



**NEAR EAST UNIVERSITY
INSTITUTE OF GRADUATE STUDIES
DEPARTMENT OF CIVIL ENGINEERING**

**ENSEMBLE RAINFALL ENSEMBLE RUNOFF MODELING
USING RAIN GAUGE AND SATELLITE BASED DATA, CASE
OF GILGEL ABAY, ETHIOPIA**

Ph.D. THESIS

Tagesse Gichamo LAFAMO

Nicosia

June, 2022

**TAGESSE
GICHAMO
LAFAMO**

**ENSEMBLE RAINFALL ENSEMBLE RUNOFF
MODELING USING RAIN GAUGE AND SATELLITE
BASED DATA, CASE OF GILGEL ABAY, ETHIOPIA**

Ph.D. THESIS

2022

**NEAR EAST UNIVERSITY
INSTITUTE OF GRADUATE STUDIES
DEPARTMENT OF CIVIL ENGINEERING**

**ENSEMBLE RAINFALL ENSEMBLE RUNOFF MODELING
USING RAIN GAUGE AND SATELLITE-BASED DATA, CASE OF
GILGEL ABAY, ETHIOPIA**

Ph.D. THESIS

Tagesse Gichamo LAFAMO

Supervisors

Prof. Dr. Hüseyin GÖKÇEKUŞ (Main Supervisor)


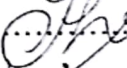
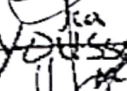


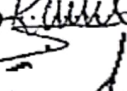
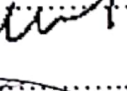
Prof. Dr. Vahid NOURANI (Co-Supervisor)

Nicosia


June, 2022

Approval

We certify that we have read the thesis submitted by TAGESSE GICHAMO LAFAMO titled "Ensemble Rainfall Ensemble Runoff Modeling Using Rain Gauge And Satellite-Based Data, case of Gilgel Abay, Ethiopia" and that in our combined opinion it is fully adequate, in scope and quality, as a thesis for the degree of Doctor of Philosophy in Civil Engineering.

| Examining Committee | Name-Surname | Signature |
|------------------------|-------------------------------------|---------------------------------------------------------------------------------------|
| Head of the Committee: | PROF. DR. MUSTAFA ERGİL |  |
| Committee Member: | ASST. PROF. DR. ELNAZ SHARGHI |  |
| Committee Member: | ASSOC. PROF. DR. YOUSSEF KASSEM |  |
| Committee Member: | ASSOC. PROF. DR. FIDAN ASLANOVA |  |
| Committee Member: | ASSOC. PROF. DR. ANOOSHEH IRAVANIAN |  |
| Supervisor: | PROF. DR. HUSEYİN GOKCEKUS |  |
| Co-Supervisor: | PROF. DR. VAHID NOURANI |  |

Approved by the Head of the Department 26./09./2022.....


Prof. Dr. Kabir SADEGHI

Head of Department

Approved by the Institute of Graduate Studies

...../...../2022

Prof. Dr. Ismail Can Başer

Head of the Institute



Declaration

I hereby declare that all information, documents, analysis, and results in this thesis have been collected and presented according to the academic rules and ethical guidelines of the Institute of Graduate Studies, Near East University. I also declare that as required by these rules and conduct, I have fully cited and referenced information and data that are not original to this study.



Tagesse Gichamo Lafamo

10/7/2022

Acknowledgment

I would like to express my deepest gratitude and sincere appreciation to my main supervisor Prof. Dr. Hüseyin GÖKÇEKUŞ for his patience, motivation, enthusiasm and immense contribution to the achievement of this goal. My deepest appreciation goes to my co-supervisor Prof. Dr. Vahid NOURANI for his uncountable guidance and support, starting from suggesting the research topic to the publication and completion of the thesis.

I would like to thank the Ethiopian Ministry of Education and Arsi University for their financial support and sponsorship of my study. I would like to thank Near East University for providing me with a 100% scholarship for my study.

I am very grateful to my wife Martha for her unwavering support, love, and passion throughout my years of study and my life in general. My gratitude also goes to my daughters Elishaday and Malela for their patience on all the days when I was unable to treat and care of them. My gratitude goes to my mother and other family members for their prayers and encouragement during the difficult days.

My profound gratitude goes to all my friends and colleagues who have always been a source of strength and aspiration.

Tagesse Gichamo LAFAMO

DEDICATED TO MY PARENTS

Abstract

Ensemble Rainfall Ensemble Runoff Modeling Using Rain Gauge and Satellite-Based Data, Case of Gilgel Abay, Ethiopia

Tagesse Gichamo Lafamo

Ph.D., Department of Civil and Environmental Engineering

Supervisors: Prof. Dr. Hüseyin Gökçekuş (main supervisor)

Prof. Dr. Vahid Nourani (Co-supervisor)

June, 2022,(149) pages

The study aimed to develop an ensemble rainfall-runoff model by Adaptive Neuro-Fuzzy Inference System (ANFIS), Feed Forward Neural Network (FFNN), Soil and Water Analysis Tool (SWAT), Hydrologic Engineering Center's Hydraulic Modeling System (HEC-HMS), Hydrologiska Byråns Vattenbalansavdelning (HBV), and Support Vector Regression (SVR) of Gilgel Abay watershed, Blue Nile basin, Ethiopia. Rainfall from 5 gauging stations (Gundel, Wetet Abay, Sekela, Dangila, and Adet) and 3 satellite sources (Climate Prediction Center (CPC) morphing technique (CMORPH), 3B42 and 3B42RT which are Tropical Rainfall Measuring Mission (TRMM) products, discharge measured at outlet, and spatial data such as Digital Elevation Map (DEM), soil map and land use land cover were used for the modeling. The most sensitive parameters of rain-runoff modeling for every model were examined, and soil curve number (CN2) and baseflow factor (ALPHA_BF) for SWAT, the initial abstraction and lag time for HEC-HMS, and soil moisture storage (FC) and lower storage recession coefficient (K2) for HBV were obtained. The appropriate input parameters for SVR, ANFIS and FFNN models were also identified using the non-linear sensitivity analysis method, and accordingly, discharge and rainfall were sensitive for rainfall-runoff modeling.

First, each model separately simulated runoff using rainfall datasets of gauge, each satellite, and their fusion. Second, each model output was imposed to ensemble modeling via proposed simple average (SAE), Neural Network (NNE) and weighted average (WAE) ensemble techniques using 3 ensemble scenarios. The scenarios applied

were i) an ensemble of AI-based models, ii) an ensemble of physically-based models, and iii) an ensemble of all models using rainfall fusion.

From the satellite rainfall products, CMORPH indicated better performance for all models but it still tends to overestimate the low flows. The rainfall-runoff modeling results using 3B42 and 3B42RT underestimate peak flow, and in particular, 3B42 gave random false peaks in the dry period. It is noted that all models were good in apprehending the rainfall-runoff relationship; nevertheless, ANFIS perceived slight supremacy by Nash-Sutcliffe Efficiency (NSE) of 0.864 and 0.875 for gauge and fusion rainfall data, respectively at the validation phase. SWAT outperformed the other semi-distrusted models with NSE of 0.81 and 0.821 for gauge and fusion rainfall data, respectively, at the validation stage. Scenario 3 ensemble modeling (fusion of rainfall datasets) was shown substantial improvement over modeling by satellite rainfall dataset owing to bias correcting capacity of rainfall dataset from the gauge over rainfall datasets obtained from the satellite. The NNE technique boosted the accuracy of low performed satellite rainfall dataset-based model by 21.2% and the rainfall datasets, fusion-based model, by 15.7% at the validation stage. Generally, the results of this study point out that the fusion of rainfall datasets from multiple satellite sources would be a worthy preference for rainfall-runoff simulation of data-scarce as well as un-gauged catchments.

Keywords: rainfall-runoff modeling, ensemble- modeling, physically-based, artificial-intelligence, gilgel -abay

Table of contents

| | |
|-------------------------|---|
| Approval..... | 2 |
| Declaration | 3 |
| Acknowledgment | 4 |
| Abstract..... | 6 |
| Table of Contents | 8 |

CHAPTER I

| | |
|------------------------------------------|----|
| Introduction..... | 17 |
| General Background..... | 17 |
| Statement of the Problem | 23 |
| Objectives of the Study | 24 |
| Significance of the Study | 25 |
| Scope and limitations of the study | 25 |

CHAPTER II

| | |
|----------------------------------------------------|----|
| Literature Review..... | 27 |
| Physically-Based Rainfall-Runoff Models..... | 31 |
| The SWAT..... | 31 |
| HEC-HMS | 33 |
| HBV | 34 |
| AI-based rainfall-runoff models..... | 35 |
| ANFIS..... | 35 |
| ANN..... | 37 |
| SVR | 38 |
| Satellite Estimated Precipitation Products | 38 |
| Concept of Ensemble Rainfall-Runoff Modeling | 44 |

CHAPTER III

| | |
|------------------------------------------------|----|
| Methodology | 48 |
| Description of the Study Area | 48 |
| Datasets | 49 |
| Gauging-Station Datasets | 50 |
| Satellite Rainfall Datasets | 50 |
| Methodology | 53 |
| Proposed Rainfall-Runoff Models | 55 |
| The SWAT Model | 55 |
| The HBV Model | 61 |
| The HEC-HMS Model | 63 |
| The ANFIS Model | 66 |
| The ANN Model | 68 |
| The SVR Model | 70 |
| Performance Evaluation | 74 |
| Ensemble Modeling | 75 |
| Non-Linear Neural Network Ensemble (NNE) | 75 |
| Simple Average Ensemble (SAE) | 76 |
| Weighted Average Ensemble (WAE) | 76 |
| Sensitivity Analysis | 77 |

CHAPTER IV

| | |
|---------------------------------------|----|
| Results and Findings | 81 |
| Results of Sensitivity Analysis | 81 |
| Results of Single Models | 84 |
| Results of Rainfall Fusion | 94 |

| | |
|---------------------------------------------------|-----|
| Results of Ensemble Modeling | 99 |
| CHAPTER V | |
| Discussions..... | 106 |
| CHAPTER VI | |
| Conclusion and Recommendations..... | 111 |
| Conclusions | 111 |
| Recommendations | 113 |
| REFERENCES | 114 |
| APPENDIX 1..... | 131 |
| Curriculum Vitae..... | 131 |
| APPENDIX 2..... | 136 |
| Graphical Presentation of Each Models Result..... | 136 |
| APPENDIX 3..... | 142 |
| Graphical Summary of Raw Data | 142 |
| APPENDIX 4 | 147 |
| Ethical Approval Letter | 147 |
| APPENDIX 5..... | 148 |
| Similarity Report | 148 |

List of Tables

| | |
|----------------|-----|
| Table 1 | 40 |
| Table 2 | 44 |
| Table 3 | 52 |
| Table 4 | 57 |
| Table 5 | 66 |
| Table 6 | 77 |
| Table 7 | 79 |
| Table 8 | 81 |
| Table 9 | 83 |
| Table 10 | 84 |
| Table 11 | 91 |
| Table 12 | 92 |
| Table 13 | 96 |
| Table 14 | 98 |
| Table 15 | 100 |
| Table 16 | 101 |
| Table 17 | 102 |

List of Figures

| | |
|-----------------|-----|
| Figure 1 | 28 |
| Figure 2 | 39 |
| Figure 3 | 40 |
| Figure 4 | 42 |
| Figure 5 | 47 |
| Figure 6 | 49 |
| Figure 7 | 54 |
| Figure 8 | 57 |
| Figure 9 | 58 |
| Figure 10 | 59 |
| Figure 11 | 60 |
| Figure 12 | 60 |
| Figure 13 | 61 |
| Figure 14 | 63 |
| Figure 15 | 65 |
| Figure 16 | 67 |
| Figure 17 | 70 |
| Figure 18 | 73 |
| Figure 19 | 87 |
| Figure 20 | 89 |
| Figure 21 | 93 |
| Figure 22 | 94 |
| Figure 23 | 97 |
| Figure 24 | 99 |
| Figure 25 | 101 |
| Figure 26 | 103 |
| Figure 27 | 104 |
| Figure 28 | 136 |
| Figure 29 | 137 |

| | |
|-----------------|-----|
| Figure 30 | 138 |
| Figure 31 | 139 |
| Figure 32 | 140 |
| Figure 33 | 141 |
| Figure 34 | 142 |
| Figure 35 | 143 |
| Figure 36 | 143 |
| Figure 37 | 144 |
| Figure 38 | 144 |
| Figure 39 | 145 |
| Figure 40 | 146 |

List of Abbreviations

| | |
|-----------|----------------------------------------------------------------------------|
| AdaBoost | Adaptive Boosting |
| AGRL | Agricultural land |
| AI | Artificial Intelligence |
| ANFIS | Adaptive neuro-fuzzy inference system |
| ANN | Artificial Neural Network |
| ARIMA | Auto-Regressive Integrated Moving Average |
| ARIMAX | Auto-Regressive Moving Average with Exogenous Input |
| AWBM | Australian Water Balance Model |
| AWC | Available water capacity of soil layer |
| BP | Back-Propagation algorithm |
| CHIRPS | Climate Hazards Group Infrared Precipitation with Stations data |
| CMORPH | Climate Prediction Center morphing technique |
| CN | Soil Curve Number |
| DEM | Digital Elevation Model |
| DPR | Dual Frequency Precipitation Radar |
| FC | Maximum Soil Storage |
| FIS | Fuzzy Inference System |
| FL | Fuzzy Logic |
| GA | Genetic Algorithm |
| GEP | Gene expression programming |
| GL | Grass Land |
| GLUE | Generalized Likelihood Uncertainty Estimation |
| GP | Genetic Programming |
| GPM | Global Precipitation Measurement |
| GSMaP-MVK | Global Satellite Mapping of Precipitation Moving Vector with Kalman filter |

| | |
|---------|-----------------------------------------------------------------------------------------|
| GWDELAY | Groundwater delay time |
| HBV | Hydrologiska Byråns Vattenbalansavdelning |
| HEC-HMS | Hydrologic Engineering Center's Hydraulic Modeling System |
| HRU | Hydrologic Response Units |
| IHECRAS | Identification of Unit Hydrograph Components from Rainfall, Evaporation, and Streamflow |
| IMERG | Integrated Multi-Satellite Retrievals for GPM |
| JAXA | Japan Aerospace Exploration Agency |
| JST | Japan Science and Technology Agency |
| KWM | Kinematic Wave Model |
| LM | Levenberg-Marquardt algorithm |
| LP | Limit of Potential Evaporation |
| LULC | Land Use Land Cover |
| MAXBAS | Length of Weighing Function |
| MCMC | Markov Chain Monte Carol |
| MF | Membership Function |
| MLP | Multi-layer Perceptron |
| MLR | Multi-linear Regression |
| MSWEP | Multi Source Weighted Ensemble Precipitation |
| NASA | National Aeronautics and Space Administration |
| NNE | Neural Network Ensemble |
| NOAA | United States National Oceanic and Atmospheric Administration |
| NSE | Nash-Sutcliffe Coefficient of Efficiency |
| P | Rainfall |
| ParaSol | Parameter Solution |
| PCA | principal component analysis |
| PED | Parameter Efficient Distributed |
| PERC | Percolation to groundwater |

| | |
|--------------|----------------------------------------------------------------------------------------------------------------|
| PERSIANN | Precipitation Estimation from Remotely Sensed Information using Artificial Neural Networks |
| PERSIANN-CDR | Precipitation Estimation from Remotely Sensed Information using Artificial Neural Networks-Climate Data Record |
| POS | Particle Swarm Optimization |
| Q | Discharge |
| RMSE | Root Mean Square Error |
| SAC-SMA | Sacramento Soil Moisture Accounting Model |
| SAE | Simple Average Ensemble |
| SCS | Soil Conservation Service |
| SCS-CN | Soil Conservation Service Soil Curve Number |
| SCS-UH | Soil Conservation Service Unit Hydrograph |
| SL | Scrub/Shrub |
| SM | Soil Moisture |
| SMA | Sacramento Soil Moisture Accounting Model |
| SMHI | Swedish Meteorological and Hydrological Institute |
| SUFI-2 | Sequential Uncertainty Fitting |
| SURLAG | Surface runoff lag coefficient |
| SVM | Support Vector Machine |
| SVR | Support Vector Regression |
| SWAT | Soil and Water Assessment Tool |
| SWMM | Storm Water Management Model |
| T | Temperature |
| TRMM | Tropical Rainfall Measuring Mission |
| TT | Threshold Temperature |
| UrL | Built area |
| UZL | Reservoir threshold |
| WAE | Weighted Average Ensemble |

CHAPTER I

Introduction

General Background

Rainfall-runoff modeling is applied as a technique to estimate methods for predicting runoff in real-time (Shamseldin et al., 1997). The rainfall-runoff modeling process is frequently used to determine the streamflow signals leaving the catchment by using rainfall and snowmelt signals received by the catchment. Rainfall-runoff explains the process that the streamflow occurred from the physical interaction of rainfall, evaporation, infiltration, surface runoff, groundwater flow, interflow, and transpiration in the hydrologic cycle that are gained to the system or lost from the system (Young et al., 2017). The rainfall-runoff modeling process is conceptualized for the specific part of the physical component called a drainage network or watershed which has a common outlet point. The real rainfall-runoff process could be simulated and predicted by the computer-based simplified representation of the hydrologic cycle which is known as modeling.

An appropriate model should be selected depending on several factors such as the interest of the researcher, input data availability, characteristics of the watershed, accuracy of the model, and its familiarity. Accurate modeling of rainfall-runoff is critical for various aspects of hydrology and environmental management, such as watershed management, siltation control, land use planning, water supply, wastewater disposal, flooding, and groundwater management. However, the modeling process is very complex due to the irregularity and non-linearity of rainfall data in time and space (Nourani et al., 2013). The process is also challenging because its physical processes are subjected to changes in space and time, revealing random and non-linear characteristics.

In rainfall-runoff modeling, the most challenging task is the accurate identification of the relationship that could exist between input and output parameters. This situation could be the worst for ungauged catchments as it lacks appropriate records of datasets mainly rainfall and discharge. Input-output parameters relationship in

ungauged catchments is often determined by regionalization of non-flow catchment entities such as soil, slope of drainage path, land use, and land cover (Mathias et al., 2016). The uncertainties in rainfall-runoff modeling could also occur due to inappropriate model structure, and forcing datasets (Chen et al., 2013). The model structures could determine their capacity to represent the physical processes of a given watershed and the observed data could also be less informative to present the real hydrologic characteristics. Measuring all the factors affecting rainfall-runoff modeling is not an easy task and is often impossible for unaccessible basins (Zegelew & Melesse, 2018). Therefore, models with simple structures, that require minimal input data, and less complex with comparable modeling accuracy should be the best models.

The other problem in the rainfall-runoff modeling process is the dynamic nature of streamflow and climatic variables in space and time and they are usually chaotic, random, and non-linear (Yaseen et al., 2016). Streamflow is highly variable in both quantity and quality at different seasons of the year and at different places along the flow path. The climatic variables such as rainfall, temperature, solar radiation, and evaporation could also be highly variable in space and time as the result of global and regional climate change due to natural or man-made effects. Therefore, the dynamic nature of input parameters and specific model structure could affect the rainfall-runoff modeling accuracy.

Several models have been developed for rainfall-runoff modeling, including physically-based distributed models, conceptual models, and artificial intelligence-based (AI) black-box models. Various conventional black-box models such as Multiple Linear Regression (MLR), Auto-Regressive integrated moving average (ARIMA), and Auto-Regressive Moving Average with Exogenous Input (ARIMAX) have been used for hydrologic modeling (Adamowski et al., 2012; Graumlich, 1987; Salas et al., 1980; Zhang et al., 2011). However, the underlying assumptions of conventional models are uniform and stationary inputs and a linear relationship between inputs and outputs, which is not the case for widely non-linear and non-stationary hydrologic data. The linear model assumes stationary input data and can lead to inaccurate results.

The physically-based semi-distributed models, for instance, Soil and Water Assessment Tool (SWAT) and Hydrologic Engineering Center's Hydraulic Modeling System (HEC-HMS) can well understand the physical relationships of the components and truthfully simulate rainfall-runoff, however, they need large spatial and temporal data and the process is time-consuming (Nourani et al., 2021). The linear classic models are simple to use and map linear relations between inputs and outputs but they are not effective for rainfall-runoff modeling because hydrologic processes are non-linear spatial and temporal phenomena. Artificial intelligence (AI) based black-box models have increased rainfall-runoff modeling performance because AI has the capability of handling spatial and temporal irregularity and non-linearity of rainfall (Nourani et al., 2011). AI techniques such as Artificial Neural Network (ANN), Adaptive neuro-fuzzy inference system (ANFIS), Support Vector Machine (SVM), Genetic programming (GP), and Support Vector Regression (SVR) were widely used for rainfall-runoff modeling (Kisi et al., 2013). In the last few decades, various artificial intelligence models have been applied to solve hydrologic and water resource engineering-related problems such as rainfall-runoff modeling, streamflow forecasting, sediment transport prediction, rainfall forecasting, water table estimation, and groundwater flow (Abbot and Marohasy 2017; Altunkaynak and Nigussie 2015; Asadi et al. 2013; Evsukoff et al., 2012; Kurtulus and Razack 2010; Rajaei, 2011; Shi et al. 2018; Si et al. 2015; Stanley Raj et al. 2017; Zeynoddin et al. 2018).

SWAT is the physically-based and semi-distributed model that has been effectively modeling rainfall-runoff relation at daily and sub-daily periods in catchment level (Arnold et al., 1998; Arnold & Fohrer, 2005). The SWAT model is verified as a credible and effective tool not only for runoff simulation but also for flood prediction and warning, nutrient transportation, soil erosion, and land use pattern change modeling (Busico et al., 2020; Deng et al., 2019; Zhang et al., 2020).

HEC-HMS is also a semi-distributed hydrological model applied for rainfall-runoff modeling at dendritic watersheds in time and space (Feldman, 2000; Kwin et al., 2016). It discretizes the catchment into smaller catchments called sub-basins to incorporate the details of each entity into the rainfall-runoff simulation results. HEC-HMS model could successfully simulate rainfall-runoff both continuous and single event

floods and the result could be used for urban flood control and wide-scale catchment hydrological management.

Hydrologiska Byråns Vattenbalansavdelning (HBV) is a conceptual semi-distributed hydrological model based on a simple continuity equation to model streamflow and the physical processes of components (Ciupak et al., 2019). The model divides the watershed into smaller sub-watersheds. HBV has been practically simulated in numerous hydrological modeling such as rainfall-runoff, climatic variability, and water level forecast (Ali et al., 2018; Kazemi et al., 2019; Pervin et al., 2021).

AI-based models are gaining popularity in rainfall-runoff modeling because they are user-friendly and can provide accurate results with a short convergence time using few input data sets. ANN has become familiar in the past few decades for modeling a complicated non-linear relation such as rainfall-runoff. The model's capability to handle large dimensionality of data, noisy and non-linear datasets has proved by many researchers over the past two decades (Alizadeh et al. 2017; Chua and Wong 2010; Hsu et al., 1995; Jain et al., 2004; Kasiviswanathan et al. 2013; Nourani 2017; Nourani et al. 2013; Nourani et al., 2009; Piotrowski and Napiorkowski 2013; Srinivasulu and Jain 2006).

Adaptive Neuro-Fuzzy Inference System (ANFIS) is a data-driven black-box model which was presented by (Jyh Shing Roger Jang, 1993) in a combined form of Artificial Neural Network and Fuzzy Inference System where its main components such as membership function and an if-then logic rule were introduced. ANFIS can detect datasets through the hybrid method of least square and backpropagation gradient descent error techniques. A fuzzy Inference System can accurately estimate compact time serious datasets (Jang et al., 1997). ANFIS is categorized into Mamdani's method (Mamdani & Assilian, 1975), and Tuskamoto's and Sugeno's (Takagi & Sugeno, 1985) methods based on the linguistic logic operational interface and membership function of the models. Mamdani's method applied fuzzy membership functions techniques while Sugeno's method uses constant or linear function techniques. ANFIS mostly relies on Sugeno's method more than Mamdani's method because Sugeno's method is more compact and its computational efficiency is high. Adaptive Neuro-Fuzzy Inference System (ANFIS) has been extensively applied to resolve non-linear and non-stationary

hydrological and water resource engineering problems such as rainfall prediction, rainfall-runoff modeling, and water level forecasting and streamflow forecasting (Güner and Yumuk 2014; Noori et al., 2013; Si et al. 2015).

SVR is the non-linear regression model that is advanced from the Support Regression Machine (SVM) with the basic perception of having the capacity to map datasets with greater dimensionality via non-linear techniques to map the relations between inputs and outputs. The objective function of SVR is the operational risk that is used to diminish the inaccuracy between observed and predicted variables (Wen et al., 2015). As compared to the other two AI models, the SVR model is superior particularly, it can significantly reduce over-fitting, provide a global optimum solution, and can parallel distribution processing (Kalteh, 2013). The limitation of SVR is complex computational processes since it uses quadratic equations for computing the regression (Wang & Hu, 2005).

Up to date, there is no single universal modeling approach that could provide the most accurate runoff simulation in every circumstance (Yaseen et al., 2016). This could be because of the fact that a given natural process develops exclusively over time whereas the modeling methodologies based on finite datasets time-series are variable in their structure and governed by the parametric forms that vary from one model to the other model. Overall, the mentioned physically-based and AI models could provide reliable rainfall-runoff outputs, nevertheless relying on a single model for rainfall-runoff, the results may not always be trustworthy and accurate because the model cannot handle various uncertainties. It is suggested to use multiple models simultaneously as alternative models that can provide an optimal result. An optimum simulation result can be achieved by combining (ensemble) the outputs of different models together as input to the ensemble model (Shamseldin et al., 1997). The assumption behind the ensemble technique is that the important feature from individual models' output would be modeled together which may reduce uncertainties and give a more reliable output. Ensemble modeling as post-processing techniques can increase the accuracy of prediction, reliability of output, and lower the error of variance (Kiran and Ravi 2008; Sharghi et al., 2018; Yamashkin et al. 2018; Zhang 2003) compared to individual models output. Ensemble modeling could ascertain and encapsulate exceptional features of each model

and data thus it increases the accuracy of the modeling. Various ensemble models have been applied such as neural network, simple linear averaging and weighted linear averaging methods are the most familiar ensemble techniques.

Rainfall is the indispensable element of the earth's hydrologic cycle and it could play a substantial role in the redistribution and replenishment of water resources and it could affect the growth of agronomy, ecosystem, and economy (Li et al., 2018). For any hydrological modeling, the result would be accurate, if the rainfall quality is good enough and evenly distributed in space and time.

Conventional rain-gauges, radars, and satellite-based rainfall measurement practices are the usual methods of obtaining rainfall for rainfall-runoff simulation. Nevertheless, ground stations for rainfall measurement are often unevenly and non-uniformly distributed in developing countries and this condition is unlikely to advance shortly (Worqlul et al., 2017). In the past few decades, satellite rainfall datasets are identified as cheap, and consistent data sources, that are available in various temporal and spatial resolutions and it has been attracting the interests of hydrologists, particularly in areas where the conventional gauging stations are unavailable or sparsely distributed (Tapiador et al., 2012).

Several space crafts have been launched aimed to estimate precipitation, for instance, the Climate Prediction Center (CPC) morphing technique (CMORPH), Tropical Rainfall Measuring Mission (TRMM), and Global Precipitation Measurement (GPM) Core Observatory. The CMORPH was set in motion in 1998 to record precipitation products as near-real-time datasets (Joyce et al., 2004) and it retrieves better temporal and spatial resolution precipitation records from more accurate passive microwave sensors. The TRMM provides rainfall data in real-time (3B42RT) and post-research real-time (3B42). The TRMM combines the relative merits of rainfall information from multi-satellite sources and provides more consistent and accurate precipitation over the specified grids (Prakash et al., 2018). TRMM is ideal for precipitation measurement with suitable spatial and temporal resolution because it consists of appropriate sets of measurement devices and is situated at low orbits with a suitable angle of inclination.

Although the satellite-based rainfall datasets are suitable inputs for rainfall-runoff simulation of non-gauged watersheds, every satellite data has its benefits, the rainfall datasets' consistencies in space and time are extremely affected by elevation and atmospheric influences (Tang & Hossain, 2012). Hence, the combination of precipitation datasets from several satellites sources as an input ensemble might improve rainfall-runoff modeling through the calibration stage; the model could apprehend better weight for more realistic satellite rainfall datasets.

Uncertainties in rainfall-runoff modeling that might arise from the input data were practically managed through calibration and assimilation of the input data (Kumar et al., 2015). In catchments where rain gauging stations could not adequately represent the area, fusion of gauge and satellite rainfall data from multiple sources proved to be highly effective in rainfall-runoff modeling. The distortion in satellite rainfall estimates could be corrected by gauging rainfall during the fusion. All models have not been able to perform equally well in rainfall-runoff modeling, and they have their merits in one aspect and their shortcomings in the other. Hence, ensemble techniques could update the modeling by combining the advantages of each model in the calibration phase and enhance the overall efficiency of rainfall-runoff modeling.

Statement of the Problem

Information about rainfall-runoff is very crucial for any water resource and hydrological problems and accurate result of rainfall-runoff, good quality rainfall data in terms of spatial and temporal resolution is important. Natural and man-made water-related environmental hazards especially drought and flooding are becoming more frequent. Rapid population increment could also increase more demands for agricultural land expansion and related deforestation leads to soil erosion and sedimentation problems. As a result of these environmental problems, water quality and quantity became worse, food insecurity and health-related issues and regional climate variabilities are aggravated.

For the intervention of mitigation and adaptation actions, well planned hydrological modeling has paramount significance as a decision supporting tool.

Temporally and spatially well-defined hydro-meteorological time series data especially precipitation is required for rainfall-runoff modeling.

In the current study area, rainfall observation gauges are inadequate, uneven, and short in space and time. Furthermore, the area is topographically flexible from hills to plains; in this case, the rainfall datasets could be subjected to orographic influences and cause bias and improper areal representations (Gebre, 2015). The rain gauge distribution in the basin is sparse and not uniform, hence the quality and quantity of climatic data from the gauges could not be good enough to obtain accurate rainfall-runoff modeling results.

Estimation of precipitation from satellites is a good option in areas where the mentioned problems are common. Satellite estimated precipitation using the appropriate algorithm can be provided as input to effectively model rainfall-runoff. Ensemble modeling, fusion of using gauge and satellite estimated rainfall as an input can accurately model rainfall-runoff relationships and the current study approach is a pioneer for the study area.

Objectives of the Study

The objectives of this study are:

- ✓ Rainfall-runoff modeling by SWAT, HEC-HMS, HBV, FFNN, ANFIS, and SVR separately using the gauge and satellite rainfall datasets along with the other spatial and time-series datasets.
- ✓ Rainfall-runoff modeling by SWAT, HEC-HMS, HBV, FFNN, ANFIS, and SVR using the fusion of gauge and satellite rainfall datasets
- ✓ Ensemble rainfall-runoff modeling using the outputs of AI-based models (FFNN, ANFIS, and SVR) as inputs to further enhance the modeling performance
- ✓ Ensemble rainfall-runoff modeling using the outputs of physically-based models (SWAT, HEC-HMS, HBV) as inputs to further enhance the modeling performance
- ✓ Overall ensemble modeling using outputs of all proposed models from rainfall fusion stage as inputs to improve the rainfall-runoff simulation accuracy

Significance of the Study

Accurate modeling of rainfall-runoff could be a good tool for water allocation, water management, and policy decisions. The exact amount of runoff generated at a given time could be used to plan and operate hydraulic structures such as dams, reservoirs, bridges, irrigation projects, and flood control facilities.

Therefore, real-time runoff modeling for the Gilgel Abay watershed would serve as an input for the planning, operation, and management of these important water infrastructures. Management and response to environmental disasters triggered by human and natural causes such as floods and droughts could also require accurate determination of runoff models. Flood and disaster response could require accurate analysis of the magnitude of peak events and lowest flows so that data can be used to intervene and protect against such disasters.

Moreover, the Nile Basin is connected to 10 riparian countries, and more than 160 million rely on it for existence (Uhlenbrook et al., 2010) and more than 60% of the river originates from the Ethiopian highlands, particularly the upper Gilgel Abay catchment. The real scientific facts supported by such studies will increase data sharing among riparian countries, transparency, and trust, which could lead to better water resource allocation, commonwealth, and regional stability.

The results of this study could therefore provide valuable data for water management, current and future planning and operation of hydraulic structures, and flood and drought protection. It could also provide high-quality flow data for Nile Basin cooperation, integration, and shared prosperity.

Scope and limitations of the study

This study was bounded in single and ensemble rainfall-runoff modeling by three AI-based (ANFIS, FFNN, and SVR) and three physically-based (SWAT, HEC-HMS, and HBV) models using three satellite and five ground-based rainfall measurement data for Gilgel Abay watershed, Ethiopia. The distribution of ground-based rainfall observation stations is not uniform but sparse. Even for existing stations, data records for some days were missing and incomplete. In addition, most of the

weather observation stations in the study area are not at a synoptic scale, making it difficult to obtain complete measured climate data. Moreover, the global covid-19 pandemic and associated travel restrictions, financial resources, and time were the limiting factors faced during this study.

CHAPTER II

Literature Review

Rainfall-runoff modeling determines the relationship between rainfall coming to the ground and the portion of that rainfall converted to runoff. Rainfall-runoff modeling is the standard process routinely applied for hydrological analysis in engineering, science, and environmental management. The rainfall-runoff process extends to river flow time series concerning space and time, to examine management methods and watershed response to land use land cover and climate change (Thorsten et al., 2003). Rainfall-runoff modeling is valuable for the planning, operation, and use of various water resources management activities such as flood control, drought management, irrigation, hydropower generation, water supply, and the design of various hydraulic structures such as dams, reservoirs, and bridges (Ghumman et al. 2011; Srinivasulu and Jain 2006).

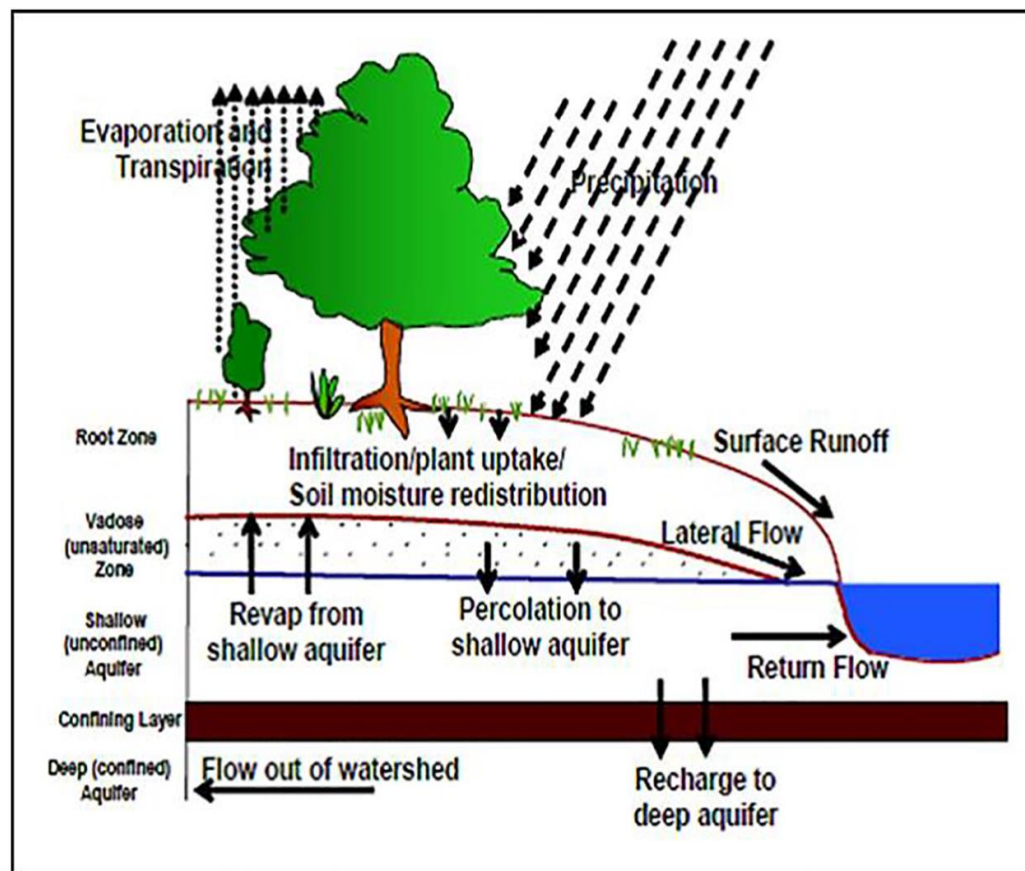
Rainfall and runoff are spatially and temporally variable and their relationship is likely to be non-linear, making the conversion of rainfall into a runoff a very complex task. The rainfall-runoff process usually includes inflow parameters to the system and outflow parameters from the system and assumes time-variant storage changes (see Fig. 1). Accurate modeling of the rainfall-runoff relationship is highly influenced by the nature of rainfall (intensity and duration), watershed characteristics (slope, storage characteristics, topography, and shape), spatial and temporal variability of parameters, watershed morphology, incomplete and noisy data, and climatic variabilities such as temperature and humidity (Srinivasulu & Jain, 2006; Amin Talei, Hock, et al., 2010).

The accurate rainfall-runoff modeling is the one that can transfer all the useful information of the inputs into the final output. In addition to the other factors, rainfall-runoff modeling can be influenced by the spatial and temporal distribution of rainfall characteristics such as intensity, duration, quantity, and antecedent soil moisture. The geomorphologic setting of the watershed such as land use, soil slope, soil composition, vegetation patterns, and size of the watershed can influence the relationship between rainfall and runoff generation (Srinivasulu & Jain, 2006).

The best rainfall-runoff model is also the one that provides runoff more similar to measured values, is less complex, and utilizes fewer inputs (Devia et al., 2015). Hydrologic models determine rainfall-runoff relationships based on the effects of several hydrological cycle components such as precipitation, evapotranspiration, percolation, infiltration, and interception. Those hydrologic cycle components are used as inputs and runoff would be generated as output.

Figure 1

Rainfall-Runoff Processes



Various methods have been presented and applied for rainfall-runoff modeling, which is mainly generalized into three groups: metric, parametric and mechanistic model structures.

The metric models are mainly data-driven empirical and black-box models and utilize observed time series to infer model structure and related parameters. The metric models solely rely on available data to acquire information but not do not consider the

catchment characteristics and flow pattern, therefore they are named black-box models. The metric models are lumped on space that they manage a whole watershed as a single unit. In metric models, the rainfall-runoff relations are principally dependent on observed data without representing processes involved in rainfall-runoff modeling (Jaiswal et al., 2020). The main drawback of this model is the lack of capacity to retrieve spatial variability of flow and rainfall on rainfall-runoff modeling in the ungauged catchment.

Parametric models are often known as conceptual models and their functional structure depends on storage equations (Thorsten et al., 2003). These models assume that the storages gain flow from rainfall, snowmelt, infiltration, and percolation, whereas it lost water by evaporation, runoff, and drainage. The model structure is determined by researchers' experience and understanding of hydrological networks and relies on the quality of input time series mainly streamflow data. The parametric modeling aggregates several processes in space and time into a single component and most of this type of model treats a catchment as a homogenous unit like metric units.

The mechanistic models are often called physically-based or white-box models and their functional structures are based on the assumption of conservation of energy, mass, and momentum (Beven, 2002). The mechanistic models could produce accurate results however, it needs large spatial and temporal input data. Mechanistic models spatially discretize the catchment into smaller sub-basins such as hydrological response units, grids, and hillslopes.

The physically-based models can study the spatial and temporal variations of hydrologic parameters such as soil, land use, and slope in a particular watershed that could be characterized as semi-distributed or fully nature. The physically-based models display the internal processes that will provide better information to understand the watershed system.

Physically-based fully/semi-distributed models are used to approximate internal subprocesses and physical mechanisms of the hydrologic cycle. Physically-based models can incorporate simple linear laws and assume time-varying, non-linear and deterministic parameters. Some examples of physically-based models include the Soil

and Water Assessment Tool (SWAT), Hydrologic Engineering Center's Hydraulic Modeling System (HEC-HMS), the Storm Water Management Model (SWMM), flood hydrograph package of Hydrologic Engineering Center of the US Army Corps of Engineers' Flood Hydrograph Package (HEC-1), and the Sacramento Soil Moisture Accounting Model (SAC-SMA). Hydrologiska Byråns Vattenbalansavdelning (HBV) is a conceptual semi-distributed hydrological model based on a simple continuity equation to model streamflow and the physical processes of components. Black-box models use various approaches to determine the relationship between rainfall and runoff without requiring complex physical processes. Examples of black-box models include ARMAX, ANN, SVR, and ANFIS which are effective in capturing non-linear and non-stationary characteristics of hydrological processes.

Accurate modeling of rainfall-runoff could provide important information for drought forecasting, flood prediction, water resources management, and planning (Alizadeh et al., 2017). Inaccurate runoff estimation can lead to misapplication of policies and loss of resources and lives. Precipitation is among the most important parameters in estimating runoff and river flow processes, and a good understanding of the quantity and characteristics of such parameters is very important for watershed modeling.

The accuracy of output for the rainfall-runoff models is affected by several factors such as input data resolution, basin size, topographic characteristics, methods of model calibration, and type of model. Therefore, selecting an appropriate model which could provide the best result should be carefully selected based on mentioned criteria. According to Wittwer, (2013), lumped hydrological models are more suitable for a small-sized watershed with flat or plain topography and input data with daily resolution. Semi-distributed models are more efficient for medium size watershed with moderate to hilly topographic features and it needs hourly or daily input data for calibration. The fully-distributed models are more suitable for large catchments, which are characterized by mountainous topography and with hourly or sub-hourly input data sets. Selecting an appropriate model extremely depends on the availability and resolution of input data sets. Some models are freely available for use but some are not open access and need purchasing, therefore, users must be careful during model selection.

Based on randomness, the hydrologic models can be categorized into two; that are stochastic and deterministic types. The results generated by stochastic models are usually characterized by partial randomness. On the other hand, deterministic models do not show randomness. For the given inputs, the deterministic models reproduce the same outputs at the given time and space. Therefore, it is concluded that stochastic hydrologic models are more suitable for prediction whereas deterministic models are more suitable for forecasting (Te Chow, 1964).

Physically-Based Rainfall-Runoff Models

The SWAT

The SWAT is a semi-distributed physically-based rainfall-runoff model developed to simulate applied to the model at daily time steps at the basin level (Arnold et al., 1998; Arnold & Fohrer, 2005). The model was released after a long time proven experimental trial by a combination of the United States Department of Agriculture Research Service, United States Department of Agriculture and Natural Resource Conservation Service, and Texas A & M University. The model was invented to simulate the effects of land use land cover changes on water resources, sedimentation, and the release of hazardous nutrients from fertilizers and pesticides in wide-scale catchments with varying land use, soil types, and agricultural practices over time (Arnold & Allen, 1996). It has increased universal acknowledgment as a novel watershed modeling software and is now used in nearly 100 countries. It has been broadly applied to study water resource management and nonpoint source contamination in the environment and hydro-ecological settings (Gassman et al., 2007). It also helps to understand complex environments and accessibility of water resources, water quality, climate variability, and crop farming over the earth (Dile et al., 2016).

SWAT is a physically-based model that uses climate, soil, terrain, vegetation, and land-use data to model the hydrologic characteristics of watersheds in the context of water management, temperature, sediment transport, and chemical exchange (Garret et al., 2018). For model application, the basin is subdivided into smaller sub-watersheds called hydrologic response units (HRUs) based on soil texture, land management practices, and draught, which increases the ability to model in spatial detail. Input

parameters to the model include hydrologic, climatic, soil erosion, nutrient, soil temperature, crop development, and streamflow data. The model predicts hydrologic conditions for each HRU by calculating the water balance, which includes daily rainfall, runoff, evapotranspiration, infiltration, and river discharge.

SWAT undertakes tasks that include dividing a watershed into sub-catchments by combining land use, soils, and digital elevation modeling (DEM) and then further dividing them into lumped units called Hydrologic Response Units (HRUs). The general hydrologic investigation is performed at the HRU level, including ET, interception loss of rainfall, horizontal sub-surface within the soil matrix, and backflow from shallow groundwater table. The modeling procedure is achieved in the upper part of the soil, the intermediate zone, the shallow and deep groundwater table, and the exposed channels. The SWAT model is proven as a powerful and efficient tool not only for streamflow simulation but also for flood prediction, nutrient transporting, soil erosion, and land use land cover change modeling (Busico et al., 2020; Deng et al., 2019; Reza Eini et al., 2020; H. Zhang et al., 2020).

Setegn et al., (2008) applied SWAT for hydrologic modeling for the prediction of streamflow using SUFI-2, Parasol, and GLUE sensitivity analysis tools in the Tana basin of Ethiopia and obtained good agreement between observed and simulated flow using SUFI-2 and GLUE algorithms. The hydrological response of the upper Blue Nile was carried out using the SWAT model and indicated that its performance was generally good but for extremely wet and dry seasons it was not satisfactory (Bizuneh et al., 2021). The SWAT rainfall-runoff model was calibrated and validated for Luvuvhu river in South Africa and concluded that the model gave acceptable at the calibration stage but not at the verification stage (Thavhana et al., 2018). Busico et al., (2020) evaluated the performance of SWAT for runoff prediction considering various soil inputs in Italy and obtained a good agreement between observed and predicted runoff with changing climate. The hydrological responses to land uses were simulated by SWAT in Australia and obtained urban land use reproduced high runoff than forest and rangeland use types and the model output was compatible with general fact.

HEC-HMS

HEC-HMS is a computer program that contains several methods for modeling dendritic watersheds and channels and characterizing hydraulic structures to predict streamflow, water level, and flooding. HEC-HMS can generally simulate five hydrologic parameters such as precipitation, evapotranspiration, surface runoff, groundwater discharge, and channel discharge, using a separate method for each parameter. In a given watershed, HEC-HMS can evaluate the temporal and spatial distribution of precipitation using a variety of approaches, including a user-specified hyetograph, gridded precipitation, inverse-distance gauge weighting, and soil conservation service (SCS) hypothetical approach. The surface runoff routine from HEC-HMS describes the fraction of precipitation infiltrated and runs off that can be calculated using the initial constant, the SCS soil curve number (CN), the exponential method, and Green's and Ampt's methods. The base flow routine simulates the slow subsurface flow from the hydrologic cycle into the watershed using a linear reservoir, exponential reservoir, constant monthly, and nonlinear Boussinesq methods. The routing component simulates the 1-dimensional discharge of an open channel and predicts downstream discharge, velocity, and stage hydrographs using kinematic wave, lag-time, and Muskingum approaches. The HEC-HMS graphical user interface includes the watershed model, meteorological model, control specification, simulation, and model calibration runs, as well as tools to verify results.

The HEC-HMS model is gaining popularity because it can simulate both long- and short-term runoff events and is user-friendly. The model is used in a variety of hydrologic problems, including flood forecasting and warning, rainfall-runoff simulation, watershed management, and project planning regardless of watershed size. The HEC-HMS model uses rainfall, temperature, discharge, land use, and soil data as inputs to generate runoff at a preferred time scale. The model has been successfully applied for rainfall-runoff and flood simulation in the different catchments and parts of the world and proved itself as powerful modeling tool (Abushandi & Merkel, 2013; Halwatura & Najim, 2013; Mandal et al., 2016; Young et al., 2017). Zelelew & Melesse, (2018) applied HEC-HMS estimation of runoff at watershed scale in the upper Blue Nile, Ethiopia using constant and initial loss method with SCS unit hydrograph

transform method gave good agreement between observed and simulated runoff. HEC-HMS for flow simulation at Tana basin, Ethiopia, using SCS-CN for loss, SCS-UH for runoff, and Muskingum method for routing estimations (Bitew et al., 2019). In this study, initial performance was low, but after calibration and sensitivity analysis, the performance was significantly improved. Young et al., (2017) applied HEC-HMS in combination with machine learning methods for accurate rainfall-runoff modeling in Chishan creek basin of Taiwan. The obtained result of the study indicated that the model could well simulate peak flow at the individual level and further improved at the hybrid level as well. HEC-HMS model was applied for rainfall-runoff simulation in the Sri Lankan watershed using SCS, Snyder, and Clark unit hydrograph loss methods (Halwatura & Najim, 2013). The result indicated that the Snyder unit hydrograph performed better than the Clark unit hydrograph in flow simulation, but SCS could not well capture the flow at the basin. Moreover, Abushandi & Merkel, (2013) compared the performance of HEC-HMS with the IHECRAS model for rainfall-runoff simulation at Wadi Dhuliel arid catchment. The obtained result of the study noted that the runoff simulation capacity of IHECRAS was lower than HEC-HMS for the particular basin.

HBV

The HBV is a conceptual semi-distributed model originally developed by the Swedish Meteorological and Hydrological Institute (Lindström et al., 1997) for continuous runoff simulations. The input data requirements of the HBV are very low, usually requiring daily precipitation and temperature. The model is simple to use but gives comparatively good results. The HBV model has flexible structures that can be used to subdivide the watershed based on different elevation bands, land use, and vegetation zones. The model has been used extensively used to fill the gaps in observed data, simulation of runoff in ungauged catchments, compute design floods, and conduct water quality studies. The HBV rainfall-runoff modeling procedures consist of several hydrologic routines representing snow, soil moisture, response, and routing. In a snow routine, the threshold temperature (TT) is used to define the temperature range where snow begins to melt. The soil routine is the main routine that controls runoff produced from the rainfall or snowmelt processes. In the response routine, transformation

functions convert the excess flow from the soil moisture box to runoff. The hydrograph of runoff at the outlet point is obtained in the routing routine by transforming the runoff from the response routine. HBV has been effectively applied for several hydrological modeling namely, streamflow simulation, climate change analysis, and water level prediction, and has shown the best modeling capability (Ali et al., 2018; Kazemi et al., 2019; Pervin et al., 2021; Uhlenbrook et al., 2010).

The hydrological response of the upper Blue Nile was carried out using the HBV model and indicated that its performance was generally good but for extremely wet and dry seasons it was not satisfactory (Bizuneh et al., 2021). The suitability of satellite rainfall datasets and the capacity of HBV and Parameter Efficient Distributed (PED) models for rainfall-runoff modeling were evaluated in the data-scarce upper Blue Nile basin, Ethiopia (Worqlul et al., 2017). The obtained result indicated that HBV could well reproduced the observed runoff better than PED for both gauge and satellite rainfall products. The watershed characteristics of the upper Blue Nile were analyzed by HBV using lumped vegetation zone and climatic data and it well well-reproduced bi-weekly and monthly flow, however, it poorly reproduced daily flow (Uhlenbrook et al., 2010). HBV model was applied to study temporal variability of streamflow of Hunza river in Pakistan and its performance was good at both calibration and validation except for slight underestimation of low flow during the dry season (Ali et al., 2018). Jia & Sun, (2012) studied the runoff prediction and modeling process in the Liao river of China using the HBV model and find out the model could successfully simulate streamflow in the basin.

AI-based rainfall-runoff models

ANFIS

ANFIS is the combination of neural network and fuzzy logic that can deliver adequate solutions while providing qualitative and heuristic information about the obtained solution (Jang et al., 1997). The fuzzy if-then rule could provide a better understanding of non-linear rainfall-runoff relations. Fuzzy Logic (FL) states the methods of computation and solving the problems based on the reasoning ability of humans (Chandwani et al., 2015). Fuzzy logic defines the problems with no fixed

boundary or no crisp numbers and it uses a set of logical values from sets of numbers ranging from 0 (totally false) to 1 (totally true) that are called memberships and the functions on which the numbers represented are known as membership functions. Several membership functions are available for ANFIS modeling and some of them are trapezoidal, triangular, Gaussian, and Sigmodal types. Fuzzy logic uses the AND/OR logical operational functions and IF-THEN fuzzy rules each has its particular definition based on membership concepts.

ANFIS has been extensively applied to resolve non-linear and non-stationary hydrological and water resource engineering problems such as rainfall prediction, rainfall-runoff modeling, water level forecasting, and streamflow forecasting (Güner and Yumuk 2014; Noori, Safavi et al., 2013; Si et al. 2015).

Talei et al., (2013) conducted rainfall-runoff modeling by the neuro-fuzzy system and compared the result with HBV, Storm Water Management Model (SWMM), and Kinematic Wave Model (KWM) and obtained fairly comparable results with the best physical model and better than the least performed physical model. ANFIS was applied to model multi-step ahead rainfall-runoff modeling and to capture non-linear characteristics of hydrologic systems in the three gorge reservoir (Zhou et al., 2019). The result of this study demonstrated that the ANFIS could successfully capture non-linear relationships of hydrological parameters and effectively integrate climatic parameters to reproduce runoff. Talei, et al., (2010) investigated the sequential rainfall time series and flow inputs for the rainfall-runoff modeling process using ANFIS and the result indicated that modeling by sequential rainfall was less performed than modeling using non-sequential rainfall inputs.

ANFIS was applied for rainfall-runoff modeling using Principal Component Analysis (PCA) to average out the rainfall and study its physiographic characteristics in the Tuscany, basin, Italy (Bartoletti et al., 2018). This study compared PCA with GIS for input preparation used to build the ANFIS rainfall-runoff model and the result demonstrated that PCA based model was more accurate in rainfall-runoff modeling. ANFIS was applied to forecast rainfall-runoff during typhoon events using a self-organized mapping method to cluster radar cells of rainfall at Shihmen Reservoir in

northern Taiwan (Chang & Tsai, 2016). It was noted that the proposed model can perfectly forecast runoff up to 4 hours ahead closely similar to observed peak flow.

ANN

ANN is a mathematical ‘black-box’ model containing numerous non-linear artificial neurons operated side by side that could be created as single or multiple layers. It process data based on the functional operation of the human mind and it has input, hidden and output layers where each neuron is connected by nodes. The information from input nodes is first transferred to hidden neurons and then summed up to the output neurons by activation functions. ANN is a nonlinear regression model that has been used for the effective modeling of non-linear relationships of water resource parameters in various hydrological settings (Nourani et al., 2009). Rajurkar et al., (2004) coupled ANN with the simple linear model to simulate runoff in India and the result demonstrated that ANN better reproduced runoff than the simple linear models. Coupling further improved the rainfall-runoff modeling. In the rainfall-runoff modeling study by (Hosseini & Mahjouri, 2016), ANN was integrated with SVR to overcome the drawbacks of ANN. The result indicated that every single model could reproduce acceptable results but integrating both models further improved the result as well as the robustness and reliability of the coupled model.

The ANN was applied for the prediction of the event-based rainfall-runoff process using a kinematic wave equation for the determination of model structure (Chua et al., 2011). Both total and effective rainfall were used as input and the method accurately predict the peak flow. Kasiviswanathan et al., (2013) constructed a two-stage ANN model for rainfall-runoff, first, only an ANN-based model was generated, second, the output was used as inputs to train the model using the Genetic Algorithm (GA) as an ensemble modeling. The ensemble model improved the rainfall-runoff result when it was compared with the result of the single ANN model. ANN was combined with wavelet transform to predict runoff two months ahead and demonstrated that wavelet-ANN could effectively predict runoff two months ahead using multiple climatic input data (Alizadeh et al., 2017).

SVR

SVR is a non-linear regression developed based on the concept of a Support Vector Machine (SVM) that could map the relationship between inputs and outputs with higher dimensionality. The SVR model considers operational risk as a target function to minimize risks in place of reducing the residue between observed and simulated values (Wen et al., 2015). Over the past 10 years, SVR has gained acceptance over other AI models due to its self-learning properties, parallel distributed processing, avoidance of overfitting problems, and provision of globally optimal results (Kalteh, 2013). The main disadvantage of modeling with SVR is the complex computational process for constrained optimization problems. These drawbacks can be offset by the application of least square support vector regression (LSSVR) algorithms, which use linear methods instead of quadratic equations (Wang & Hu, 2005).

The SVR model was applied along with ANN for rainfall-runoff modeling and revealed its superiority over ANN (Ateeq-ur-Rauf et al., 2018). Hosseini & Mahjouri, (2016) coupled SVR with ANN for rainfall-runoff modeling and the result indicated that the disadvantages of ANN were well managed by SVR strength and each model could reproduce good outputs however, coupling both models further enhanced the result as well as the robustness and reliability of the coupled model. SVR was applied for real-time flood prediction in Lan-Yang River, Taiwan and the result demonstrated that SVR could predict 1 to 6 hours ahead of floods in the catchment (Yu et al., 2006).

Satellite Estimated Precipitation Products

Remotely sensed rainfall products have been applied for various hydrological and agricultural research over the past three decades because it is verified that cheap, uninterrupted, and large spatial coverage for rain gauge void areas (Collins et al., 2013; Prakash et al., 2018; Tapiador et al., 2012). Satellite-based precipitation datasets are an alternative source of rainfall for ungauged and sparsely gaged watersheds.

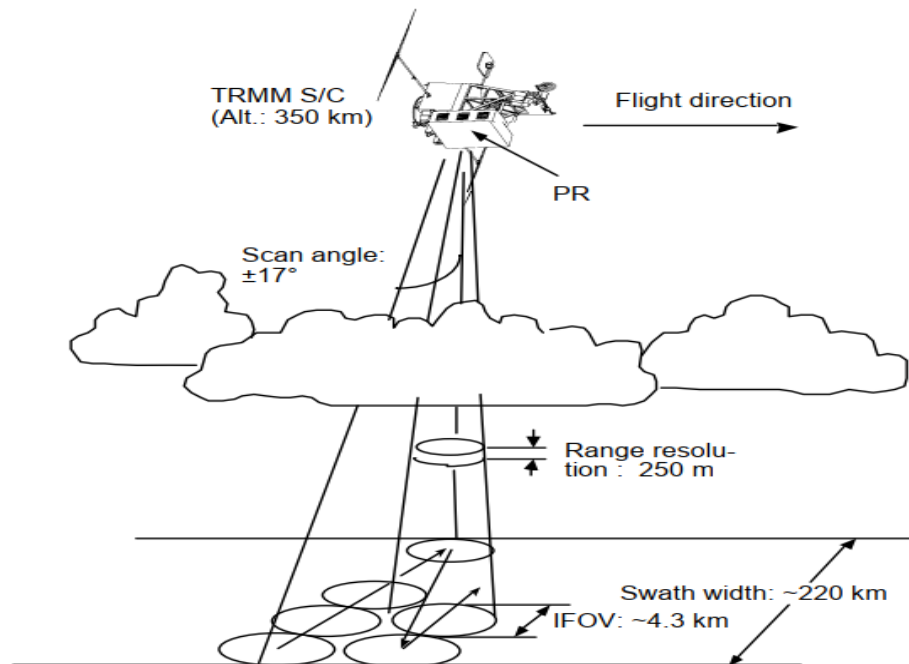
TRMM was jointly launched in 1997 by the Japan Aerospace Exploration Agency (JAXA) and the National Aeronautics and Space Administration (NASA) to estimate precipitation in humid tropics (Le et al., 2020). A TRMM precipitation sensor comprises sets of devices such as precipitation radars, microwave imagers, and visible and infrared ray scanners. TRMM estimates precipitation in three steps: i) the obtained

raw data obtained are calibrated and geo-referenced, ii) the geographic features of the site are updated with the resolution and location of the raw satellite data, iii) the temporal average data are mapped uniformly in space and time.

The TRMM spacecraft used for the estimation of precipitation is a unique instrument to observe the vertical pattern of precipitation distribution operated at 13.8 GHz frequency (more details are given in Table 1). It can effectively observe the quantity of precipitation over land and the ocean. Initially, TRMM was positioned at an altitude of 350 km but it changed to 402.5km after August 2001 for better efficiency (Fig 2).

Figure 2

TRMM Precipitation Observation Arrangements



TRMM contains the precipitation radar (PR), infrared and visible scanners, cloud and earth radiant energy system, and imaging and lighting systems (see Fig 3).

Figure 3

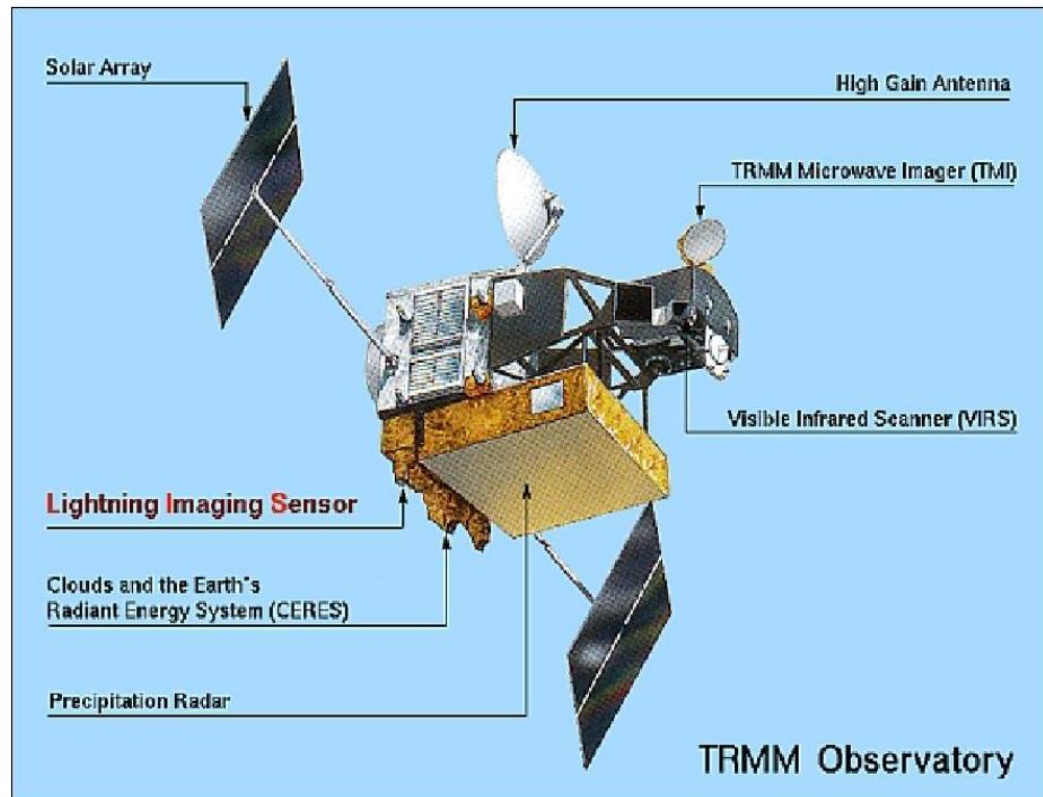
Sets of Instruments in TRMM Spacecraft

Table 1

Main Parameters of TRMM Spacecraft

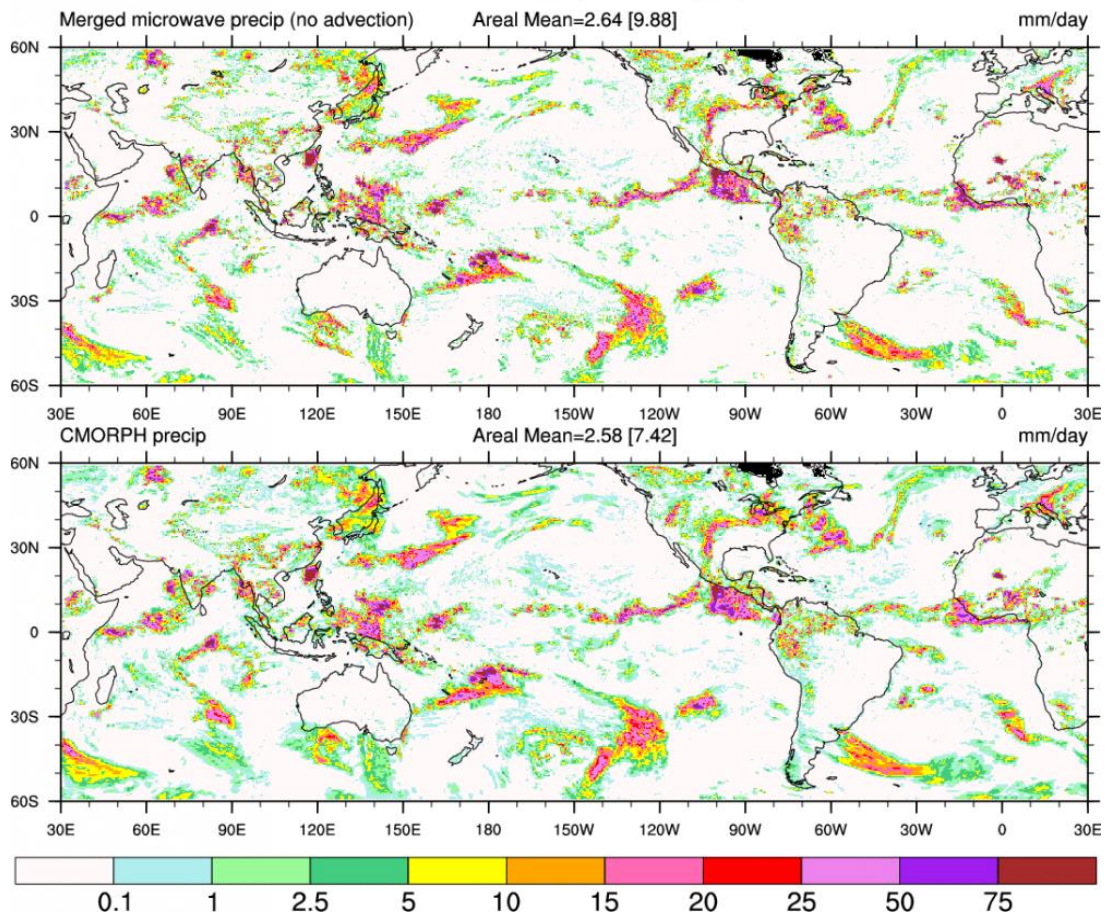
| Parameters | Specification |
|------------------------------|------------------------|
| Frequency | 13.8 GHz |
| Sensitivity | < 0.7 mm/hr |
| Swath width | 220 km (End to End) |
| Observable range | Ground to 15 km height |
| Scanning angle | 17° |
| Horizontal Resolution | 0.25 km |

| | |
|----------------------------|--------|
| Vertical Resolution | 4.3 km |
|----------------------------|--------|

The PR is used to measure three-dimensional precipitation and measure rainfall quantity on earth and ocean. The infrared and visible scanners are used to sense radiation in 5 spectral bands available as the visible and infrared spectrum. The image sensors and lighting system is an optical telescope that is used to acquire in between cloud and cloud to ground lighting propagations. The image sensors and lighting system could also use to correlate the global lighting with precipitation and other storm characteristics. TRMM includes 3B42RT which is a near-real-time product and 3B42 which is post research precipitation product.

CMORPH is another satellite-based precipitation measurement method established by the United States National Oceanic and Atmospheric Administration (NOAA) and operated since 1998 to estimate near-real-time precipitation, which is regularly available after 18 hours of observation time (Gebremichael et al., 2014; Joyce et al., 2004) and globally, CMORPH covers 60° N to 60° S (Fig. 4).

Figure 4

Global Coverage of CMORPH Precipitation Estimation

Global Precipitation Measurement (GPM) Core Observatory has been operated since 2014 to provide real-time rainfall and snowfall. GPM includes thirteen passive radiometric microwaves such as; a microwave imager, combined with Ka (26 to 40 GHz) or Ku-band (12 to 18 GHz) dual-frequency precipitation radar (DPR) that helps as a benchmark to combine and modify estimated precipitation by patterning operational microwave sensors and research data (Prakash et al., 2018).

The Integrated Multi-SatellitE Retrievals for GPM (IMERG) precipitation measures was first introduced at the beginning of 2015 and precipitation is available 0.1°x0.1° spatial resolution and half-hourly temporal resolution. This method includes features from CMORPH, TRMM, and Precipitation Estimation from Remotely Sensed Information using Artificial Neural Networks (PERSIANN) (Hsu et al., 1995). The

IMERG precipitation estimation satellite is usually available in late, early, and final runs, based on the latency of versions and availability. The 03D is the post-research version of the IMERG product that was available since the beginning of 2015 (Yong et al., 2015) and the precipitation measurement inputs of IMERG are obtained from different passive and infrared microwave satellites.

Climate Hazards Group Infrared Precipitation with Stations data (CHIRPS) provides precipitation with monthly temporal resolution and $0.05^{\circ} \times 0.05^{\circ}$ spatial resolution which available with global coverage of 50° north to 50° south since 1981 (Gao et al., 2017). The CHIRPS was introduced by satellite imagery incorporation to measure in-situ precipitation and highly-resolution climatologic parameters. It utilizes cold cloud period Global Precipitation Index analysis of infrared temperature, modified with TRMM precipitation products. CHIRPS have been widely applied to monitor drought and climate change on the global and regional scales.

Precipitation Estimation from Remotely Sensed Information using Artificial Neural Networks-Climate Data Record (PERSIANN-CDR) was another precipitation measurement satellite that was introduced by the University of California, Center for Hydrometeorology and Remote Sensing (Gao et al., 2018). The PERSIANN-CDR could provide daily precipitation data with a spatial resolution of $0.25^{\circ} \times 0.25^{\circ}$ with global coverage of 60° south to 60° north starting from 1983 to the present. The objective of this satellite spacecraft was to provide consistent time series precipitation products that could be used for studying extreme climatic and hydrological events imposed by global or regional climate change such as drought and flooding. To estimate precipitation, the satellite uses complex algorithms based on ANN usually retrieving the information from the thermal brightness temperature.

Global Satellite Mapping of Precipitation Moving Vector with Kalman filter (GSMap-MVK) was developed by Japan Science and Technology Agency (JST) and it was aimed to map the worldwide distribution of precipitation with $0.1^{\circ} \times 0.1^{\circ}$ spatial and hourly temporal resolution (Ma et al., 2018). GSMap utilizes Kalman filters to update precipitation amount subsequently as it propagates each pixel laterally with the atmospheric signal vector.

Multi-Source Weighted Ensemble Precipitation (MSWEP) was designed and launched to provide trustworthy and globally available precipitation that covers 1979 to the present time (Ma et al., 2018). The spatial resolution of MSWEP precipitation measurement is $0.25^{\circ} \times 0.25^{\circ}$ and its temporal resolution is 3 hours. This satellite merges the optimal precipitation data to obtain high-quality precipitation datasets. Bias correction for over or underestimation and orographic effects were applied by assuming catchment mean precipitation multiple in the drainage basins which was distributed globally. The temporal precipitation pattern of MSWEP was specified by weighted average precipitation anomalies of mean gauge and several satellite precipitation measurement methods namely, CMORPH, GSMaP-MVK, and 3B42RT. The most common satellites used for precipitation measurement are summarized and indicated in (Table 2).

Table 2

Summary of Common Satellites Used for Precipitation Measurement

| Satellite precipitation source | Spatial resolution | Temporal resolution | Precipitation availability |
|---------------------------------------|------------------------------------|----------------------------|-----------------------------------|
| CMORPH | $0.25^{\circ} \times 0.25^{\circ}$ | 3-Hourly | 1998- present |
| 3B42RT | $0.25^{\circ} \times 0.25^{\circ}$ | 3-Hourly | 1997-present |
| 3B42 | $0.25^{\circ} \times 0.25^{\circ}$ | 3-Hourly | 1997-present |
| GSMaP-MVK | $0.1^{\circ} \times 0.1^{\circ}$ | Hourly | 2014-present |
| MSWEP | $0.25^{\circ} \times 0.25^{\circ}$ | 3-Hourly | 1979-present |
| (PERSIANN-CDR | $0.25^{\circ} \times 0.25^{\circ}$ | Daily | 1983-present |
| CHIRPS | $0.05^{\circ} \times 0.05^{\circ}$ | Monthly | 1981-present |
| IMERG | $0.1^{\circ} \times 0.1^{\circ}$ | Half-hourly | 2015-present |

Concept of Ensemble Rainfall-Runoff Modeling

Although several rainfall-runoff models were available, none of them were confirmed as the best performing model for all the catchments and under all conditions. The conclusion was drawn by the World Meteorological Organization by

intercomparison of rainfall-runoff studies carried out using diverse models (WMO, 1992). This study suggested that there is no superior single model has been introduced yet for the rainfall-runoff modeling. The performance of a particular model could not be completely perfect in all aspects for all types of input datasets, hence for the same problem, different models could produce different outcomes (Abba et al., 2020). Trusting a single model may cause potential danger to the accuracy of rainfall-runoff model results because a specific model may be unlikely to reproduce accurate results for every watershed in all circumstances. The reason could be, that either the model's structural invalidity or the conditions assumed that the model should be operated are not fulfilled.

In the practical experience of model calibration, the single objective functions could not be good enough to well capture specific entities of inputs and transmit them into the output (Liu et al., 2014). Even the fully distributed physically-based models might successfully depict the spatial features but may not well capture the temporal variations of flow. The combination of several models output via ensemble modeling could help to capture the benefits of each model and enhance the accuracy of the modeling (Sharghi et al., 2018). The principle of ensemble modeling is that each model could capture certain beneficial information about the rainfall-runoff modeling, thus providing important information which may not be similar to the other models. Therefore, assimilating the entire model's output could provide valuable input entities and a source of information about rainfall-runoff modeling. The ensemble modeling may also help to better understand the fundamental physical processes convoluted in every single model thus enabling to development of efficient single models. This could be via the modification of the specific model structure and the assumptions where the model pre-designed.

The ensemble modeling improves the performance of models because it apprehends the useful patterns of each dataset and structural strength of each model and converts them into the unit output pattern. The ensemble techniques are mainly categorized into the linear and non-linear operated by regression-based algorithms. For instance, simple linear average and weighted average ensemble methods (linear), neural

network, Adaptive Boosting (AdaBoost), and Gene expression programming (GEP) ensemble techniques (non-linear) are among the common ensemble methods.

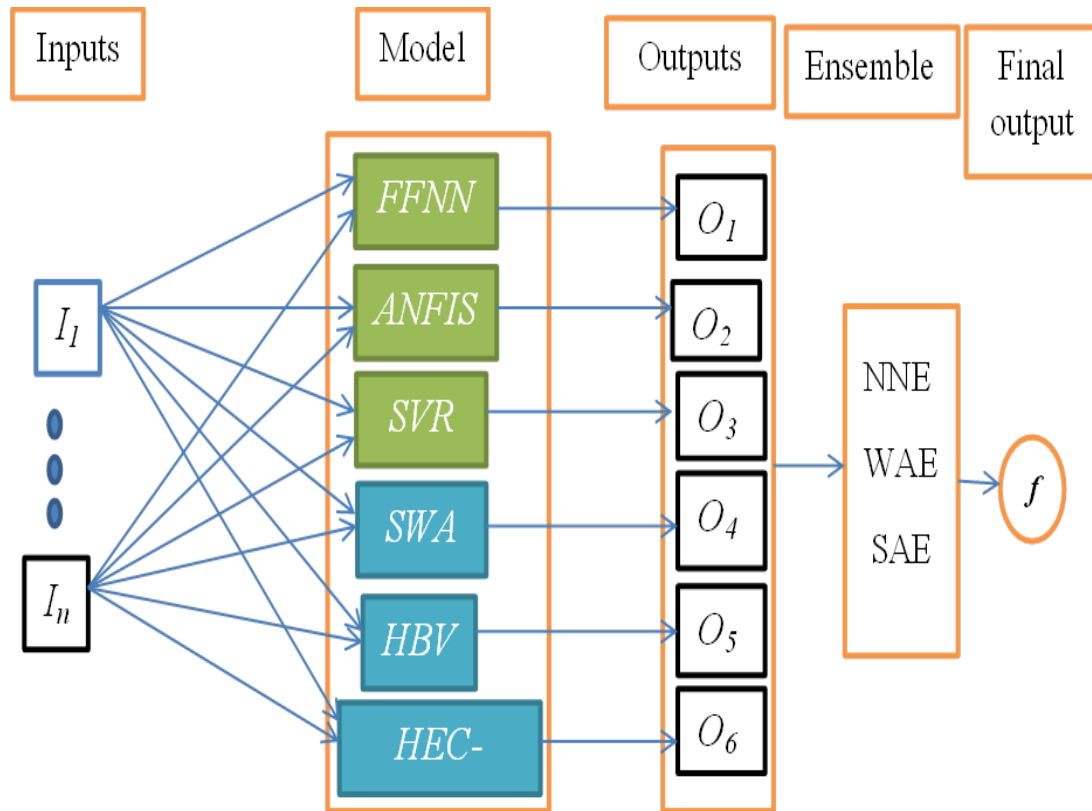
The simple average ensemble (SAE) method directly computes the arithmetic average of the single model's output whereas the weighted average ensemble technique assigns weight for each single model output based on their measure of goodness fit (Nourani et al., 2019). SAE method is the simplest technique that has been applied to combine model outputs of several single models. The SAE method needs only a little effort and no need for any curve fitting for combining the individual model output combination (Makridakis et al., 1982). In this ensemble method, equal weights are allocated for all model outputs during combination. The drawback of this technique is errors from each model involved may linearly propagate into the output.

The weighted average ensemble (WAE) applies weights for each model's output according to their significance, thus it could effectively capture the most important information especially since the accuracy level of the models is highly variable. The WAE is often subjected to multiple co-linearity which may lead to inaccurate determination of the weights for each model and it is considered its drawback (Winkler, 1983).

The neural network-based ensemble technique is a non-linear kernel ensemble method that could map the non-linear relationships of each model concerning the target. The AdaBoost algorithm considers the sample and re-assigns the weight for the determination of the error which is among the best ensemble techniques (Liu et al., 2014). It was basically developed for classification problems but accurately applied for regression problems as well. The ensemble techniques applied in this study are presented in (Fig 5) which combined the outputs of all proposed models.

The study conducted by Nourani, et al., (2021) studied two linear and 2 non-linear ensemble modeling of outputs suspended sediment load from multi-linear regression (MLR), SVM, ANFIS, and FFNN. It is noted that the non-linear ensemble (ANFIS) improved the output of MLR up to 37% and it improved SVM up to 19%.

Figure 5

The Structure of the Developed Ensemble Model

The study by (Bates & Granger, 2016) proved that a combination of several models outputs via ensemble modeling could enhance the performance of modeling. GEP ensemble technique was applied to combine the rainfall-runoff modeling outputs of five hydrological methods namely SWAT, HBV, identification of unit hydrograph components from rainfall, evaporation, and streamflow (IHECRAS), Australian Water Balance Model (AWBM), and SMA (Esmaeili-Gisavandani et al., 2021) and the GEP ensemble significantly improved the modeling accuracy at both calibration and validation phases. Ensemble modeling of reference evapotranspiration by both linear and non-linear ensemble techniques using the outputs of AI-based and empirical models (Nourani, et al., 2019), and the result indicated that ensemble modeling enhanced the accuracy up to 22% for AI-based models and up to 55% for empirical models.

CHAPTER III

Methodology

Description of the Study Area

The Gilgel Abay catchment is positioned in the upper Blue Nile basin, the northern-west part of Ethiopian highlands. The catchment covers an area of 1635km² and is situated at the latitude of 10⁰56' to 11⁰51' N and longitudes of 36⁰44' to 37⁰23'E (Fig.6). It is one of the sub-catchments of Lake Tana basin, which provides more than 60% of the flow to the basin (Wale et al., 2009). Most of the basin is dominated by highland topographic classes, and its elevations range from 1866 m to 3543 m above mean sea level.

The watershed is characterized by plain to gentle slopes ranging from 0% to 43%. The basin is under the influence of a tropical highland monsoon which shows cool and humid climate characteristics with an average yearly temperature of 17 - 22 degrees Celsius. The basin has distinct wet and dry seasons, the major rainfall occurs from early June to mid-September which includes 70-90% yearly rainfall in the basin, while a dry climate prevails from October to May, with an average annual rainfall of 1420mm.

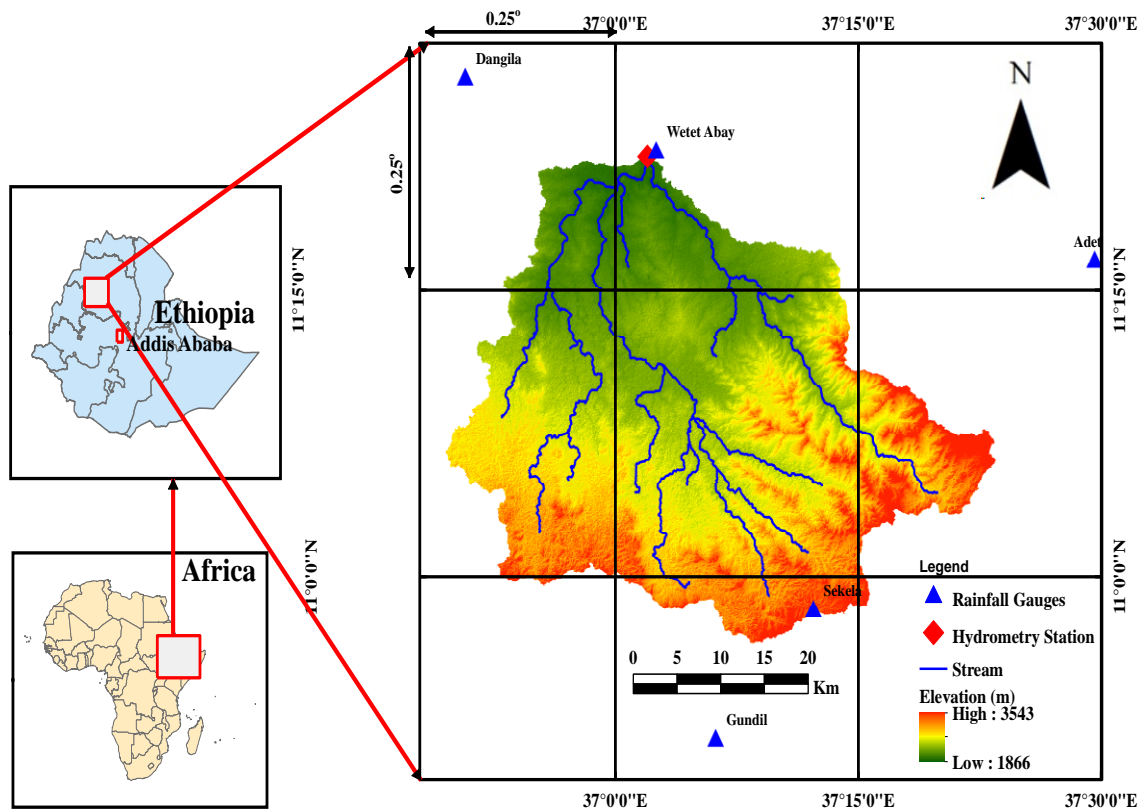
The watershed has a hydrometric station at the outlet of the watershed. Gilgel Abay is the main river flowing along the flow path of a watershed and which raises from the mountains areas of Gojjam. The river has four small tributaries namely, Jamma, Kogar, Ashar, and Kelti that fed it at different locations. Gilgel Abay river is believed as the initiating source of the Nile river. The river is 71m wide near its mouth and its slope gradient is 0.7m/km in length. The river transports 22185 tonnes/year of bedload and 7.6 million tonnes/year of suspended sediments to the lake Tana (Lemma et al., 2019). Besides natural erosion, anthropogenic impacts such as deforestation, intensified land use and associated land degradation resulting in excess sediment transport to the river.

The geology of the basin is predominantly characterized by quaternary basalts. The soil textures of clay, clay loam, and silt loam are evenly distributed in the watershed with 33% each. Haplic luvisols are the main soil type of the watershed and there is a mixed land use with 74% intensive agriculture, 15% grassland, and 11% forests and

woodlands. The economic activities of the area are dominated by mixed rainfed agriculture and animal production usually less productive and destructive agriculture has been practiced which leads to soil erosion and associated delta growth downstream of the river.

Figure 6

The Map of the Gilgel Abay Watershed and Satellite-Rainfall Measurement Grid Lines



Datasets

Several temporal and spatial datasets from multiple sources have been utilized by the proposed models. The daily climatic time series (rainfall, maximum and minimum temperature), and discharge of 12 years (2007-2018) are utilized as inputs for rainfall-runoff simulation. The rainfall datasets are used from both gauge and satellite sources. The fundamental spatial inputs for delineating the watershed into sub-basins and hydrologic response units (HRUs) are a digital elevation model (DEM), land use and

land cover map (LULC), and soils map. The DEM of the Gilgel Abay watershed with a spatial resolution of 12.5mx12.5m was downloaded from the Alaska Satellite Facility Service (<https://search.asf.alaska.edu/#/>). The LULC map for the year 2020 was downloaded from ESA's Sentinel-2 imagery, which is a high-resolution with a 10mx10m grid and includes detailed land use classes.

Gauging-Station Datasets

Daily rainfall and temperatures (maximum and minimum) for Adet, Dangila, Gundel, Sekela, and Wetet Abay stations for the mentioned periods was obtained from the National Meteorological Agency of Ethiopia. Daily discharge time series of the mainstream at the gauging station located at the outlet was collected from the Ministry of Irrigation, Water, and Energy. The datasets series were tested for homogeneity using the double mass curve method. The test indicated that there are no significant discontinuities between the observed data sets, so no homogeneity problems were found.

Satellite Rainfall Datasets

Precipitation data could alternatively be available from special space crafts launched for this purpose. The satellites emit infrared and microwave rays and collect information from the lower atmospheric cloud then the information is received by special devices and translated to meaningful data. In the current study, two TRMM version 7 products (3B42RT and 3B42) and CMORPH satellite precipitation products were used for rainfall-runoff modeling.

The 3B42RT precipitation dataset is available in real-time after 6 hours and covers the earth from 60°N-60°S latitude. The 3B42RT uses the combined precipitation radar and microwave imager datasets to calibrate precipitation data derived from radiometers and microwave sensors in low Earth orbit (Ochoa et al., 2014). The gauge-calibrated 3B42 is the research version after real-time, available two weeks later at the end of each month with global coverage from 50°N-50°S latitude (Li et al., 2018). CMORPH uses infrared ray and passive microwaves information from geostationary and low-orbit radiometric satellites, respectively, at worthy resolution in space and time for the estimation of precipitation.

Precipitation data were estimated by the CMORPH algorithm using passive microwave information from near-orbit infrared information and satellite radiometers from geostationary satellites. CMORPH estimates precipitation from the combination of low-orbit passive microwave satellite scans and infrared information derived from geostationary satellites (Joyce et al., 2004) with high spatial and temporal resolution. Precipitation information obtained from the passive microwaves is transmitted to space via motion vectors obtained from infrared ray satellites (Dinku et al., 2007).

Infrared data are abundant almost everywhere and at all times in the world, but they measure the temperature on top of a cloud, which may not always have a good correlation with precipitation. Cold clouds can sometimes exist in a vast region where there is no rain at all. If only infrared data are used to estimate precipitation, the precipitation estimate may be inaccurate because it captures wide areas of cold clouds that may be non-precipitating. Passive microwave senses the thermal radiation of rain and the scattering of the rising emission from the surface into the atmosphere. However, deploying microwave sensors in geostationary orbit is technically difficult, making it difficult to collect precipitation data in space and time unless they are averaged in time (Joyce et al., 2004). To take advantage of each sensor, precipitation data from the disparate sensor could be combined.

CMORPH estimates precipitation using the information derived from low-orbiting microwave satellites, and this information is mediated by spatial propagation features derived exclusively from geostationary infrared datasets. To transmit precipitation information, the vector matrices were formed by computing spatial delay relationships on consecutive images derived from geostationary infrared sensors and then used to transmit precipitation acquired from passive microwave sensors in the absence of spatially and temporally updated passive microwave data. The infrared information provides transportation services for the microwave obtained precipitation data when microwave data are not available at a particular location. The transmission vector matrices are formed by calculating spatial delay relationships on consecutive images from geostationary infrared satellites, which are then used to transmit the microwave-derived precipitation data. At a given location, the intensity and shape of precipitation detected with passive microwaves can be determined by time-weighted

interpolation between measurements obtained with passive microwaves propagating forward from the last available measurement and backward from the next available microwave measurement. This process could provide complete precipitation information in space and known as morphing techniques. First, the temporal sequences of information motion are derived from the infrared ray satellites, and then they carry out displacement motion to morph from one microwave estimate to the next. The CMORPH precipitation estimation technique obtains precipitation amount from passive microwave information, but infrared radiation information is also used to motivate a cloud motion field that consequently propagates rain forming cloud pixels. The precipitation estimated by CMORPH is a high quality because the microwave-scanned precipitation information is morphed and interpolated by linear time-weighted techniques. This method of measuring precipitation by satellite is more flexible because any precipitation estimated by any microwave-based sensor can be included. The satellite rainfall datasets applied in this study are available on the daily time scale and with a spatial resolution of $0.25^{\circ} \times 0.25^{\circ}$. The entire watershed is represented by 8 satellite precipitation grids (Fig. 6). The three satellite precipitation products were selected because they have shown good performance in previous studies (Bitew et al., 2012; Nourani et al., 2013) for the Gilgel Abay and the datasets are available at a daily temporal resolution that is an appropriate time scale for selected models. The statistical details of both gauge and satellite rainfall and streamflow data sets were given in (Table 3).

Table 3

Statistics of Gauge and Satellite Rainfall and Discharge at the Catchment

| Rainfall (mm/day) | | | | |
|--------------------------|---------|---------|------|--------------------|
| Stations | Maximum | Minimum | Mean | Standard deviation |
| Adet | 71.2 | 0 | 3.50 | 7.29 |
| Dangila | 62 | 0 | 4.42 | 8.61 |
| Gundil | 90.8 | 0 | 6.74 | 11.81 |
| Sekela | 73.1 | 0 | 6.05 | 9.92 |

| | | | | |
|-------------------------------------------------------|---------|------|------|-------|
| Wetet Abay | 71 | 0 | 5.32 | 9.89 |
| 3B42 | 49.32 | 0 | 3.54 | 6.12 |
| 3B42RT | 55.10 | 0 | 3.73 | 6.60 |
| CMORPH | 71.5 | 0 | 5.82 | 9.40 |
| Discharge at gauging station (m³/s) | 406.846 | 4.71 | 58.4 | 61.01 |

Methodology

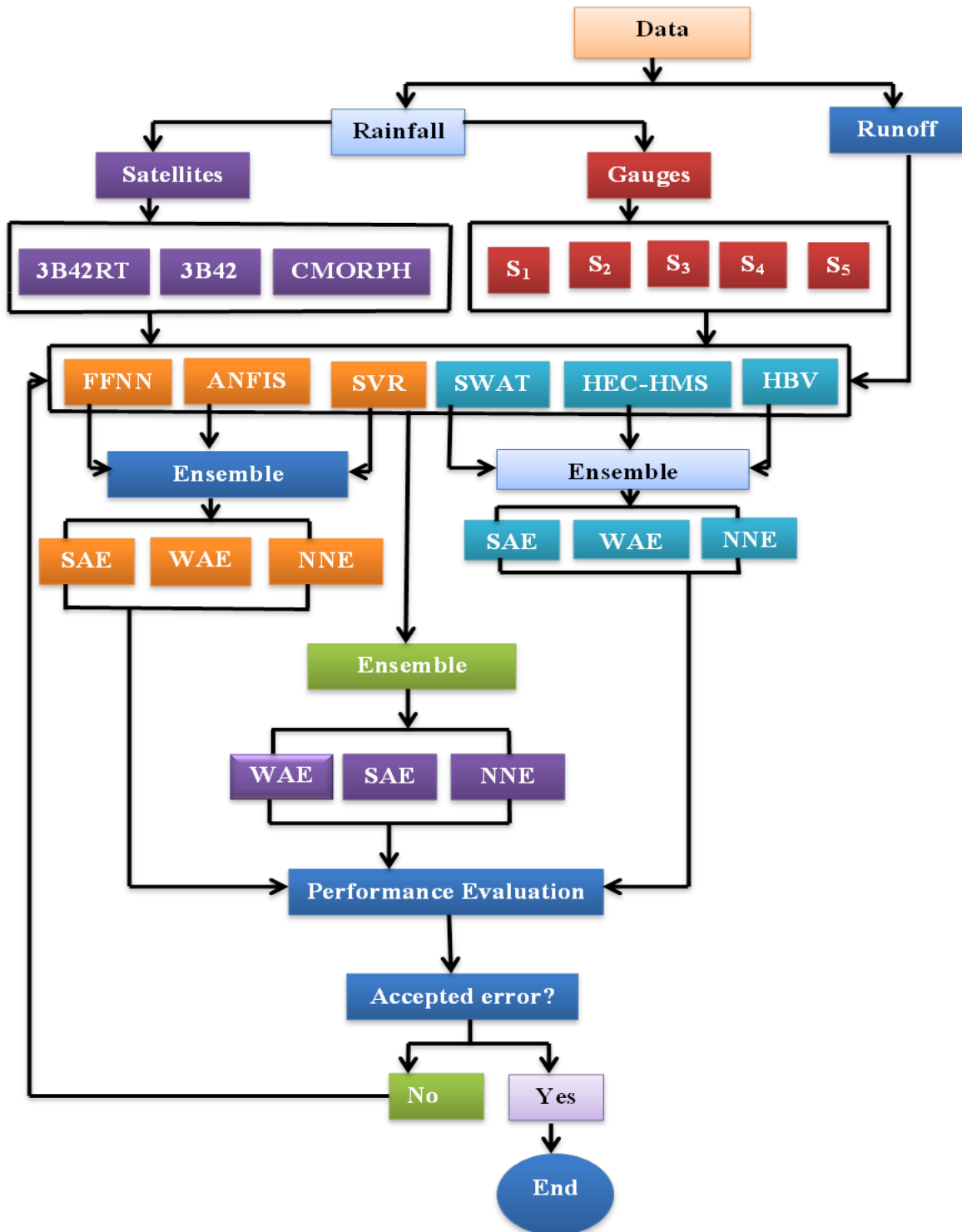
In the current study, 3 AI-based (FFNN, ANFIS, and SVR) and 3 semi-distributed (SWAT, HEC-HMS, and HBV) models were used to model rainfall-runoff for the Gilgel Abay catchment. The study has been carried out in 2 stages as presented in (Fig. 5). In the first stage, all the proposed models individually simulate the rainfall-runoff process using gauge-based and satellite-based rainfall data separately and the fusion of them as well. In the second step, the results of each model were used as input to the ensemble modeling methods via Weighted Average (WAE), Simple Average (SAE) and Neural Network (NNE) see (Fig 7) in three ensemble scenarios. Stage one modeling has comprised two sub-stages.

First, each proposed model simulated runoff for both gauge and satellite rainfall datasets separately. Second, the fusion of rainfall from both gauge and satellite data sources was used to simulate runoff by each model.

The three ensemble scenarios applied are i) ensemble of AI-based models, ii) ensemble of physically-based models, and iii) ensemble of all models output from the input fusion phase via SAE, WAE, and NNE techniques.

Figure 7

Schematic Diagram of Planned Methodology (S1, S2, S3, S4, and S5 Represent the Five Gauging Stations)



Proposed Rainfall-Runoff Models

In this study, semi-distributed (SWAT, HBV, and HEC-HMS) and AI-based (ANFIS, FFNN, and SVR) models were proposed for rainfall-runoff modeling processes. All the proposed models are well described in the following sections.

The SWAT Model

SWAT is the semi-distributed and physically-based hydrologic model that operates in sub-daily, daily time, and monthly steps to model runoff, sediment transport, and nutrient cycling in complex watersheds (Arnold et al., 1998). SWAT is process-based and effective in computation, and capable of simulating time series data. The SWAT splits the basin into smaller sub-watersheds that are more divided into several hydrological units (HRUs) where each of them is featured by distinctive soil, land use, and slope characteristics (Leong & Yang, 2020). Rainfall-runoff processes in SWAT can be executed in two distinct steps. First, all existing hydrologic and meteorological inputs are used to simulate runoff in each sub-basin. The second step is the routing step, where the outflows from every sub-basin are connected to the major channel and the cumulative runoff flows to the final basin outlet (Busico et al., 2020). The SWAT modeling process is performed in the soil upper portion, intermediate zone, light and deep groundwater table, and surface channels. SWAT uses the water balance equation for rainfall-runoff simulation as follows;

$$SW_f = SW + \sum_{i=1}^t [R_{day} - (Q_{surface} + ET + W + Q_{ground})] \quad (1)$$

where SW_f is final soil moisture availability in a day (mm), SW is the initial soil moisture content in a day (mm), t is time (days), R_{day} is daily precipitation (mm), $Q_{surface}$ is daily surface runoff (mm), ET is the combination of daily evaporation and transpiration (mm), W is daily percolation (mm), Q_{ground} is daily groundwater discharge (mm).

The surface runoff in SWAT could be reproduced by using Soil Conservation Service (SCS) run-off curve number (CN) method (Welde & Gebremariam, 2017) or Green and Ampt's infiltration procedure (Gassman et al., 2007; Sardoii et al., 2012).

$$Q_{surface} = \frac{(R_{day} - 0.2S)^2}{R_{day} + 0.8S}, R_{day} > 0.2S, Q_{surface} = 0$$

$$R_{day} < 0.2S, S = 25.4 \left(\frac{100}{CN} - 10 \right) \quad (2)$$

where $Q_{surface}$ is surface flow per day; R_{day} is rainfall per day in (mm); S is retention storage (mm) and CN is curve number.

The stream base flow is computed as:

$$Q_{gw,i} = Q_{gw,i} \times \exp[-\alpha_{gw}\Delta t] + W_{rchrq} \times (1 - \exp[-\alpha_{gw} \times \Delta t])$$

$$\text{if, } aq_{sh} > aq_{shthr,q}, Q_{gw,i} = 0, aq_{sh} \leq aq_{shthr,q} \quad (3)$$

where $Q_{gw,i}$ is a base flow contribution to the major stream on the day i (mm); $Q_{gw,i-1}$ is the groundwater discharge into the major stream on the day $i-1$ (mm); α_{gw} is the base flow recession constant; Δt is the time (1 day); $wrchrq$, is the quantity of recharge inflowing the shallow soil profile on the day i (mm); aq_{sh} is the quantity of water deposited in the shallow soil profile at the start of day i (mm); and $aq_{shthr,q}$ is the threshold water level in the shallow aquifer for groundwater input to the major stream bed to occur (mm).

Six major land use and cover types were identified and analyzed by SWAT for the Gilgel Abay catchment (see Fig. 8) and the proportion of each particular land use land cover type was presented in (Table 4). Agricultural land use was dominating in the study area since the people living in the basin rely on rainfed agriculture for the production of cereal crops, cash crops, and vegetables.

The major soil types identified in the study area are Haplic Luvisols, Haplic Alisols, Haplic Nitisols, Utric Regosols, and Utric Vertisols (see Table 4 and Fig. 8). The catchment is predominantly covered by Haplic Luvisols which is the family of Luvisols and extremely weathered soil, characterized by high accumulation of clay at subsurface and lower nutrient retention, crusting on the surface, and exposed to high erosion hazards.

Figure 8

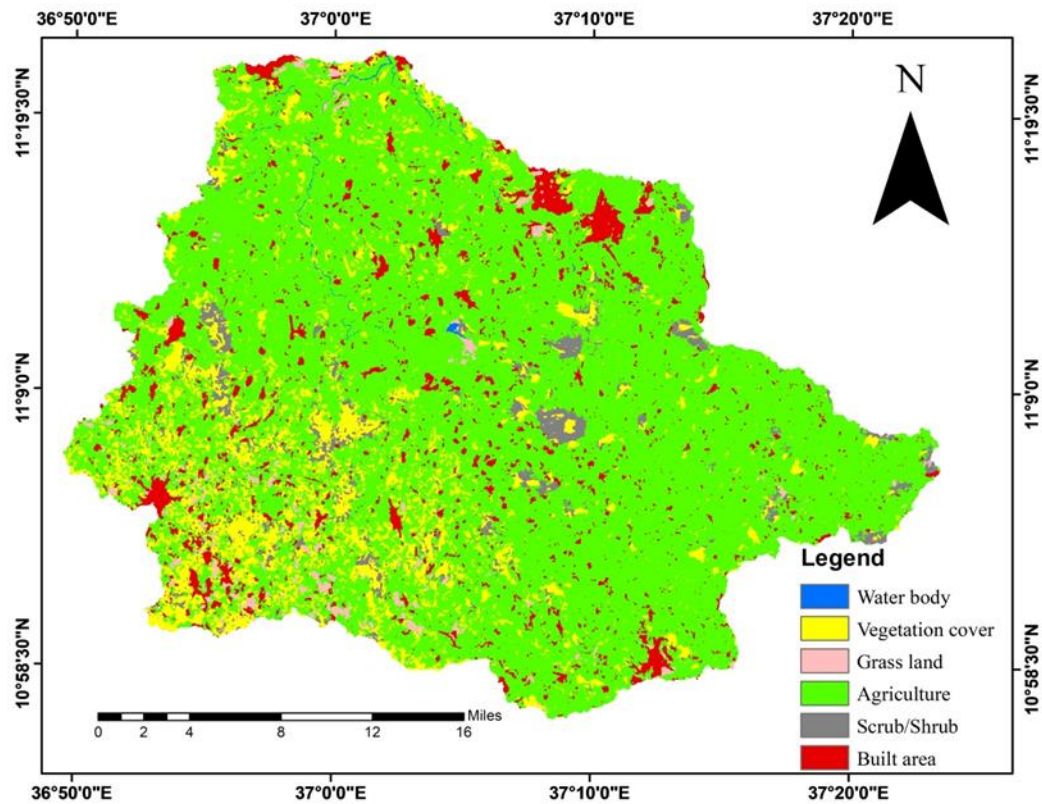
Land Use Land Cover Details of the Study Area

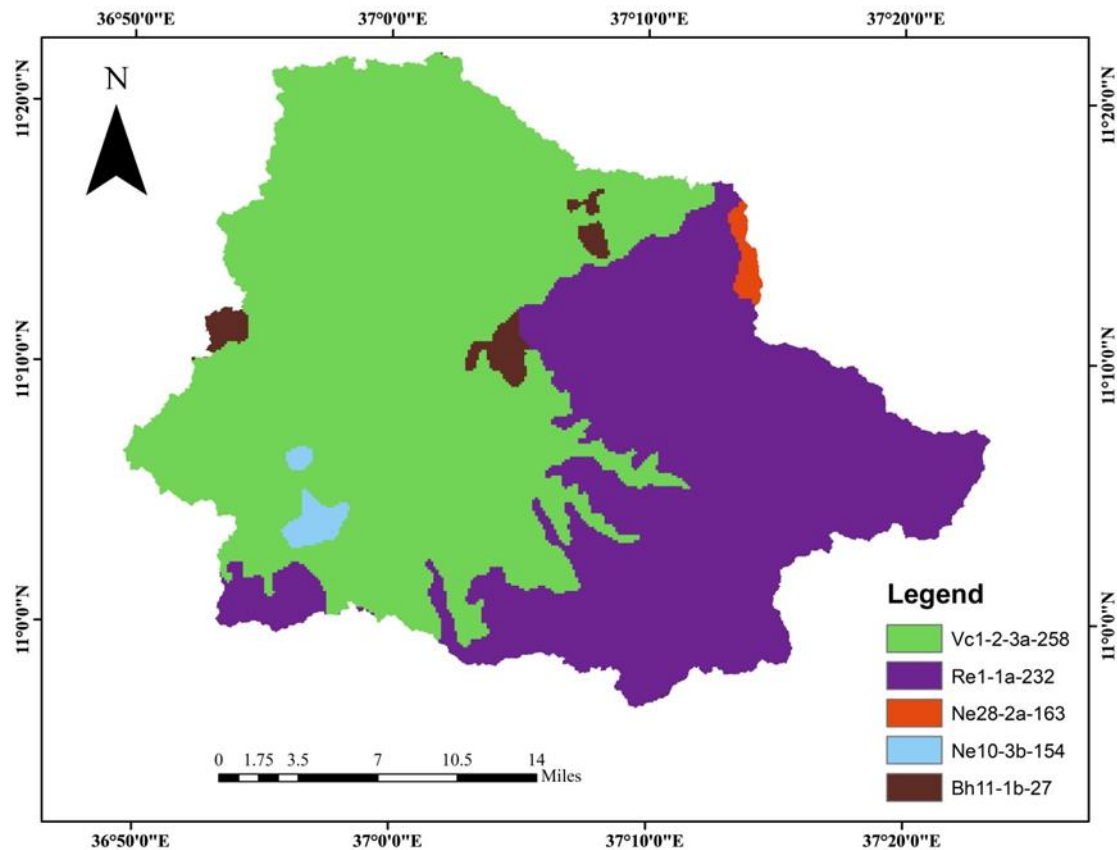
Table 4

Land Use Land Cover, Soil Types and their Proportions in the Study Area

| Parameters | Name | FAO code | Proportion (%) |
|----------------------------|------------------|--------------|----------------|
| Soil | Haplic Luvisols | Vc1-2-3a-258 | 57.2 |
| | Haplic Alisols | Re1-1a-232 | 40.25 |
| | Haplic Nitisols | Ne28-2a-163 | 0.68 |
| | Utric Regosols | Ne10-3b-154 | 0.71 |
| | Utric Vertisols | Bh11-1b-27 | 1.16 |
| Land use/land cover | Waterbody | Wa | 0.66 |
| | Vegetation cover | VcL | 5 |
| | Grass Land | GL | 2.8 |

| | | |
|-------------|------|-------|
| Agriculture | AGRL | 86.64 |
| Scrub/Shrub | SL | 1.75 |
| Built area | UrL | 3.15 |

Figure 9

The Soil Types of Gilgel Abay Catchment

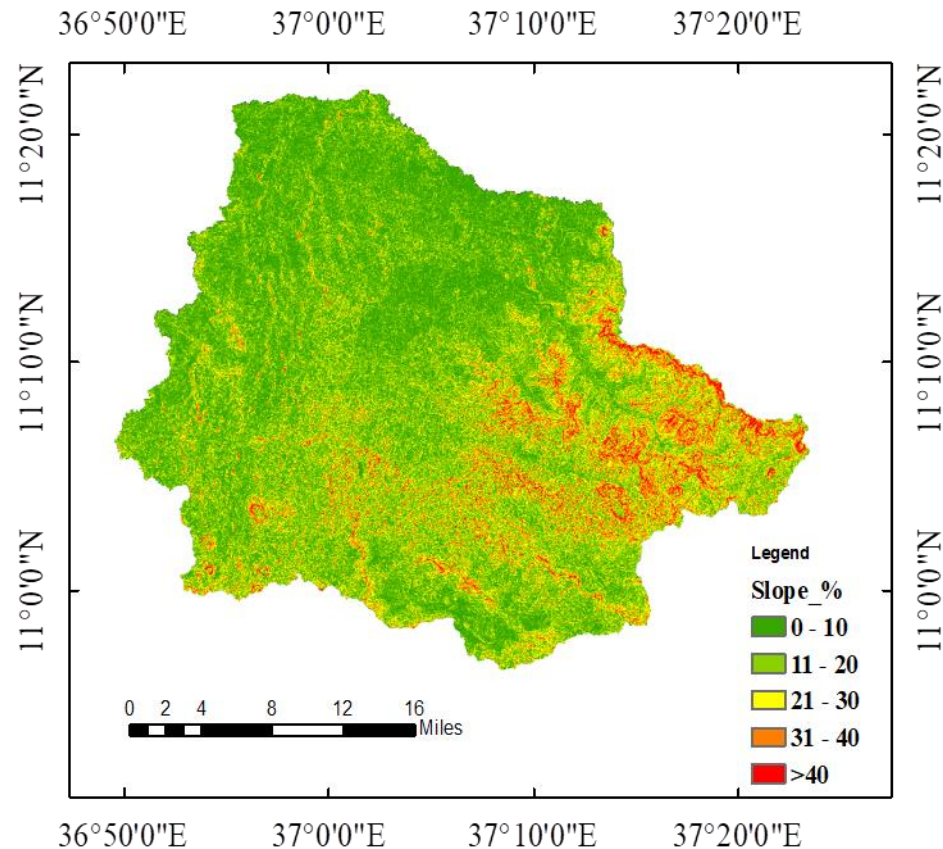
In the current study, the SCS-CN has been applied to reproduce runoff simulation. The land use land cover and soil grids (Figs. 8 and 9) were layered to develop a rainfall-runoff model for the catchment.

In setting up the SWAT model, the watershed was first delineated from the DEM (Fig 11), then land use, soil, and slope maps were layered together (Figs. 8, 9, and 10) and HRUs were created (Fig 12), which are sub-basins portion that provides details about soil properties, slope, and land use. HRUs is the smallest basic spatial unit which is a unique composition of the soil, land use land cover, and slope information for the

particular catchment having similar hydrological properties. The HRUs lump together soil, land use land cover, and slope similar characteristics into a unit feature. After loading soil, land use land cover, and slope maps, the HRUs layer was successfully defined and ready for rainfall-runoff modeling.

Figure 10

The Slope Classification of Gilgel Abay Catchment



After creating the HRUs, SWAT input tables were written, basically loading the weather data for each station one by one, specifying methods to calculate evapotranspiration, and the SWAT database was updated. Once the weather data was loaded, the SWAT watershed data was updated and finally, the SWAT model was run for the basin and the rainfall-runoff simulation was performed for the catchment.

Figure 11

Watershed Delineated by the SWAT Model for the Study Area

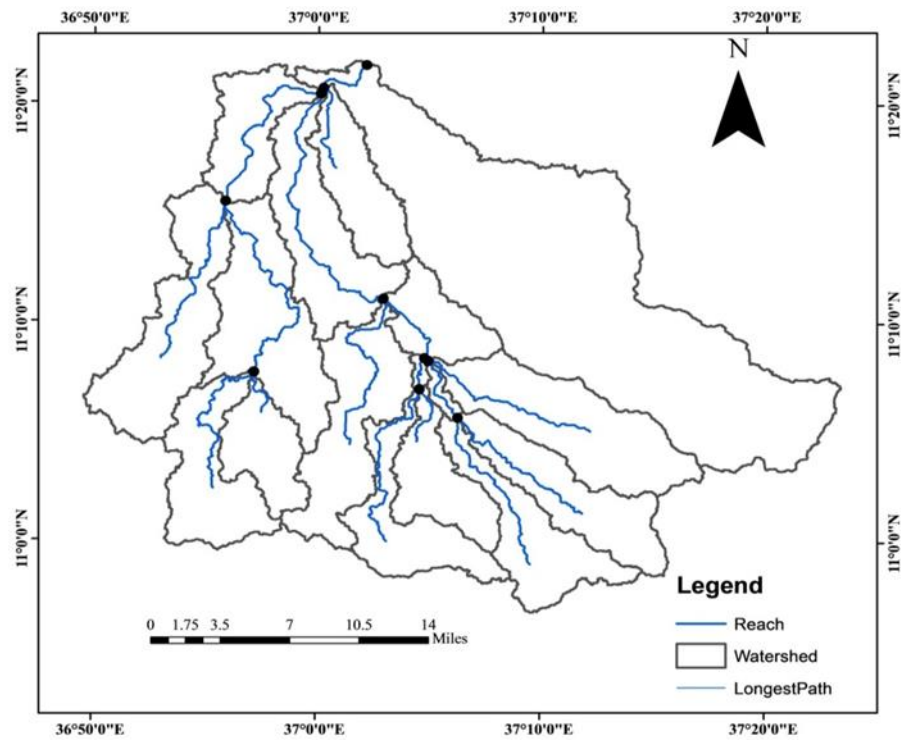
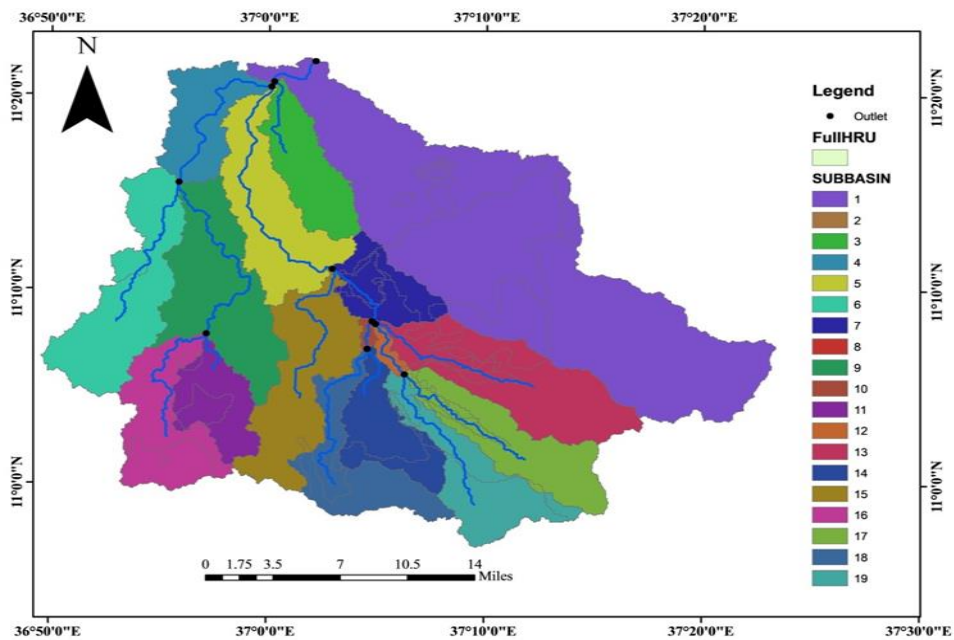


Figure 12

The Complete HRUs Created by SWAT for Gilgel Abay

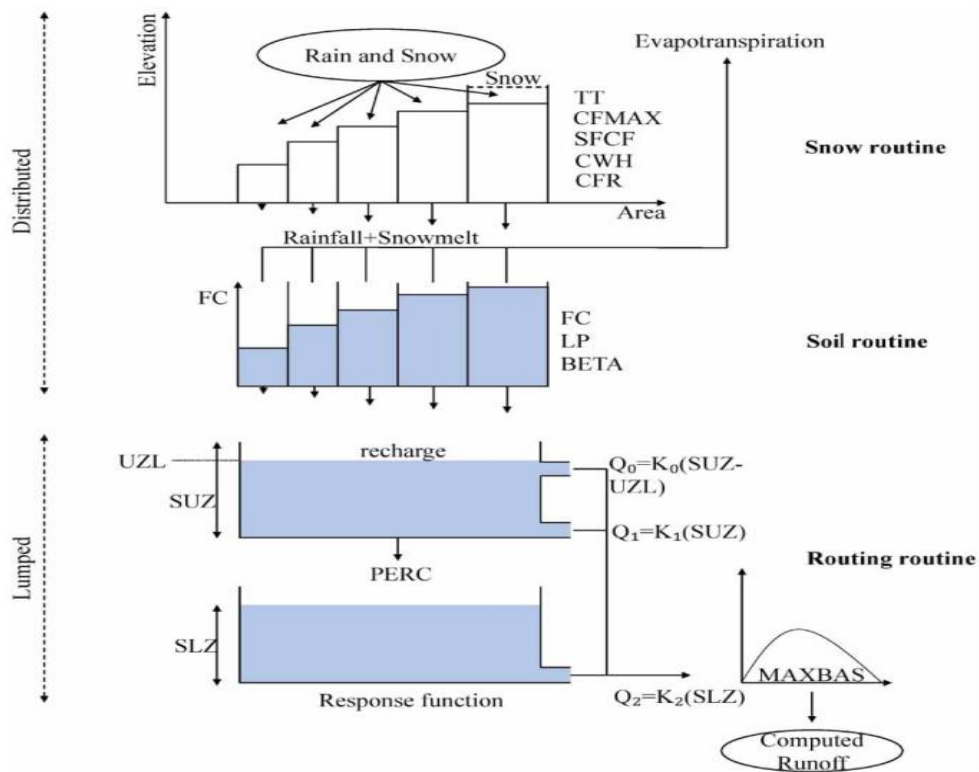


The HBV Model

HBV is a conceptual and semi-distributed hydrological model for runoff simulations, flood planning, and climate change predictions (Lindström et al., 1997) that was developed by the Swedish Meteorological and Hydrological Institute (SMHI). The version of the HBV applied for runoff simulation in the current study is HBV light which updated groundwater contribution and delay factors. HBV simulates daily runoff using daily rainfall, evapotranspiration, temperature, vegetation, and elevation zones. The HBV rainfall-runoff modeling procedures consist of various hydrological routines representing snow, soil moisture, response, and routing (see Fig. 13).

Figure 13

Schematic View of HBV Model (Al-Safi & Sarukkalige, 2019)



The runoff components are computed by three linear reservoir equations namely, Q_0 (direct runoff component), Q_1 (intermediate runoff component), and Q_2 (base runoff component) using recession coefficients K_0 , K_1 , and K_2 , respectively. The soil moisture subroutine is based on the parameters Beta (β) (shape coefficient for non-linear storage

properties of the soil zone), maximum soil storage (FC), and limit of potential evaporation (LP). Beta controls the influence of precipitation on the response function. MAXBAS (length of weighing function) is used as a transformation function to compute outflow from the catchment.

The snow routine represents snowmelt processes and their contribution to streamflow and is not appraised in this study because snow is not available in the catchment area. The variations in soil moisture (SM) and groundwater contribution are measured by soil moisture routine based on the quantity of flow approaching from preceding routine (P) and FC represented by Eq. 4.

$$\frac{recharge}{P_t} = \left[\frac{SM_t}{FC} \right]^\beta \quad (4)$$

If the ratio of SM to FC is greater than LP, the actual soil evaporation is similar to potential evaporation, or else the actual evaporation could be linearly minimized as:

$$ET_{act} = E_{pot} \times \min\left(\frac{SM_t}{FC \times LP}, 1\right) \quad (5)$$

The groundwater outflow is represented as a summation of two or three outflows based on upper zone storing (SUZ) that is located above or below the threshold zone (UZL):

$$Q_{gw}(t) = K_2 \times SLZ + K_1 \times SUZ + K_0 \times \max(SUZ - UZL, 0) \quad (6)$$

The runoff is simulated using the MAXBAS parameter and triangular weighting function as:

$$Q_{sim}(t) = \sum_{i=1}^{MAXBAS} C(i) \times Q_{gw}(t-i+1) \quad (7)$$

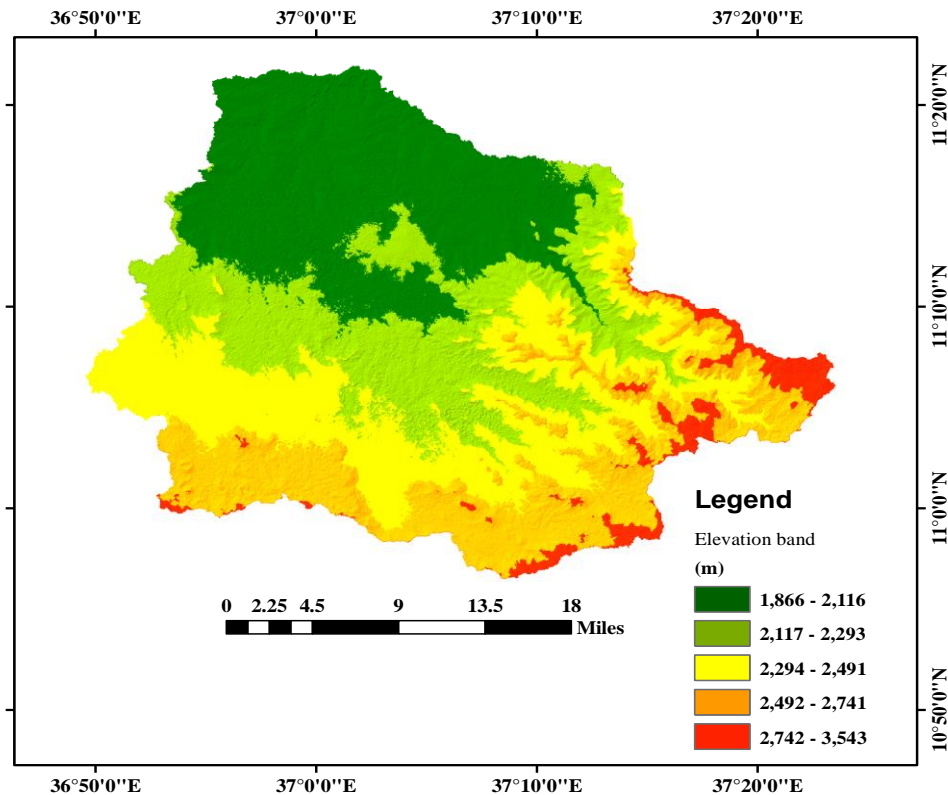
$$C(i) = \int_{i-1}^i \frac{2}{MAXBAS} - \left| U - \frac{MAXBAS}{2} \right| \times \frac{4}{MAXBAS^2} dU \quad (8)$$

Elevation zones of the area were analyzed using a (10mx10m) DEM downloaded from (<https://sentinels.copernicus.eu/web/sentinel/missions/sentinel-1>) SENTINEL1 database

for free. The area was divided into 5 elevation zones at appropriate intervals (Fig. 14). The vegetation classes of the area have been re-classified into 3 majors namely, Grassland, Mixed Agriculture, and Forest classes from the land use raster.

Figure 14

Elevation Bands of the Watershed



The HEC-HMS Model

HEC-HMS is a semi-distributed, physically-based conceptual hydrological model that was developed by the US Army Corps of Engineers to simulate runoff from dendritic watersheds (Feldman, 2000). The model has been updated every time and different versions are available, therefore, the extended HEC-HMS version 4.7 was used in this study. HEC-HMS could effectively undertake four hydrological processes such as; loss, transform, base flow, and routing models. The model determines effective rainfall in the watershed by characterizing antecedent soil moisture situations (Young et al., 2017) as presented in Eq. 9. In this study, the SCS-CN loss technique was chosen to

define direct runoff, because it was extensively applied in several watersheds and revealed better outcomes as compared with initial and constant loss methods (Sardoii et al., 2012).

$$P_e = \frac{(P - I_a)^2}{P - I_a + S} \quad (9)$$

where P_e and P are the precipitation excess and accumulated rainfall depth at time t , respectively, I_a is the initial abstraction (e.g., infiltration loss), and S is the potential maximum retention. S (mm) and I_a can be determined by the SCS method based on CN as:

$$S = \frac{25400}{CN} - 254 \quad (10)$$

$$I_a = 0.2S \quad (11)$$

Soil CN ranges from 1 to 100 and it is a function of land use, land cover, and soil hydrological group. For this study, CN was determined from the global hydrologic soil group and soil class texture grid using the ArcGIS zonal statistics tool. The peak flow (Q) is computed using Eq. (12) as:

$$Q = \frac{(P - 0.2S)^2}{(P - I_a + S)} \quad (12)$$

HEC-HMS has numerous transform approaches to covert rainfall into runoff. In this study, the SCS unit hydrograph with standard graphs has been used as a transform method because it is simple and requires only lag time as an input parameter. The SCS method developed the relationship between time of concentration and lag from watershed features such as reach length and slope (see Eqs. 13 and 14).

$$T_c = \frac{l^{0.8} (S + 1)^{0.7}}{1140Y^{0.5}} \quad (13)$$

$$T_{lag} = 0.6T_c \quad (14)$$

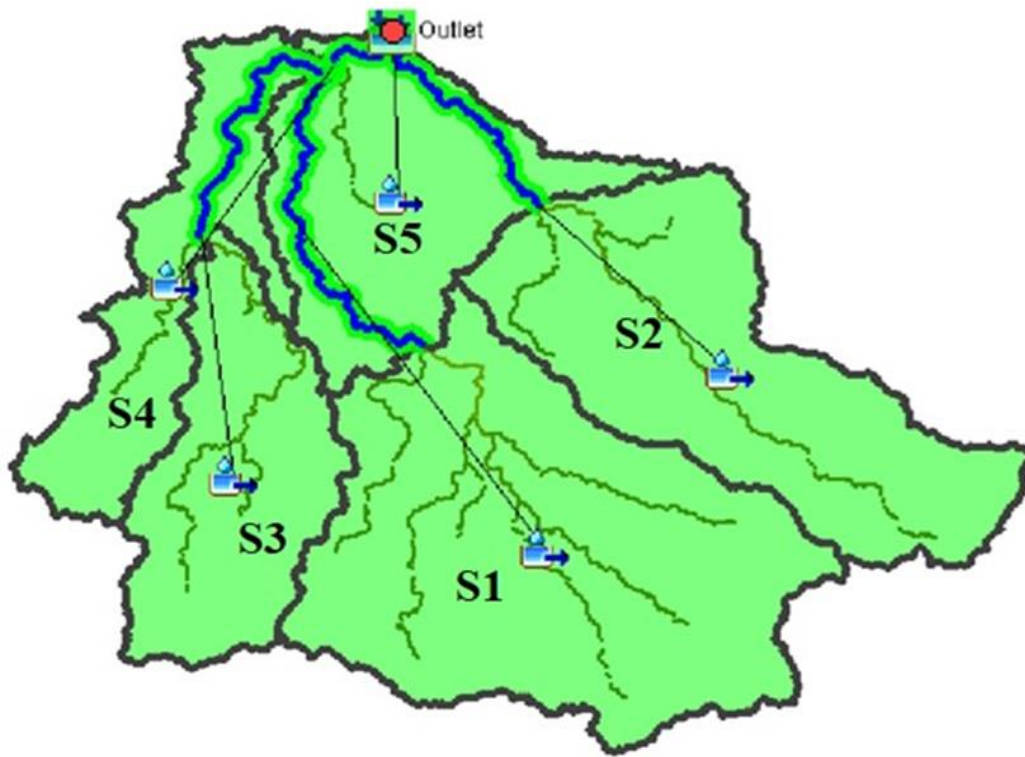
where T_c is the time of concentration (hours), T_{lag} is lag time (hours) l is flow length (feet), Y is the average watershed slope (%).

The developed HEC-HMS basin model was presented in (Fig. 15) and runoff was simulated at the outlet point. In the current study, base-flow recession and Muskingum methods were used for base flow and routing models respectively as the methods are most often applied and are more effective methods (Seong et al., 2008). The Muskingum method is a simple and lumped flow routing technique that could compute outflow hydrograph at sink point (Bitew et al., 2019). In this routing method, the propagation time (K) of the flood wave through reach and dimensionless weight (X) corresponding to the reduction of the flood wave is required (Eq. 15).

$$S = [XI + (1 - X)Q] \quad (15)$$

Figure 15

The Catchment Model Developed by HEC-HMS (S_n Represents n Sub-Basins of the Catchment).



The watershed characteristics of the study area that provide the information for simulation of rainfall-runoff by HEC-HMS were analyzed (see Table 5). Accordingly, the longest sub-basin was sub-basin 1 which took more than 4 hours for runoff to arrive at the outlet point.

Table 5

Physiographic Features of the Watershed

| Sub-basin | Area (km ²) | Slope (%) | CN | Lag (hr) |
|------------------|-------------------------|-----------|-------|----------|
| Sub-basin 1 (S1) | 561.34 | 22.5 | 85.2 | 4.43 |
| Sub-basin 2 (S2) | 386.12 | 15.18 | 83.87 | 3.12 |
| Sub-basin 3 (S3) | 233.58 | 14.45 | 84.26 | 2.71 |
| Sub-basin 4 (S4) | 188.97 | 19.51 | 83.75 | 2.42 |
| Sub-basin 5 (S5) | 268.24 | 17.33 | 84.57 | 1.92 |

The ANFIS Model

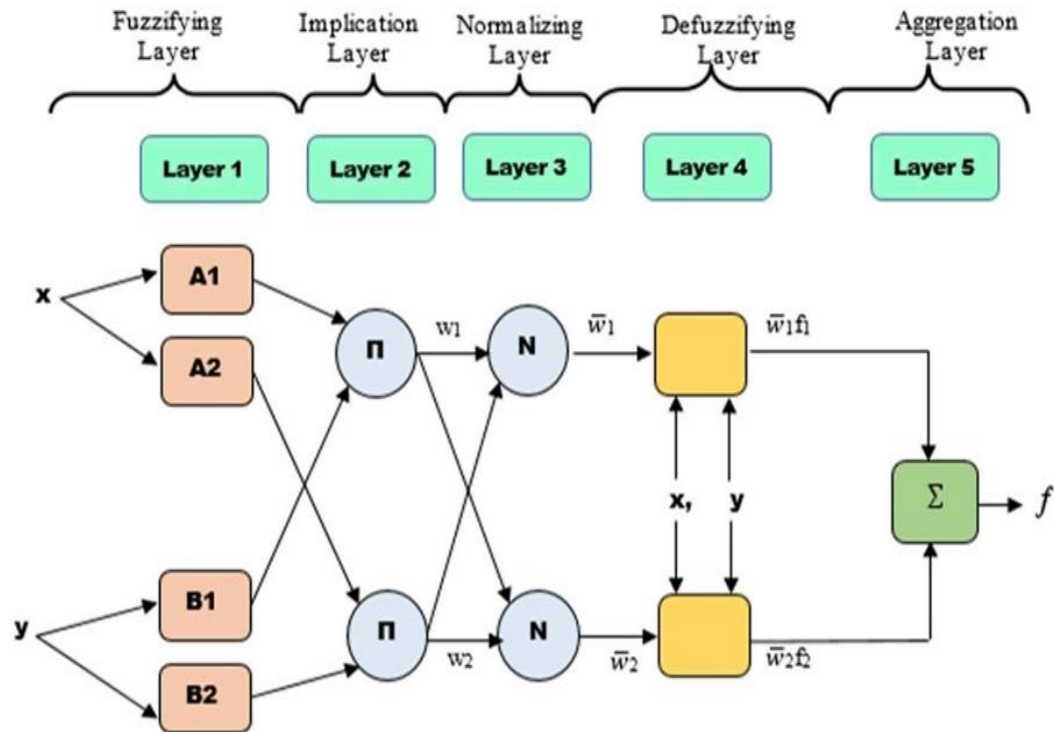
Fuzzy Logic (FL) explains commutative approaches to thinking and improves the deciding capability of humans via enhanced reasoning (Chandwani et al., 2015). ANFIS is the combination of ANN and FL that provides an acceptable solution and it was presented first by (Jang, 1993). Unlike classic models, in FL the values of the parameters, are defined linguistically and then linked by if-then rules, and the results of the fuzzy subset outputs are defuzzified to the crisp numbers.

The ANFIS hybrid model represents a rational system that synergistically combines FL and ANNs by adjoining human intellectual abilities with neural networks and FL (Hock, et al., 2010) to circumvent of their drawbacks. The ANFIS model consists of Back-propagation Least Square and Gradient Descent algorithms formed by a hybrid training approach and it can regulate the structures of fuzzy membership functions by iteration tuning. The major reason for ANFIS training is to control the outcome variables and optimal premises by training the Fuzzy Inference System (FIS) with ANFIS to modify the membership functions and match them with the training datasets based on the particular error criterion. The ANFIS structure contains five layers,

namely, the product layer, fuzzy layer, normalized layer, an output layer, and defuzzifying layer similar to the multilayer FFNN and is named after its mode of functional operation (Fig. 16).

Figure 16

Schematic View of First-Order Sugeno FIS and ANFIS Structure (Jang, 1993)



Calibration of ANFIS requires the specification of fuzzy language rules as contrasting to neural networks that tune weights. Calibration of ANFIS membership functions is carried out by backpropagation and/or least mean square. However the conventional least square method is used for calibration of Takagi Sugeno fuzzy model. Taking account of FIS with x , y inputs and f output the first-order Sugeno fuzzy model applied in the current study has optimal sets of rules, which are stated by if-then:

$$\text{Rule - 1: If } \mu(x) = A_1 \text{ and } \mu(y) = B_1, \text{ then } f_1 = p_1x + q_1y + r_1 \quad (16)$$

$$\text{Rule - 2: If } \mu(x) = A_2 \text{ and } \mu(y) = B_2, \text{ then } f_2 = p_2x + q_2y + r_2 \quad (17)$$

where A_1 and A_2 are x-input membership functions, B_1 and B_2 are y-input membership functions and the output function factors are p_1, q_1, r_1 and p_2, q_2 and r_2 and five-layer ANFIS structure with Q_i^1 is input and x or y membership ranks are designated as:

Layer 1: Every node i is an adaptive node in this layer with a node function of:

$$Q_i^1 = \mu_{A_i}(x) \text{ for } i = 1, 2 \text{ or } Q_i^1 = \mu_{B_i}(y) \text{ for } i = 3, 4 \quad (18)$$

Layer 2: T-norm operator linking every rule in this layer between inputs ‘AND’ operator as:

$$Q_i^2 = w_i = \mu_{A_i}(x) \cdot \mu_{B_i}(y) \text{ for } i = 1, 2 \quad (19)$$

Layer 3: “Normalized firing strength” is the output in this layer

$$Q_i^3 = \bar{w} = \frac{w_i}{w_1 + w_2}, i = 1, 2 \quad (20)$$

\bar{w} is the output of layer 3

Layer 4: Every node i in this layer is an adaptive node and realizes the outcomes of the rules as:

$$Q_i^4 = \bar{w}(p_i x + q_i y + r_i) = \bar{w} f_i \quad (21)$$

Layer 5: In this layer, the overall output of all incoming signals is calculated:

$$Q_i^5 = \bar{w}(p_i x + q_i y + r_i) = \sum w_i f_i = \frac{\sum w_i f_i}{\sum w_i} \quad (22)$$

The ANN Model

ANN is an AI-based 'black-box' model that includes multiple non-linear artificial neurons that are run laterally and can be trained as a particular or several layers. ANN is a modeling tool that interconnects neurons one with another to form complex non-linear input-output interfaces. It is explicitly defined by network architecture, training and verification algorithms, and activation functions (Tongal & Booi, 2018). The greatest merit of ANN is that it does not require complicated physical routes, and the modeling routes are designated by systematic calculations (Ramana et al., 2013).

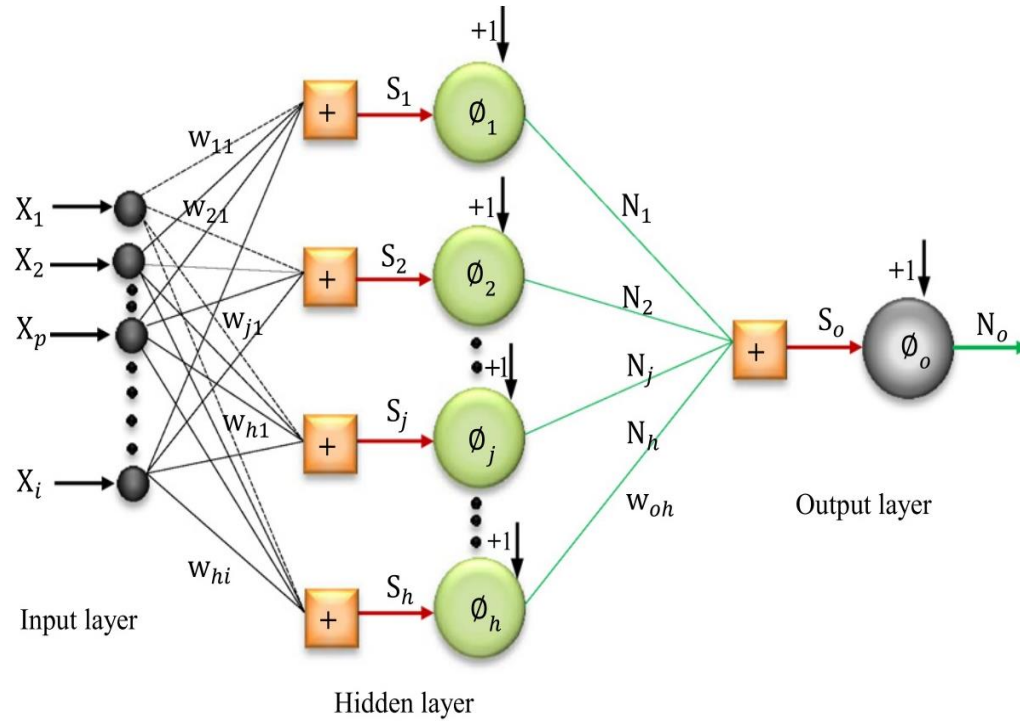
ANN provides a very effective approach to dealing with noisy, non-linear, and non-stationary data, especially in cases where the data do not conform to basic physical relationships, making ANN an appropriate model for time series prediction. The most common ANN structure in rainfall-runoff modeling is the multi-layer perceptron (MLP), which is trained with the back-propagation algorithm (BP) and comprises layers of input, and output. Among the most widely used algorithms, the Brodyen-Flecher-Goldfarb-Shanno and Levenberg-Marquardt (LM) are the popular and most effective approaches due to their fast convergence. The FFNN model calibrated with the BP algorithm is the widely used ANN structure for predicting hydrologic simulations and is also used in this study. The FFNN topology contains inputs, hidden and output layers, as well as activation functions and weights (Fig. 17). The inputs are converted into outputs using Eq. 23.

$$y_1 = f_1 \left[\sum_{K=1}^K w_{1k} f_2 \left(\sum_{J=1}^J w_{kjxj} + b_k \right) + b_l \right] \quad (23)$$

$$f_2(p) = \frac{2}{1 + e^{-2p}} - 1 \quad (24)$$

where W_{kj} is weight that connects input and output layers, W_{lk} represents the connection weight among the hidden and output neuron, b_k and b_l represents the bias of the corresponding hidden and output layer neurons, $f_1(.)$ is symbolizes the linear activation function and $f_2(.)$ designates the sigmoidal activation function of the network.

Figure 17

A Distinctive Topology of Three-Layered FFNN**The SVR Model**

SVR has been developed based on the idea of a Support Vector Machine (SVM), that has been applied for non-linear regression and grouping of the problems (Nourani et al., 2020). SVR is the AI-based model of a supervised learning method with 2 layered structures, unlike the other black-box forecasting models; it minimizes operational risk as an objective function other than decreasing the inaccuracy between the observed and simulated variables. The weights in the first layer of the SVR are non-linear, while in the second layer they are linear. Initially, the model creates a linear regression between input and target variables then the outputs are set to non-linear kernels to smooth the non-linear behavior of the input data sets (Wang et al., 2013). The model uses the modified alternate loss function, which includes a distance measure and accurately represents the regression relationship between the variables. The topological view of the model is given in Fig. 18. Assuming the problem of approximation, with the datasets $(x_1, y_1), \dots, (x_l, y_l), x \in \mathbb{R}^N, y \in \mathbb{R}$ having a linear relation.

$$f(x, a) = (w^* x) + b \quad (25)$$

The ideal regression equation is attained by diminishing the empirical risk is:

$$R_{emp}(w, b) = \frac{1}{l} \sum |y_i - f(x_i, \alpha)|_\varepsilon \quad (26)$$

The maximum general loss function with the ε -insensitive zone is described as:

$$y - f | (x, \alpha) | = \begin{cases} \varepsilon, & \text{if } |y - f(x, \alpha)| \leq \varepsilon \\ |y - f(x, \alpha)| & \end{cases} \quad (27)$$

If not, the goal is to determine a function $f(x, \alpha)$ having the maximum ε deviance from the actual variables y_i for all calibration data sets while being as smooth as possible. This corresponds to the minimization of the function:

$$\phi(w, \xi^*, \xi) = \|w\| / 2 + C(\sum \xi_i^* + \sum \xi_i) \quad (28)$$

where C is a predefined value and ξ^* , ξ are slack variables that are representing the upper and lower constraints of the outputs and it is designated by the following equations:

$$\begin{aligned} y_i - ((wx_i) + b) &\leq \varepsilon \xi_i, i = 1, 2, \dots, l \\ ((wx_i) + b) &\leq \varepsilon + \xi_i^*, i = 1, 2, \dots, l \\ \xi_i^* &\geq 0 \text{ and } \xi_i \geq 0, i = 1, 2, \dots, l \end{aligned} \quad (29)$$

The Lagrange function would be formulated from the objective function and the appropriate constraint by applying a double set of variables such as the following equation:

$$\begin{aligned} L = & \|w\|^2 / 2 + C \sum (\xi_i + \xi_i^*) \\ & - \sum \alpha_i [\varepsilon + \xi_i - y_i + (wx_i) + b] \\ & - \sum \alpha_i^* [\varepsilon + \xi_i^* - y_i + (wx_i) + b] \\ & + \sum (\eta_i \xi_i + \eta_i^* \xi_i^*) \end{aligned} \quad (30)$$

Starting from the state of the saddle point, the partial derivatives of L with respect to the main variables (w , b , ξ_i^* , ξ_i) must vanish for ideality. Substituting the result of the derivative into equation (28), and obtaining a dual optimization.

$$\begin{aligned} W(\alpha^*, \alpha) = & -\varepsilon \sum (\alpha_i^* + \alpha_i) + \sum y_i (\alpha_i^* - \alpha_i) - (1/2) \\ & \times \sum \sum (\alpha_i^* - \alpha_i)(\alpha_j^* - \alpha_j)(x_i x_j) \end{aligned} \quad (31)$$

it has to be maximized subject to constraints

$$\begin{aligned} \sum \alpha_i^* &= \sum \alpha_i, 0 \leq C, \text{ and} \\ 0 \leq \alpha_i &\leq C \text{ for } i = 1, 2, \dots, l \end{aligned} \quad (32)$$

Afterward, the coefficients α_i^* and α_i are obtained from equation (30) the compulsory vectors can now be defined as:

$$\begin{aligned} w_0 &= \sum (\alpha_i^* - \alpha_i) x_i \text{ and} \\ \sum (\alpha_i^* - \alpha_i) (x_i, x) + b_0 \end{aligned} \quad (33)$$

For the non-linear SVR model, a non-linear mapping kernel could be applied to map the datasets into larger dimensional features to which linear regression is fitted. The quadratic equation to be maximized can be rewritten as follows:

$$\begin{aligned} w(\alpha^*, \alpha) &= -\varepsilon \sum (\alpha_i^* + \alpha_i) + \sum y_i (\alpha_i^* - \alpha_i) - (1/2) \\ &\times \sum \sum (\alpha_i^* - \alpha_i) (\alpha_j^* - \alpha_j) K(x_i, x_j) \end{aligned} \quad (34)$$

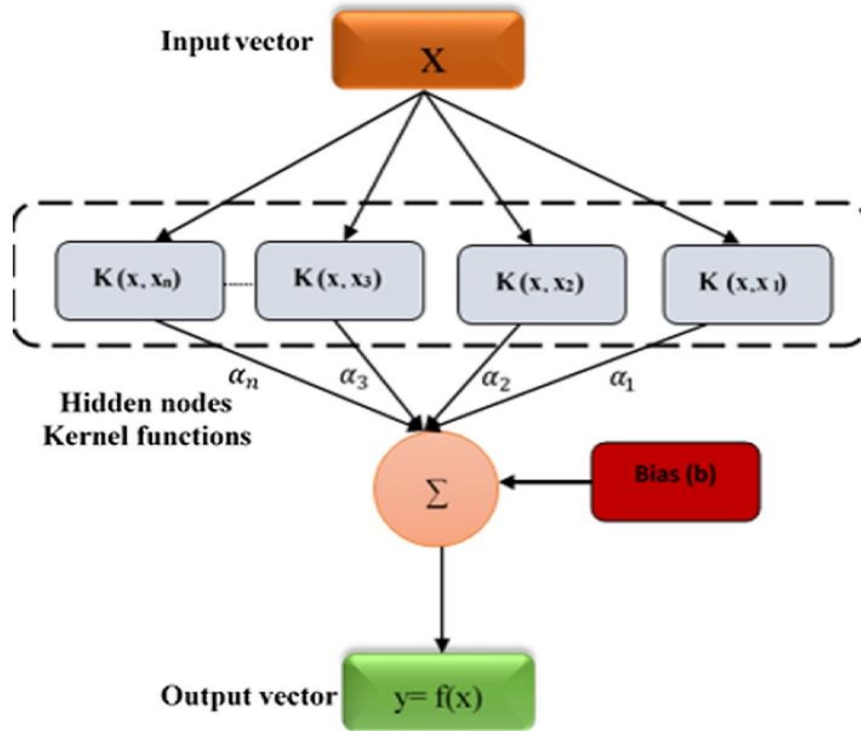
and the regression function is specified as:

$$f(x) = w_0 + b_0 \quad (35)$$

And the independent variables are defined as:

$$\begin{aligned} w_0 x &= \sum (\alpha_i^0 - \alpha_i^{0*}) k(x_i, x) \text{ and} \\ b &= -(1/2) \sum (\alpha_i^0 - \alpha_i^{0*}) [k(x_r, x_i) + k(x_s, x_j)] \end{aligned} \quad (36)$$

Figure 18

The Architecture of the SVM Model

AI-based models (ANFIS, ANN, and SVR) could effectively map the non-linear relationship between rainfall and runoff in fast convergent time. They can also generalize and smooth the noise of rainfall and flow time series. However, the AI-based models are usually prone to overtraining and their structures could not accurately apprehend the physical relation between rainfall and runoff in the catchment.

SWAT could model hydrologic and agricultural management processes in combination with climate change but it requires extensive inputs and the representation of HRUs in each sub-basin is non-spatial (Glavan & Marina, 2012). The groundwater modeling routine of the SWAT model could accurately estimate the groundwater contribution to rainfall-runoff modeling. The SWAT can incorporate the spatial input data into the modeling and that makes it a powerful tool to apprehend the effects of climate change on rainfall-runoff modeling (Jaiswal et al., 2020).

HBV model requires fewer input data; minimal convergence time and its results could often be comparable with complex models. However, the structure of

HBV is not capable to appraise the effects of climate change on rainfall-runoff modeling (Fowler et al., 2016). The structure of the HBV model requires further improvements to comprehensively quantify the effects of climate and land-use changes that could affect long-term catchment water balance (Huang et al., 2019).

The HEC-HMS has a simple structure and comprehensively examines climatic conditions and could select various computational techniques adapted to various watersheds and datasets. The HEC-HMS is very effective in short time event-based simulations of peak flow hydrographs characterized by the rapid rise and recession but it tends to overestimate peak flows for long time series streamflow simulations (Chen et al., 2019).

Ensemble of multiple models could produce a good robust simulation via better representation of models structure and reducing allied uncertainties (Velázquez et al., 2011). Therefore, ensemble modeling is important to reduce uncertainties resulting from individual model structures, input data, and model parameters and it takes over the merits of each model.

Performance Evaluation

The accuracy of the proposed models in this study was evaluated by two standard statistical tools namely; Nash-Sutcliffe Coefficient of Efficiency (NSE) and Root Mean Square Error (RMSE). NSE measures the relative amount of residual variance compared to observed variances and it expresses how simulated data fits with observed in one-to-one line. RMSE measures the accuracy based on the difference between observed and simulated datasets and it aggregates the residuals into a single performance measure as presented in (Eq. 38).

$$NSE = 1 - \frac{\sum_{i=1}^N \left(Q_o - Q_s \right)^2}{\sum_{i=1}^N \left(Q_o - \bar{Q}_o \right)^2} \quad (37)$$

$$RMSE = \sqrt{\frac{1}{N} \sum_{i=1}^N \left(Q_o(t) - Q_s(t) \right)^2} \quad (38)$$

where Q_o is actual flow, N is the number of observations, \bar{Q} is the mean of the actual flow and Q_s is the simulated flow at time t .

Ensemble Modeling

For the same data sets, one model could obviously outperform the others, and when multiple input data sets are used, the output of each model could be exclusively different. To take advantage of every model while not neglecting the overall characteristics of the datasets, the ensemble modeling practice has been developed, which uses the output of each model as input, assigning each model a certain prominence level owed to all with the support of relating functions to give the output (Kiran & Ravi, 2008). The precision of the ensemble of results of diverse single models would typically be superior to the precision of the preeminent particular model (Shamseldin & Connor, 1999). Moreover, in ensemble modeling, the outputs of every single model could represent the sources of input datasets that might be unique to that specific model then combining all those information could optimize input datasets to the model. In this study, one non-linear (neural network) and two linear (simple average, and weighted average) ensemble models are applied to boost the rainfall-runoff modeling efficiency of proposed individual models. In this study, 3 different ensemble scenarios were considered, ensemble of 3 AI-based models, ensemble of 3 physically based models and ensemble of all models using fusion of input data from different sources.

Non-Linear Neural Network Ensemble (NNE)

In NNE methods, the outputs of the distinct models are used as inputs of the NNE; each is allocated to a neuron of the input layer. The procedure of the NNE modeling is the same as FFNN, where the preeminent model architecture and number of iterations of the optimum model structure should be achieved using the trial-error method, and the sigmoid activation function was used as a output and hidden activation function. The other non-linear ensemble kernels such as Gene Expression Programming (GEP) and ANFIS can also be used, but FFNN was chosen for this study because of its simplicity,

rapid trainability, and providing results comparable to other non-linear ensemble techniques.

Simple Average Ensemble (SAE)

In the SAE method, the outputs of separately simulated SWAT, HBV, HEC-HMS, FFNN, ANFIS, and SVR are used as inputs. The SAE model was created by linear averaging of the single model outputs as:

$$\bar{Q}_o = \frac{1}{Q_n} \sum_{i=1}^{Q_n} Q_{oi} \quad (39)$$

where \bar{Q}_o , Q_{oi} and n are flow from the SAE, flow from the i^{th} individual model and the number of single models ($n= 6$).

Weighted Average Ensemble (WAE)

The WAE applies particular weights to the outputs of every single model based on the relative importance and its accuracy. The WAE modeling technique is given in Eq. 40.

$$\bar{Q}_o = \frac{1}{Q_n} \sum_{i=1}^{Q_n} w_i Q_{oi} \quad (40)$$

where w_i is the assigned weight for the i^{th} model output and could be defined from the model's performance measure as:

$$w_i = \frac{NSE_i}{\sum_{i=1}^{NSE_n} NSE_i} \quad (41)$$

NSE_i is the performance measure (e.g., Nash-Sutcliffe efficiency coefficient) of the i^{th} single model

Sensitivity Analysis

The most influential parameters of the watershed and inputs to the runoff simulation were determined for each of the proposed models during an early phase of model calibration and validation. Sensitivity analysis is an important process in any modeling because it identifies the critical variables and their level of importance that are used for model calibration and verification.

The sequential uncertainty fitting (SUFI-2) algorithm of the SWAT-CUP tool was used for the global sensitivity analysis and calibration of the SWAT model (Abbaspour, 2015). The SUFI-2 sensitivity analysis tool takes into account the suspicions resulting from the model conceptualization, the properties of the measured data sets, and their relationship to the calibration parameters (Singh et al., 2013). The sensitivity of each parameter was determined using the Latin hypercube sampling method and the upper and lower bounds of each parameter were adjusted and optimized using the SUFI-2 uncertainty algorithm. The parameters range would be amended for entire iterations till the objective function is attained. The sensitive parameters are listed (Table 6) and are used to select the correct range of parameters that could give the best result as compared to the measured flow.

Table 6

Lists of Parameters Used for SWAT Model Sensitivity Analysis

| Parameter | Description | Lower bound | Upper bound | Optimal value | Process |
|--------------|-------------------------------------------------------------|-------------|-------------|---------------|-------------|
| CN2* | * Initial SCS runoff curve number for moisture condition II | -0.2 | 0.2 | 0.04 | Runoff |
| GW_DEL AY | Groundwater delay time (days) | 35 | 450 | 45 | Groundwater |
| ALPHA_B | Baseflow alpha factor- | 0.01 | 1.2 | 0.68 | Runoff |

| | | | | | |
|-----------|----------------------------------------------------------------------|------|-----|------|--------------|
| F | Baseflow recession constant | | | | |
| SOL_AWC | Available water capacity of soil layer (mm H ₂ O/mm soil) | -0.8 | 0.8 | 0.16 | Soil channel |
| HRU_SLP | Average slope steepness | 0 | 1 | 0.18 | HRU |
| GW_REV AP | Groundwater “revap” coefficient | 0.02 | 0.2 | 0.05 | Groundwater |
| SURLAG | Surface runoff lag coefficient | 1 | 24 | 1.21 | Runoff |
| SOL_K | Saturated hydraulic conductivity | 0.7 | 0.8 | 0.72 | Soil |
| SOL_BD | Moist bulk density | 0.9 | 2.5 | 0.12 | Soil |

Rainfall-runoff modeling using HEC-HMS, the best-known approaches to sensitivity analysis are partial derivation and changing the ranges of each parameter turn by turn (Hamby, 1994). One at a time perturbation of parameters values between $\pm 25\%$ and $\pm 30\%$ with an interval of 5% has shown a good performance of the model (Bitew et al., 2019; Zelelew & Melesse, 2018) and it is the simplest method to carry out. For the current study, the sensitivity of parameters was investigated by altering the ranges of the parameters between -25% and 25% at 5% intervals until the measured and simulated data sets were significantly matched. In this technique, a single parameter was tested and optimized at a time, while the other parameters remained constant. The parameters used for HEC-HMS model sensitivity analysis are the curve number (CN), the initial abstraction, the Muskingum k and x coefficients, and the base flow.

The automatic Monte Carlo technique was applied to detect sensitive parameters of the HBV model and explore the random parameters with predefined ranges and objective functions. Before calibration, the upper and lower limits of the parameters representing the watershed characteristics were established. Each parameter was

calibrated within the predefined range until the objective function was optimized (Table 7).

Table 7

The Calibration Parameters of HBV Model

| Parameters | Explanation | Unit | Lower | Upper |
|-------------------|---------------------------------------------------|-------------------|--------------|--------------|
| UZL | Reservoir threshold | mm | 0 | 100 |
| MAXBAS | Base of weight function | Day | 13 | 24 |
| LP | Soil moisture threshold for evaporation reduction | - | 0.4 | 0.7 |
| FC | Soil moisture storage | mm | 100 | 1000 |
| PERC | Percolation to groundwater | mm/d | 0 | 0.25 |
| K0 | Recession coefficient | Day ⁻¹ | 0.05 | 0.5 |
| K1 | Recession coefficient (upper storage) | Day ⁻¹ | 0.01 | 0.1 |
| K2 | Recession coefficient (lower storage) | Day ⁻¹ | 0.001 | 0.1 |
| β | Shape coefficient | - | 1 | 6 |

In AI-based models (FFNN, ANFIS, and SVR), the neural network has proven to be an effective model for evaluating the sensitivity of input datasets to output, as the neural network was able to successfully capture the non-linear characteristics and dimensionality of hydrologic and meteorological datasets (Nourani & Fard, 2012). In this study, the key inputs to the runoff were identified using the ANN-based sensitivity assessment technique. The AI-based models, inputs such as rainfall, temperature, and discharge time series with different lags, were used to forecast runoff using FFNN.

Then, the performance of each input was evaluated by NSE goodness of fit and ranked according to their significance for rainfall-runoff modeling.

CHAPTER IV

Results and Findings

The current study was conducted in two major stages. First, all the proposed models simulated rainfall-runoff for both gauge and the satellite rainfall datasets separately, as well as for the combination of both datasets. Second, the output of each model was used as inputs for ensemble modeling by NNE, SAE, and WAE aimed at improving the accuracy of the modeling. The ensemble modeling was carried out for 3 different scenarios for each rainfall data sources: i) ensemble of AI-based models, ii) ensemble of physical-based models and iii) ensemble of all proposed models using the fusion rainfall data sets.

Results of Sensitivity Analysis

SUFI-2 algorithm was applied to analyze the sensitivity of the parameters for verification and calibration of the SWAT model. The calibration parameters were determined based on recommendations from different works of literature. Thus, nine parameters were identified and ranked according to their level of prominence in rainfall-runoff modeling (Table 8). The global sensitivity of the parameters is determined by automatic calibration based on t-stat and p-value. The parameter with the maximum t-stat and minimum p-value is the most sensitive and vice versa. Accordingly, CN is the most sensitive and SURLAG is the least sensitive parameter for SWAT flow simulation (Table 8).

Table 8

Sensitive Parameters for SWAT Runoff Simulation

| Parameter | P-value | t-stat | Rank |
|------------------|----------------|---------------|-------------|
| CN2 | 0 | -56 | 1 |
| ALPHA_BF | 0 | 11 | 2 |

| | | | |
|----------------|------|-------|---|
| Sol_K | 0 | 6.2 | 3 |
| HRU_SLP | 0 | 3.72 | 4 |
| SOL_BD | 0 | -3.62 | 5 |
| SOL_AWC | 0.24 | -1.3 | 6 |
| GW_REVA | 0.3 | -1.25 | 7 |
| P | | | |
| GW_DELA | 0.41 | -0.95 | 8 |
| Y | | | |
| SURLAG | 0.55 | 0.62 | 9 |

The sensitive parameters of the HEC-HMS rainfall-runoff model were identified by one a time perturbation of their values. Based on their ability to improve the efficiency of the simulations, 4 parameters were identified as sensitive to the HEC-HMS runoff simulation of the watershed. Soil CN, lag time, initial abstraction, and Muskingum k and x coefficients were detected as the most sensitive parameters. When the ranges of parameters were changing to the optimum, the observed and simulated data sets are converged, at the same time it could optimize model performance. The result shows that soil CN value is the most sensitive parameter for both SWAT and HEC-HMS modeling in the calibration and validation phases. This could be because most of the runoff-causing factors such as soil, land use, land cover, and slope are lumped in the respective CN as also stressed by Fanta & Sime (2022). Moreover, the land-use trend practiced in the study area, mainly dominated by destructive farming activities that lead to less infiltration rate and high runoff, erosion, and siltation rate during the wet season. The land use pattern in the Gilgel Abay watershed is dominated by destructive agricultural practices that could affect the natural infiltration and runoff relationship of the soil. Therefore, it is logical to mention that runoff in the catchment is highly dependent on the CN of the soil.

The sensitivity of the HBV model parameters to rainfall-runoff simulation was tested using automated Monte Carlo optimization techniques. The maximum and minimum bounds for each parameter were defined and the model was set to perform 700,000 runs for the catchment. The result of the Monte Carlo simulation was used to spot the lowest possible changes in the objective function. The parameter that could cause a high range of change in the objective function (NSE) is the most sensitive parameter, and a parameter that could cause a small range of changes in the objective function is considered a less sensitive parameter and the sensitive parameters are presented in (Table 9).

Table 9

Sensitive Parameters and their Rank for HBV Rainfall-Runoff Model

| Parameter | Change in objective function (%) | Rank |
|---------------------------|-----------------------------------------|-------------|
| FC | 22 | 1 |
| K2 | 16 | 2 |
| β | 12 | 3 |
| LP | 7 | 4 |

The sensitivity of the input parameters for the AI-based model was analyzed using neural network modeling, and the sensitivity of each parameter was ranked based on its effect on the simulated runoff as evaluated by the NSE in the validation phase of the FFNN modeling (see Table 10). The inputs for AI-based models are discharged (Q), rainfall (P), and temperature (T), each with 4 lag times. From the given sets of inputs, the most sensitive inputs for the runoff simulation were selected by a t-student test and used for rainfall-runoff modeling. Accordingly, discharge and rainfall each with 4 lags were relevant to rainfall-runoff modeling. However, to avoid complexity of modeling due to too much inputs, Q_{t-1} , Q_{t-2} , Q_{t-3} , P_t , and P_{t-1} , combinations were used as inputs.

Table 10

Inputs Sensitivity for AI-Based Models

| Inputs Parameters | Mean DC | Rank |
|--------------------------|----------------|-------------|
| Q_{t-1} | 0.8317 | 1 |
| Q_{t-2} | 0.8242 | 2 |
| P_t | 0.7826 | 3 |
| P_{t-1} | 0.7724 | 4 |
| Q_{t-3} | 0.7704 | 5 |
| Q_{t-4} | 0.7698 | 6 |
| P_{t-2} | 0.7549 | 7 |
| P_{t-3} | 0.7421 | 8 |
| P_{t-4} | 0.7392 | 9 |
| T | 0.1877 | 10 |
| T_{t-1} | 0.1855 | 11 |
| T_{t-2} | 0.1824 | 12 |
| T_{t-3} | 0.1786 | 13 |
| T_{t-4} | 0.1755 | 14 |

Results of Single Models

The six proposed models (SWAT, HEC-HMS, HBV, ANFIS, FFNN, and SVR) were simulated runoff using gauge and satellite-based rainfall data sets separately. The models were calibrated and validated using 12 years of daily rainfall and flow data. In addition to climatic data, physically-based semi-distributed models used spatial data

such as LULC, soil, and slope maps. The result obtained for each model using both data sources is presented in Table 11.

In SWAT modeling, the watershed was delineated from DEM then sub-basins were generated and further divided into smaller HRUs. The SWAT model discretizes the watershed into smaller units by lumping LULC, soil, and slope data and reproduced HRUs with similar physical and hydrologic characteristics. The SWAT split the catchment into 6 sub-basins and 19 HRUs (see Fig 12). After the setup of the model, 4 SWAT models (1 for each rainfall data source) were run from 2007 to 2018 of which the first 2 years of data were used to warm up the model. The climatic and discharge data series from 2009-2015 were used for model calibration and 2016-2018 were used for validation purposes. The model was automatically calibrated by the SUFI-2 algorithm of SWAT-CUP. Based on the performance criteria NSE (see Table 11, Figs 19, and 20), the SWAT model using satellite and gauge-based rainfall displayed a better performance than HBV and HEC-HMC in daily runoff simulation at both calibration and validation phases, however, it less performed than AI-based models. The result obtained by SWAT exhibited NSE values of 0.872 and 0.81 for gauge driven dataset at the calibration and validation stages, respectively. It was noted that the NSE obtained as 0.836 and 0.784 using CMORPH rainfall products at the calibration and validation stages, respectively. From the satellite-driven rainfall products, the CMORPH-based rainfall-runoff model outperformed over 3B42RT and 3B42 rainfall product-based models. The performances of 3B42RT and 3B42 based rainfall products were nearly similar at both calibration and validation phases.

The gauge-rainfall data-based models are more accurate than satellite rainfall-based models; this could be because of the bias that occurred by the satellites during apprehending rainfall information. As presented by Nourani et al., (2021), the 3B42 and 3B42RT underestimate most of the peak rainfall which could reduce the performance of the rainfall-runoff modeling. As indicated in Table 11, the performance of the SWAT model for both datasets was far better than the acceptable range (NSE - 0.5). Hence, it is normal to conclude that SWAT can effectively simulate rainfall-runoff by using satellite-driven rainfall products.

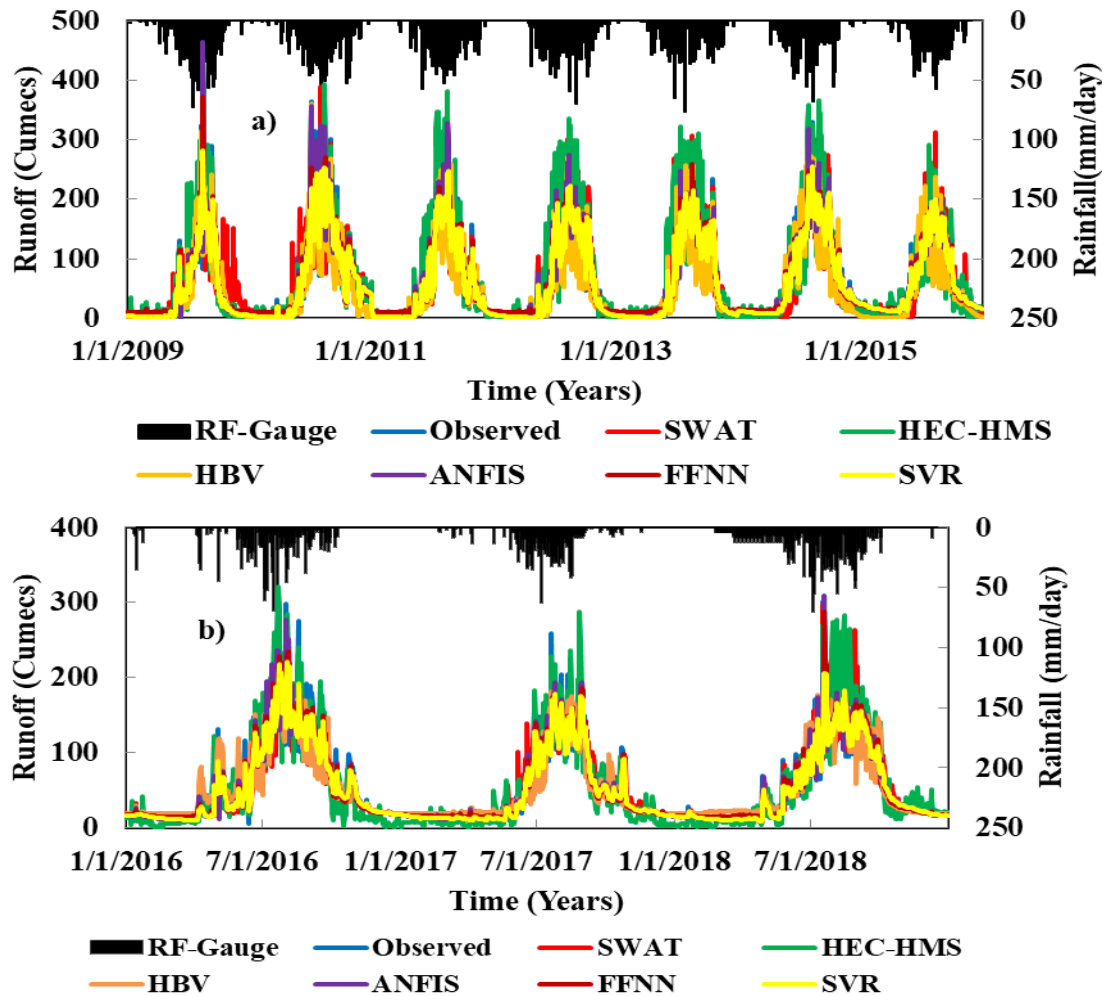
A semi-distributed physically-based hydrologic model is more appropriate for a medium-sized watershed with moderate to hilly topographic conditions (Wittwer, 2013). Gilgel Abay watershed has heterogeneous physiographic characteristics and is a medium-sized watershed. The result of this study shows that SWAT reproduces most of the observed discharges and is superior to the other physically-based models. Therefore, it is worth mentioning that the SWAT model is suitable for modeling rainfall-runoff in the Gilgel Abay catchment.

The configuration of the HEC-HMS model began with the watershed delineation from DEM (Fig. 15) and the model split the catchment into 5 sub-basins and the physiographic characteristics of each sub-basin were determined (see Table 5). Before running the model, the basin, meteorological, and control specifications models were created. For the HEC-HMS rainfall-runoff modeling, soil CN was determined from the global hydrologic soil group and soil class texture grid using the zonal statistics tool of ArcGIS. The hydrologic soil groups for the watershed were identified as A, B, and D and the percentage of area for each group was 33%, 12%, and 55%, respectively, and the weighted CN value was computed as 83-85. Like to SWAT model, the HEC-HMS model was run for gauge and satellite-driven rainfall data. Similar to the other proposed models, four rainfall-runoff models were created for HEC-HMS for each source of rainfall data.

The daily rainfall-runoff modeling performance evaluation of the models in terms of NSE and RMSE are given in Table 11 for both gauge and satellite rainfall datasets. Concerning both performance measures, the model well-simulated runoff with the NSE values of 0.837 and 0.776 and for the gauge rainfall data-based model and 0.809 and 0.759 for the CMORPH rainfall dataset-based model in the calibration and validation stages, respectively, (see Fig 19 and Fig 20). Nevertheless, the result reveals the minor overestimation of peak flows and underestimation of low flow (see Fig 19 and Fig 20).

Figure 19

Observed versus Simulated Runoff by SWAT, HEC-HMS, HBV, ANFIS, FFNN, And SVR Using Gauge Rainfall, a) at Calibration Phase, b) at Validation Phase



The HBV model was arranged for five elevation zones of the catchment (Fig 14) and three vegetation zones (Table 12) using nine model parameters (see Table 7). The Monte Carlo automatic calibration and validation were carried out using 2007-2018 daily climatic and discharge data. The data sets 2007-2008 were used to spin up the model, and 2009-2015 and 2016-2018 were used for calibration and validation, respectively. Similar to the other models, four rainfall-runoff models were created for the HBV model (one gauge rainfall-based and three satellite-based). Average precipitation and temperature in the watershed were calculated from the recorded data sets of the 5 gauging stations using the Thiessen polygon method, and

evapotranspiration was computed using the Hargreaves method using maximum and minimum daily temperatures.

The performance of HBV concerning NSE was 0.842 and 0.792 for the gauge rainfall-based model at calibration and validation steps, respectively, and its NSE was noted that 0.812 and 0.763 for the CMORPH rainfall data-based model during the calibration and validation phase, respectively (Table 11). The runoff simulated by HBV showed good agreement with the measured runoff during the calibration and validation phase for both the gauge and satellite-based datasets. Therefore, it is worth mentioning that the HBV is well calibrated and its parameter optimization is physically reasonable and the satellite dataset could be used for hydrological modeling in the basin. As can be seen in Figs. 19 and 20, the HBV model was able to accurately simulate low and mean flows, while slightly underestimating peak flows. This illustrates that the HBV model is capable of well representing the physical processes of the catchment and establishing a reliable relationship between precipitation and runoff.

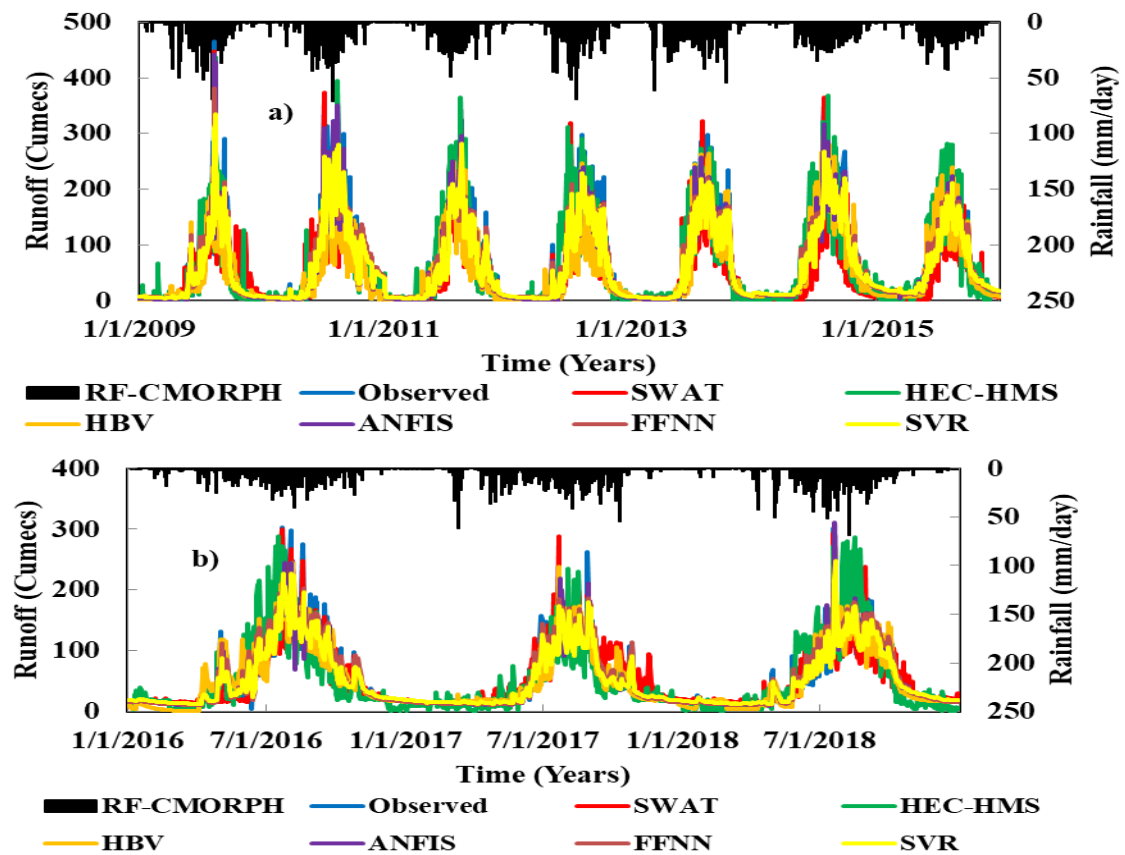
In this study, a Sugeno-type ANFIS was used and the membership functions (MFs) were determined by hybrid optimization algorithms. The Gaussian, Triangular and Trapezoidal types of MFs were iterated until the best runoff result and ANFIS architecture were obtained. The ANFIS structure and MFs that reproduced the best rainfall-runoff result with optimal epoch are given in Table 11 for both the gauge and satellite datasets. Four different ANFIS models were also created for all rainfall products.

The ANFIS model produced the best result in the validation phase with NSE of 0.885 and 0.838 for CMORPH rainfall products at calibration and validation stages, respectively (see Figs. 21d and 22d). The model was best performed with NSE of 0.913 and 0.864 for gauge rainfall-based modeling at calibration and validation phases, respectively. For CMORPH rainfall-based models, the ANFIS performed best with NSE of 0.885 and 0.838 at calibration and validation phases, respectively. For both gauge and satellite-based rainfall data, ANFIS accurately reproduced peak runoff in the wet season, nevertheless; it marginally overrated low runoff in the dry season (see Figs. 19 and 20). In this study, the ANFIS model outperformed all the other proposed models and

reproduced accurate runoff that best fits with observed streamflow. This could be because of the strength of the model to accurately map the input-output relationships since the model has incorporated the strength of the neural network and fuzzy inference system.

Figure 20

Observed versus Simulated Runoff by SWAT, HEC-HMS, HBV, ANFIS, FFNN, And SVR Using Satellite Rainfall, a) at Calibration Phase, b) at Validation Phase



The FFNN trained via BP and ML algorithm with one hidden layer and unstable hidden neurons were used to model rainfall-runoff. The ideal size of the hidden neurons was determined by trial and error in a range of 9-16 for both the satellite and gauge rainfall-based models. It is noted that the gauge rainfall-based FFNN rainfall-runoff model is superior to the satellite-driven rainfall-runoff models in both the calibration and validation phases.

The NSE of FFNN rainfall-runoff modeling was 0.857 and 0.816 for gauge rainfall-based models and 0.839 and 0.805 for CMORPH rainfall-based modeling at calibration and validation steps, respectively. In FFNN modeling, it is practical to choose rainfall datasets with a smaller number of hidden neurons. Among the satellite datasets, the FFNN modeling based on the CMORPH rainfall dataset is superior to the modeling based on the 3B42RT and 3B42 rainfall datasets. Hence, FFNN modeling with the CMORPH rainfall dataset could model runoff with a short running time and minimal cost. Moreover, FFNN was able to accurately reproduce low flows, but it is less accurate at modeling peak flows (see Figs. 19 and 20).

The radial base function (RBF) kernel has been used to build SVR rainfall-runoff models based on both satellite and gauge rainfall datasets. SVR also has other kernels such as polynomial and sigmoidal, but RBF was selected because it requires fewer tuning parameters and has already been shown to outperform over the other kernels (Sharghi et al., 2018). Similar to the other proposed models, four SVR rainfall-runoff models (one gauge rainfall-based and three satellites rainfall-based) were created for the Gilgel Abay catchment.

The results of SVR modeling for gauge and satellite rainfall data were presented in Table 11. The performance of SVR rainfall-runoff modeling in terms of NSE value was 0.848 and 0.809 for the gauge rainfall-based modeling and 0.831 and 0.79 and CMORPH precipitation dataset-based modeling in the calibration and validation phases, respectively. As depicted in Fig. 19 and 20, SVR could better reproduce low flow but underestimated high flows for both gauge and satellite rainfall datasets based on modeling. It is noted that the SVR model could well reproduce the rainfall-runoff but its performance was slightly lower than ANFIS and FFNN modeling.

Among the applied AI-based rainfall-runoff models, ANFIS was superior to FFNN and SVR in both the calibration and validation phases. This could be due to the fact that ANFIS incorporates the fast learning capability of ANN and the fuzzy inference system, which makes it a more accurate model.

Table 11

Results of Proposed Single Models

| Model | Rainfall source | Structure | NSE | | RMSE (m3/s) | |
|-------------|--------------------|------------|-------------|------------|-------------|------------|
| | | | Calibration | Validation | Calibration | Validation |
| SWAT | Gauge | - | 0.872 | 0.81 | 23.267 | 26.818 |
| | CMORPH | - | 0.836 | 0.784 | 25.334 | 29.742 |
| | 3B42RT | - | 0.814 | 0.762 | 26.52 | 31.345 |
| | 3B42 | - | 0.805 | 0.752 | 28.42 | 32.68 |
| HEC- HMS | Gauge | - | 0.837 | 0.776 | 25.837 | 29.701 |
| | CMORPH | - | 0.809 | 0.759 | 26.84 | 32.067 |
| | 3B42RT | - | 0.782 | 0.744 | 27.452 | 33.462 |
| | 3B42 | - | 0.7724 | 0.734 | 29.24 | 35.547 |
| HBV | Gauge | - | 0.842 | 0.792 | 25.045 | 31.271 |
| | CMORPH | - | 0.812 | 0.763 | 26.31 | 32.35 |
| | 3B42RT | - | 0.805 | 0.754 | 27.621 | 33.24 |
| | 3B42 | - | 0.786 | 0.748 | 28.54 | 34.465 |
| ANFIS | Gauge | Gaussian | 0.913 | 0.864 | 20.147 | 23.588 |
| | CMORPH | Triangular | 0.885 | 0.838 | 22.734 | 25.82 |
| | 3B42RT | Gaussian | 0.862 | 0.812 | 24.52 | 27.52 |
| | 3B42 | Gaussian | 0.846 | 0.794 | 26.52 | 29.25 |
| FFNN | Gauge | 5-10-1 | 0.857 | 0.816 | 23.454 | 27.814 |

| | | | | | | |
|-----|--------|--------|-------|-------|--------|--------|
| | CMORPH | 5-9-1 | 0.839 | 0.805 | 24.7 | 29.57 |
| | 3B42RT | 5-13-1 | 0.816 | 0.782 | 25.65 | 31.42 |
| | 3B42 | 5-16-1 | 0.805 | 0.772 | 27.22 | 32.52 |
| SVR | Gauge | RBF | 0.848 | 0.809 | 23.871 | 28.67 |
| | CMORPH | RBF | 0.831 | 0.790 | 24.927 | 31.333 |
| | 3B42RT | RBF | 0.808 | 0.772 | 26.34 | 32.52 |
| | 3B42 | RBF | 0.785 | 0.764 | 28.42 | 34.21 |

Table 12

The HBV Sensetive Parametrs and their Optimized Values for Each Vegetation Zones.

| Parameter | Range | Vegetation class | | |
|-----------|----------|------------------|-------|-------|
| | | 1 | 2 | 3 |
| FC | 100-1000 | 625.7 | 957.3 | 566.2 |
| K2 | 0.01-0.1 | 0.04 | 0.02 | 0.05 |
| β | 1-6 | 0.91 | 0.54 | 0.47 |
| LP | 0.3-0.7 | 0.37 | 0.41 | 0.53 |

Figure 21

Scatter Plot of Observed versus Simulated Flow a) SWAT, b) HEC-HMS, c) HBV, d) ANFIS, e) FFNN, f) SVR, Using Gauge Rainfall Data.

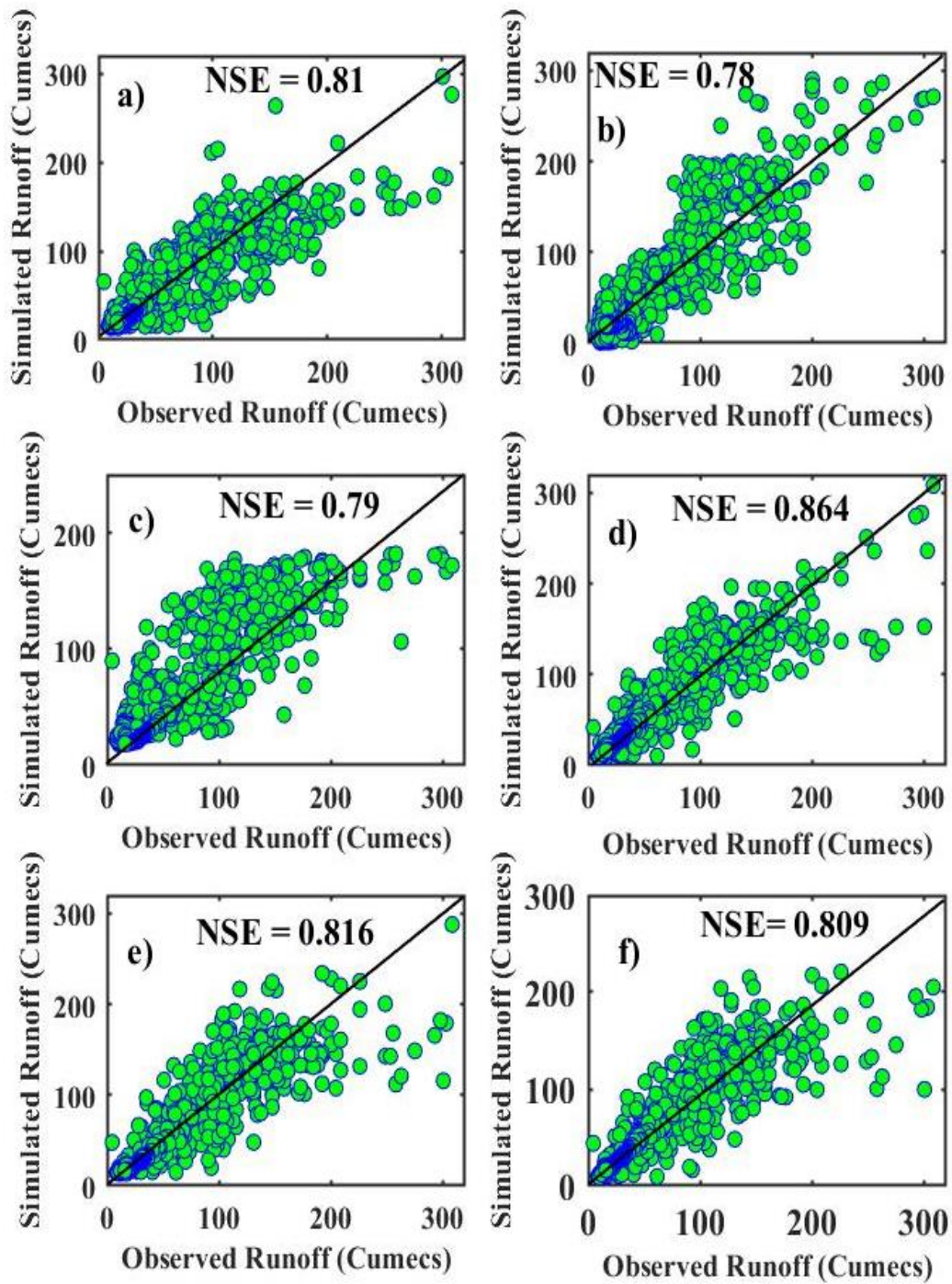
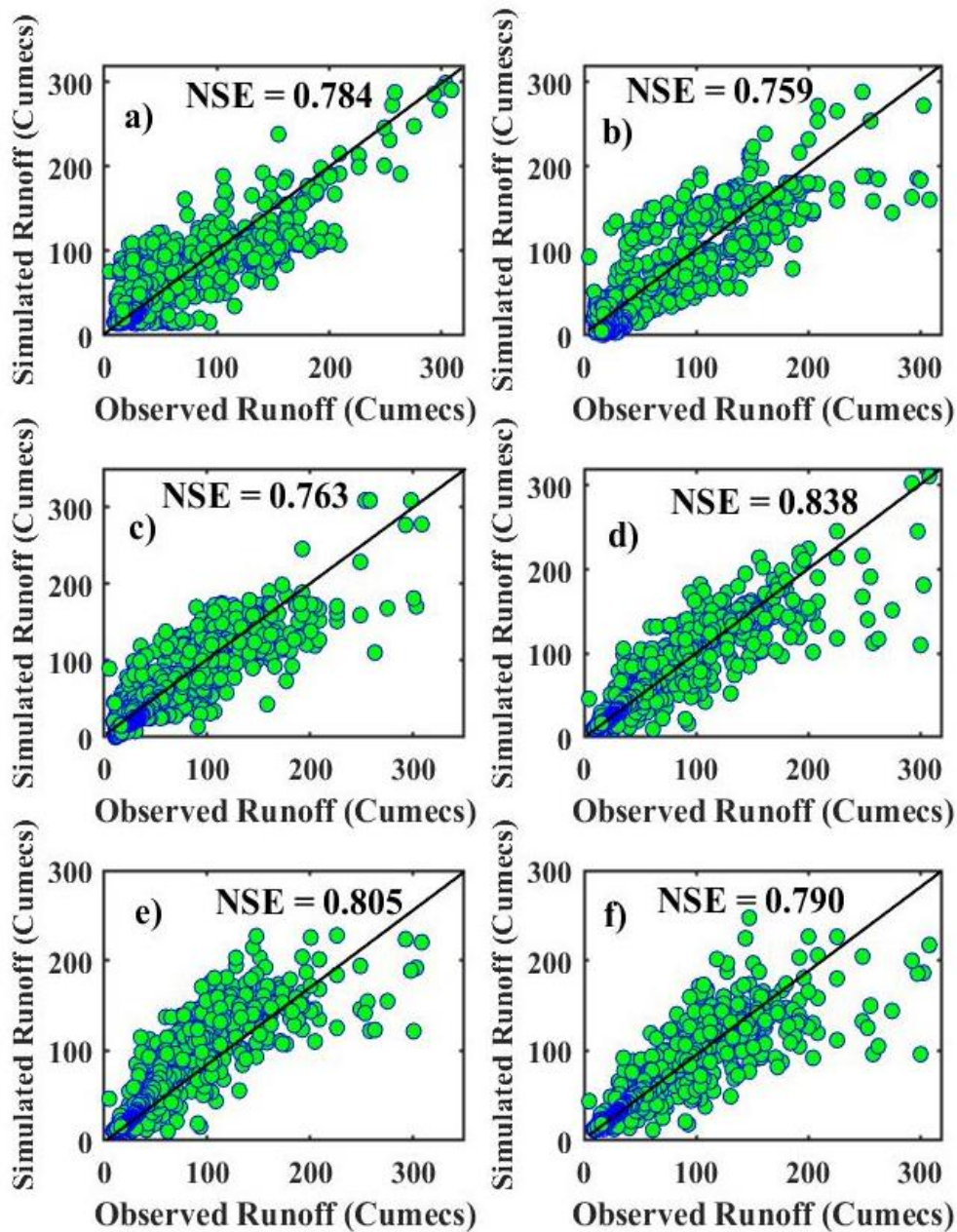


Figure 22

Scatter Plot of Observed versus Simulated Flow a) SWAT, b) HEC-HMS, c) HBV, d) ANFIS, e) FFNN, f) SVR, Using CMORPH Rainfall Data.



Results of Rainfall Fusion

In this modeling, gauge and satellite-driven rainfall products were combined to simulate runoff and the effects of rainfall fusion on runoff simulation were also

evaluated (Table 14). The fusion of rainfall datasets from the 3B42, 3B42 RT, and CMORPH satellite sources as well as gauges were deployed into the proposed models to simulate runoff. Before satellite-derived rainfall data is used for hydrologic modeling, it should usually be "bias-corrected" by a statistical relationship to gauge precipitation data (Bitew et al., 2012). The most common approaches to correcting the bias of satellite precipitation data are based on the following processes. First, the bias of the satellite rainfall dataset is calculated as the ratio of the daily average satellite rainfall products on the specific grid covered by the gauging station to the corresponding gauge precipitation records. Second, the originally obtained satellite rainfall dataset is multiplied by the bias obtained in step 1, and the bias could be removed. However, in the present study, the raw satellite dataset has been imposed into the models along with measured data, which could serve as a strategy to correct the bias of satellite data.

For HBV, the weighted average of rainfall records from both data sources was used as a combined input because the HBV model accepts only a single climate file. The rainfall-runoff results of rainfall fusion (Table 14 and Fig 23) indicated that it could meaningfully enhance the performance of modeling when compared with individual satellite modeling but it only marginally improved the gauge rainfall data-based modeling results (see Table 11).

The rainfall-runoff modeling using the rainfall data fusion improved the modeling accuracy of low-performed (3B42) satellite rainfall-based modeling by 8%, 9%, 8.4%, 8.5%, 8%, and 8.5% for HBV, SWAT, HEC-HMS, ANFIS, FFNN, and SVR, respectively, at the calibration stage. The fusion modeling also improved the modeling performance of HEC-HMS, HBV, SWAT, SVR, FFNN, and ANFIS by 6.5%, 8%, 8.4%, 6.6%, 6.6%, and, 9.2%, respectively, at the validation step.

In the specific case of using satellite rainfall datasets, the rainfall-runoff modeling was significantly enhanced as it is compared with modeling using individual rainfall datasets. The gauge rainfall data reproduced more accurate runoff than satellite rainfall products. The logic behind this could be fact that gauge-based rainfall could capture the most accurate and valid hydrological information that can represent physical processes at the watershed level. The quality of satellite estimated rainfall depends on several

factors such as cloud coverage condition of the sky, algorithm they used, revisit time of rainfall measuring space crafts, and their corresponding orbital locations. The unsteady characteristics of the mentioned factors could cause bias in the rainfall estimation process. The fusion of rainfall products from several sources enhanced the robustness of the models when it is compared with the results simulated from single source rainfall data. Therefore, it is worth mentioning that gauge rainfall data have corrected the bias of satellite rainfall datasets and enhanced the rainfall-runoff simulation capability of the models.

Table 13

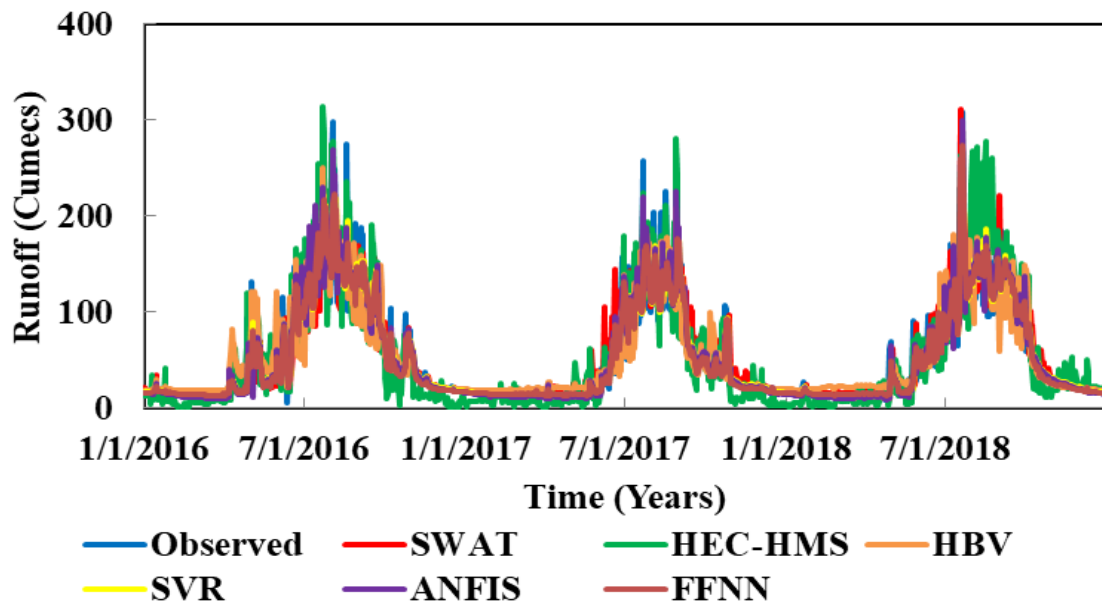
Modeling Performance for Rainfall Datasets Fusion

| Model | Structure | NSE | RMSE (m ³ /s) | | | |
|---------|-----------|-------|--------------------------|------------|-------------|------------|
| | | | Calibration | Validation | Calibration | Validation |
| SWAT | - | 0.884 | 0.821 | 21.846 | 26.075 | |
| HEC-HMS | - | 0.843 | 0.785 | 24.561 | 28.643 | |
| HBV | - | 0.855 | 0.814 | 23.526 | 28.042 | |
| ANFIS | Gaussian | 0.925 | 0.875 | 18.426 | 21.84 | |
| FFNN | 8-12-1 | 0.875 | 0.827 | 21.547 | 25.258 | |
| SVR | RBF | 0.858 | 0.818 | 22.542 | 27.681 | |

The performance of all the proposed models was generally good in both calibration and validation stages. Nevertheless, satellite rainfall-based models indicated slight deviations from observed runoff thus, the modeling performance was lower in both the calibration and validation stages for all the proposed models (see Table 11).

Figure 23

Observed versus Simulated Runoff by SWAT, HEC-HMS, HBV, ANFIS, FFNN, And SVR Using the Fusion of Rainfall at the Validation Phase



The runoff simulation for the period of consideration indicates that the proposed models can reproduce most of observed runoff in the catchment for both individual rainfall data and rainfall fusion data (see Tables 11 and 14). However, it is noted that each model is not performed equally in rainfall-runoff modeling and could not apprehend the physical process of the watershed. For example, the performance of ANFIS surpassed the other models at both calibration and validation phases for both rainfall datasets (see Figs. 21 and 22).

When the details of the runoff simulated by each model for each season are considered, the strengths and weaknesses of each model can be better identified. Therefore, to further evaluate the modeling capability in wet and dry seasons, two different points were randomly selected for each season and the runoff values simulated by each model were compared to the observed runoff. The details of simulated and observed runoff by each model on the specific day of each season are given in Table 15 and Fig. 24. For the dry season, February 2 and December 13, 2017 (indicated as points 1 and 4 in Fig 14), respectively, were selected and for the rainy season, July 10 and August 6, 2017 (points 2 and 3), respectively, were picked up.

As shown in Table 14, the simulated runoff values by HBV and SVR are closer to the observed runoff values in dry seasons, however, HEC-HMS underestimated low flows. ANFIS overestimated low flows but it well-captured peak flows. It is noted that SWAT and FFNN are fairly good at simulating low flow but they could well capture average flow. From this results, the modeling performance of models are highly varying, hence some models are good as wet season modeling while they did not well captured at dry seasons.

The result on the selected dates indicated that each model could derive different results at different times of the year. Therefore, combining the results of different models through the ensemble method could improve the simulation capacity of the modeling and lead to more accurate results. To this end, the results of each model were used as inputs, and two linear (SAE and WAE) and one non-linear (NNE) ensemble modeling were carried out in three ensemble scenarios and described in the following section.

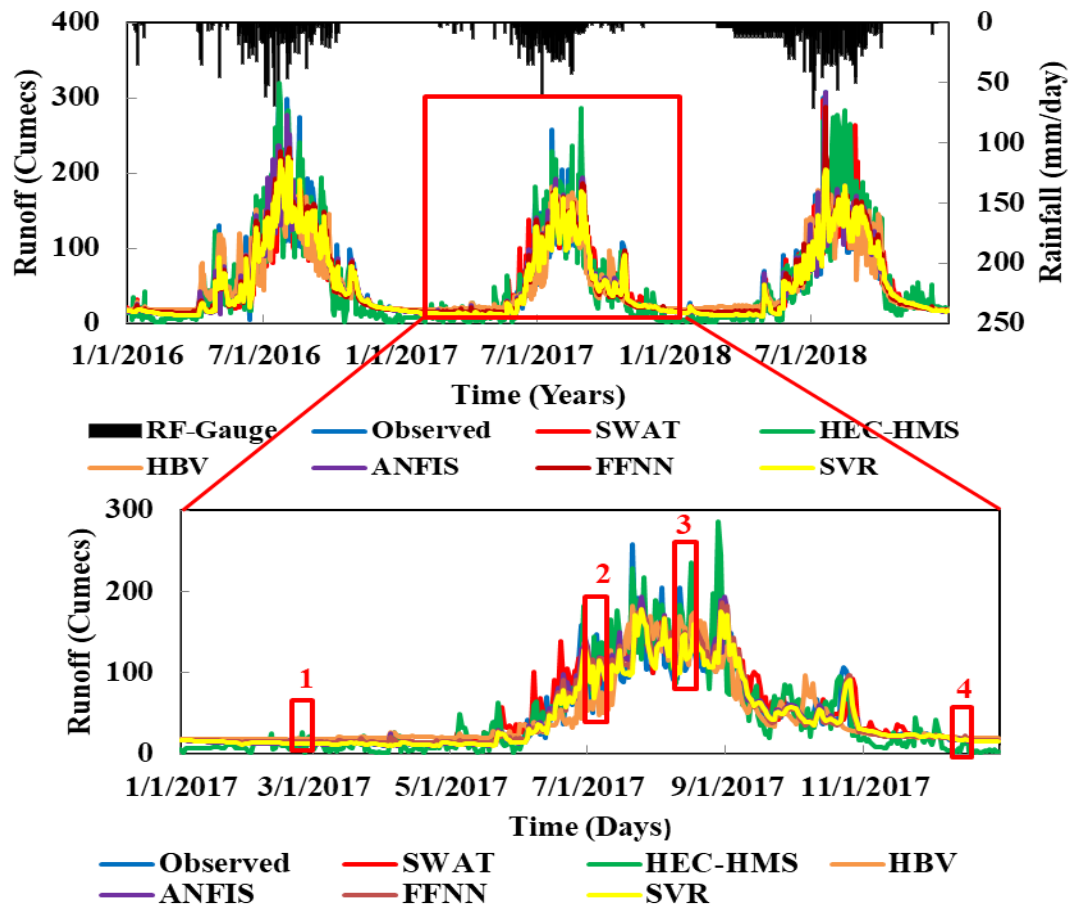
Table 14

The Observed and Simulated Runoff by Each Model on Randomly Selected Days

| Date | Observed Runoff(m ³ /s) | Simulated Runoff (m ³ /s) | | | | | |
|-------------------|---------------------------------------|--------------------------------------|---------|-------|-------|-------|-------|
| | | SWAT | HEC-HMS | HBV | ANFIS | FFNN | SVR |
| 2/18/2017 | 12.9 | 15.03 | 6.2 | 13.19 | 17.4 | 15.01 | 12.8 |
| 7/10/2017 | 75.9 | 71.2 | 102 | 55.11 | 83.8 | 98.04 | 86.9 |
| 8/6/2017 | 147.7 | 158.5 | 145 | 114.5 | 147.5 | 136 | 121.2 |
| 12/13/2017 | 17.4 | 18.9 | 7.8 | 17.3 | 19.6 | 17.8 | 17.19 |

Figure 24

Simulated Runoff Using Gauge Rainfall via SWAT, HEC-HMS, HBV, ANFIS, FFNN, And SVR a) at Validation Step, b) Details for the Year 2017



Results of Ensemble Modeling

Ensemble modeling was able to improve the rainfall-runoff modeling capacity of the individual models (SWAT, HEC-HMS, HBV, ANFIS, FFNN, and SVR). To further improve the efficiency of rainfall-runoff modeling, the ensemble technique was performed in 3 different scenarios. In scenario 1, the best results of the AI-based models (FFNN, ANFIS, and SVR) were used as input to the ensemble modeling by SAE, WAE, and NNE techniques. In scenario 2, the best results of physically-based models (SWAT, HBV, and HEC-HMS) were forced as inputs and SAE, WAE and NNE techniques were performed. In the scenario 3, outputs of the individual models obtained from the input fusion phase were forced into the SAE, WAE, and NNE ensemble methods. The weight

of WAE was determined by NSE at the validation stage according to Eq. 41. The NNE ensemble technique was developed by FFNN via BP trained with one hidden layer and variable numbers of neurons until the optimal epoch was reached.

The results of ensemble modeling are given in Tables 15, 16 and 17, for scenarios 1, 2, and 3, respectively. From the employed ensemble models, it is noted that the performance of NNE surpasses SAE and WAE techniques in both calibration and validation phases for all ensemble scenarios. NNE modeling of scenario 1 was improved the modeling accuracy of low-performed (3B42) satellite rainfall-based modeling by 17.4%, 14.16%, 16.5% for SVR, ANFIS, and FFNN, respectively, at the validation phase (see Tables 11 and 15). Likewise, the NNE scenario 1 improved the fusion modeling of SVR, ANFIS, and FFNN by 11.6%, 5.4%, and 10.6%, respectively, at the validation step (see Tables 13 and 15).

Table 15

Results of AI-based Ensemble Modeling (Scenario 1)

| Ensemble model | NSE | | RMSE (m ³ /s) | |
|----------------|-------------|------------|--------------------------|------------|
| | Calibration | Validation | Calibration | Validation |
| SAE | 0.884 | 0.848 | 20.422 | 24.564 |
| WAE | 0.894 | 0.862 | 19.256 | 23.724 |
| NNE | 0.957 | 0.925 | 15.452 | 18.265 |

In scenario 2 ensemble modeling, NNE technique improved 3B42 rainfall-based models 17%, 15.4%, and 14.9% for HEC-HMS, HBV, and SWAT, respectively, at the validation phase (see Tables 11 and 16). Similarly, it enhanced the performance of fusion modeling by 11.2%, 8%, and 7.1% for HEC-HMS, HBV, and SWAT, respectively, at the validation phase (see Tables 13 and 16).

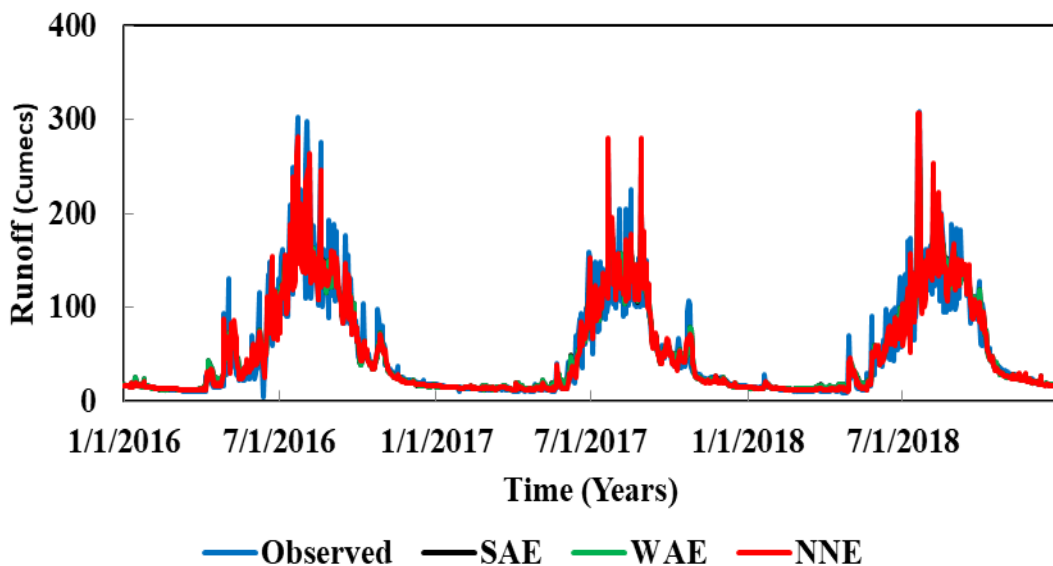
Table 16

Results of Physically-based Ensemble Modeling (Scenario 2)

| Ensemble model | NSE | | RMSE (m ³ /s) | |
|----------------|-------------|------------|--------------------------|------------|
| | Calibration | Validation | Calibration | Validation |
| SAE | 0.862 | 0.801 | 23.413 | 27.767 |
| WAE | 0.874 | 0.812 | 22.414 | 26.522 |
| NNE | 0.926 | 0.884 | 16.405 | 19.547 |

The performance of the SAE and WAE techniques was better in Scenario 1 than in Scenario 2 because the performance of the AI-based models was better than that of the physical models in the individual modeling phase, so the accuracy propagated to the ensemble modeling as well. The NNE technique outperformed the other applied ensemble techniques in both the calibration and validation phases in all scenarios of the modeling (see Fig. 25).

Figure 25

Observed versus Simulated Runoff by SAE, WAE, and NNE Techniques at the Validation Phase for Scenario 3

Based on the applied performance evaluation criteria values, scenario 3 ensemble modeling could meaningfully enhance the rainfall-runoff modeling performance of single models when it is compared with modeling using separate rainfall from each source and rainfall fusion (see Tables 11, 13, and 17). From the employed ensemble models, it is noted that the performance of NNE surpasses SAE and WAE methods at both calibration and validation phases. The NNE modeling in scenario 3 using fusion of rainfall data enhanced the modeling accuracy of low-performed (3B42) satellite rainfall-based modeling by 21.2%, 19.7%, 19.2%, 18%, 17%, and 14.7% for HEC-HMS, HBV, SWAT, SVR, FFNN, and ANFIS, respectively, at the validation stage. Similarly, the NNE improved the gauge and satellite rainfall fusion modeling of HEC-HMS, HBV, SWAT, SVR, FFNN, and ANFIS by 15.7%, 12.6%, 11.8%, 12.1%, 11.2%, and, 6%, respectively at the validation step. The ensemble modeling also substantially improved the performances of the models at calibration stages.

Comparing the accuracy of the 3 scenarios of the ensemble techniques considered in this study, it is noted that the ensemble technique of scenario 3 was more accurate than scenarios 1 and 2 in both the calibration and validation phases. In this scenario, the ensemble technique was able to take advantage of the individual models involved and the input rainfall data sets. It can be concluded that the fusion of precipitation data allows the models to capture the most important features of rainfall from each source. The physically-based models are generally able to understand the physics of hydrologic parameters involved in the rainfall-runoff process. AI-based models are also good at representing nonlinear relationships among watershed parameters.

Table 17

Results of Rainfall Fusion Ensemble Modeling (Scenario 3)

| Ensemble model | NSE | | RMSE (m ³ /s) | |
|----------------|-------------|------------|--------------------------|------------|
| | Calibration | Validation | Calibration | Validation |
| SAE | 0.935 | 0.881 | 19.221 | 22.467 |

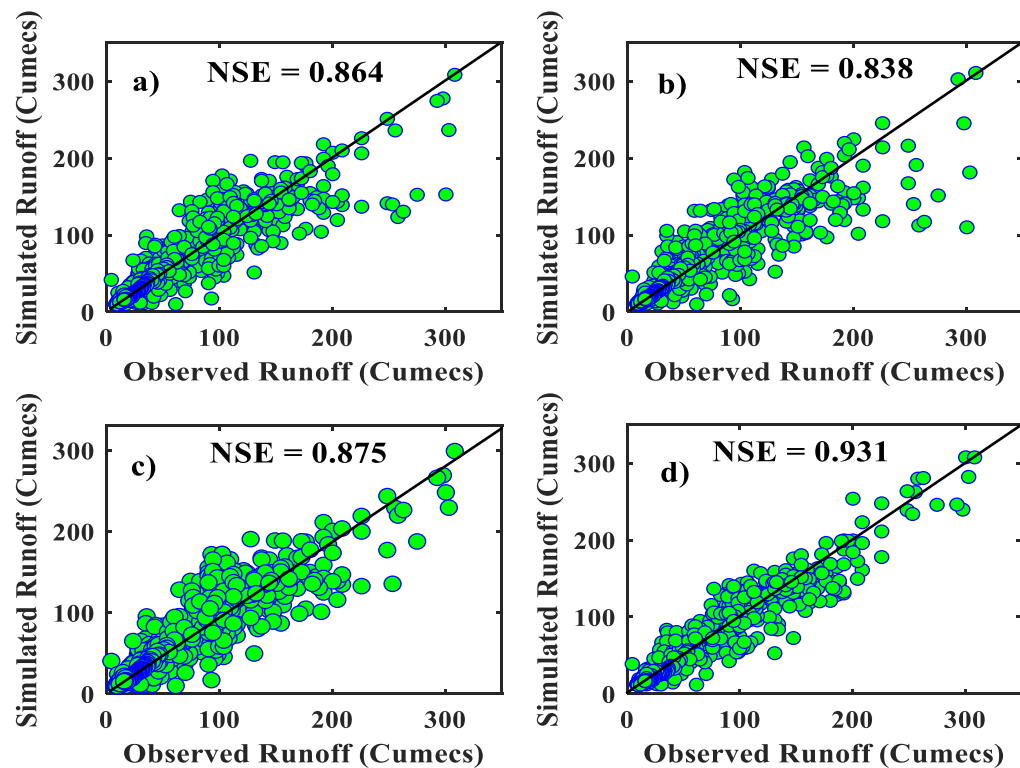
| | | | | |
|-----|-------|-------|--------|--------|
| WAE | 0.948 | 0.891 | 18.054 | 21.623 |
| NNE | 0.964 | 0.931 | 14.306 | 17.468 |

The ensemble technique in scenario 3 combines the outputs of both groups of models and therefore could further improve modeling efficiency by combining the benefits of all models involved in rainfall-runoff modeling. Based on the results, it is worth noting that the ensemble of runoff modeling could meaningfully increase the simulation performance of individual models using separate rainfall data from diverse sources.

Scatter plots of simulated runoff at the validation phase for a single best model (ANFIS) using both rainfall datasets separately; a fusion of both sources and the NNE model versus observed runoff are shown in Fig. 26.

Figure 26

Scatter Plots for a) ANFIS-Gauge, b) ANFIS-CMORPH, c) ANFIS-Fusion, d) NNE Ensemble of Fusion in the Validation Phase

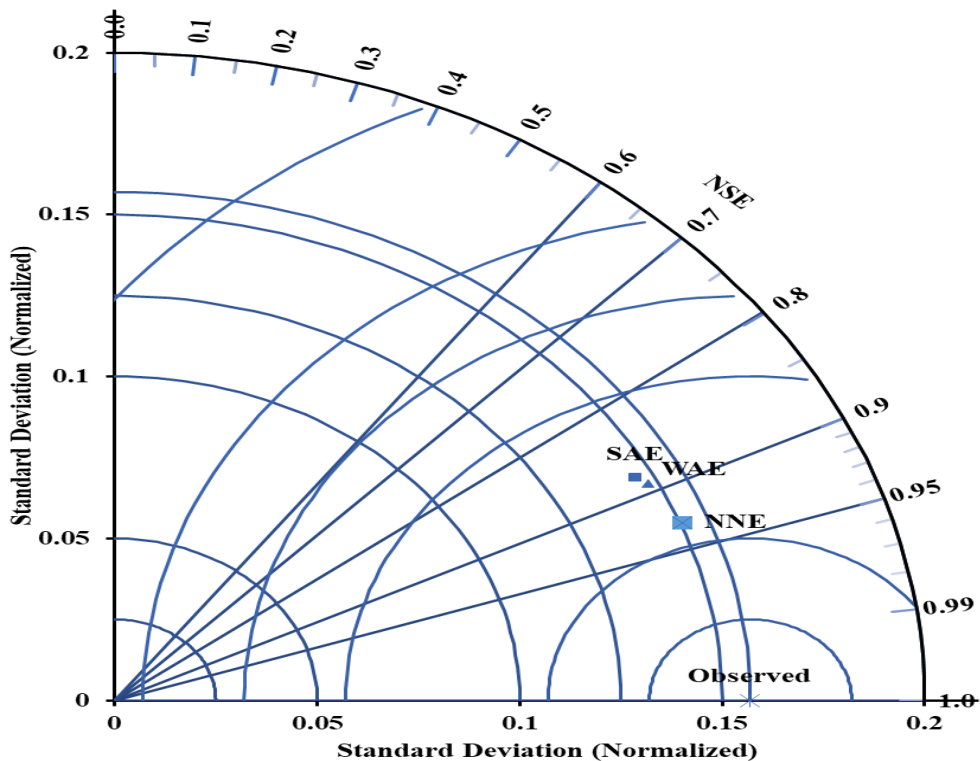


As can be seen from the scatter plots, NNE significantly enhanced the performance of the models. It is noted that the non-linear NNE ensemble rainfall-runoff modeling was superior modeling over the other two linear ensemble modeling both in the calibration and validation stages.

The modeling performance of SAE, WAE, and NNE at scenario 3 is also illustrated by the 2-dimensional transparent Taylor diagram (see Fig. 27), which can visualize the simulated runoff by each ensemble method and the observed runoff for accurate comparisons. In the Taylor chart, NSE and standard deviation were combined to form multiple performance evaluation matrices in a single chart that can describe the statistical relationship between the simulated and observed runoff. This chart aims to combine the different performances into a single array that assesses how close the simulated runoff is to the observed runoff.

Figure 27

Taylor Diagram Presentation of Performances for SAE, WAE, and NNE Ensemble Methods



The Taylor diagram for the three ensemble techniques is shown in Fig. 27. In this method, the model is more accurate when the ensemble modeling result is closer to the observed flow. As shown in Fig. 27, NNE is closer to the observed flow than SAE and WAE and is, therefore, more accurate than the other techniques.

CHAPTER V

Discussions

The contribution of all physical components involved in rainfall-runoff modeling may not be necessarily the same, and the modeling requirements for these components may also vary. The degree of importance of each component was determined by appropriate sensitivity analysis during the calibration of the models. The modeling of the rainfall-runoff could be affected by several physical components and each proposed model has several methods for uncertainty analysis. However, only a few parameters and sensitivity analysis methods were selected and applied in this study due to time and logistic limitations.

The SWAT-CUP provides five approaches to uncertainty analysis, namely SUFI-2, Generalized Likelihood Uncertainty Estimation (GLUE), Parameter Solution (ParaSol), Particle Swarm Optimization (POS), and Markov Chain Monte Carol (MCMC). In this study, the SUFI -2 algorithm was selected for the sensitivity analysis of SWAT modeling because it is more efficient and less time-consuming (Zhang et al., 2020). For the sensitivity analysis, the nine most common parameters were selected (Table 6) and ranked according to their order of importance and contribution to runoff generation (Table 8). Based on the result, the soil curve number was placed in the first position and the surface runoff coefficient lag was placed in the last position. The most influential parameters (soil curve number and base runoff coefficient) belong to the runoff component of the model. The soil curve number is a function of hydrologic soil group, land use, soil type, and soil infiltration capacity. The Gilgel Abay watershed is characterized by low infiltration capacity with high runoff potential. The reason why the soil curve number was the most sensitive could be because the study area was dominated by destructive agricultural land use type, which favors surface runoff.

The most sensitive parameters for HEC-HMS were selected by changing values in between the assigned ranges of each parameter sequentially. Accordingly, soil CN, lag time, initial abstraction, and Muskingum k and x coefficients were ranked the first to the fourth, respectively. Similar to the SWAT model, the most sensitive parameter for HEC-HMS is also the soil curve number. This could be because most of the runoff-

causing factors such as soil, land use, land cover, and slope are lumped in the respective CN. A similar result was obtained in a previous study by Fanta & Sime (2022). It is concluded that land-use practices in the area could cause high surface runoff, sediment transport and deposition, low infiltration, soil erosion, and gully formation.

The hydrologic soil group in the Gilgel Abay watershed is dominated by group D, which is characterized by low infiltration, high surface runoff potential, and high swelling potential, in which clay pans form more frequently. The CN value of the soil can be directly influenced by the aforementioned physical properties of the soil and is therefore the most sensitive parameter for both SWAT and HEC-HMS models.

The sensitivity of the most common model parameters for HBV was analyzed using the automated Monte Carlo method, with soil moisture storage (FC) or field capacity ranking first, followed by the lower soil box storage coefficient. FC is one of the components in the model's soil routine box (see Fig. 13), i.e., the main section that controls runoff initiation. If the soil is dry (low soil moisture), its contribution to runoff from rainfall could be low, and if the soil is wet, its contribution could be high.

The proposed models were generally classified into two main categories, AI-based models (ANFIS, FFNN, and SVR) and physically-based models (SWAT, HBV, and HEC-HMS). For each model, four runoff models were simulated for gauge, CMORPH, 3B42RT, and 3B42 rainfall products. For hydrologic modeling, the validation result with $NSE > 0.5$ is a generally acceptable, $NSE > 0.75$ is a very good and $NSE > 0.8$ is the best performance (Whittemore, 2002). In general, all the proposed models reproduced the observed runoff well for all rainfall datasets in the validation phase, but their performance was not quite the same. In the group of physically-based models, the SWAT rainfall-runoff modeling outperformed the HBV and HEC-HMS modeling in both the calibration and validation phases. The reason for the better performance of SWAT could be its ability to better discretize the catchment into more detailed sub-catchments with similar spatial and hydrological characteristics. The results from HEC-HMS show slight variations in peak and low flows. This is the usual limitation of hydrological models (Zhang & Savenije, 2005) due to uncertainties arising from the structure of the models and the input data.

Among the AI-based models, ANFIS performed better than FFNN and SVR in both the calibration and validation phases for all rainfall datasets. ANFIS reproduced more accurate runoff because its structure is a hybrid of fuzzy logic and artificial neural network, and it has adopted the hybrid training that uses the learning advantages of both models. The ANFIS model can universally approximate a given set of continuous data to the compact set with the required degree of accuracy (Nourani & Komasi, 2013). The input-output parameters and their membership functions were trained using the back-propagation algorithm, in which the weights of each input are tuned and then connected with fuzzy if-then rules. FFNN and SVR models produced nearly similar performance compared to other models. In FFNN modeling, multiple pieces of training were performed by changing the number of hidden neurons until the optimal objective function was achieved.

The gauge rainfall resulted in a better runoff simulation for all proposed models in both the calibration and validation phases (see Table 11). This could be due to the accuracy of the gauges' rainfall records compared to satellite-estimated rainfall products. The gauges typically record each raindrop and provide the actual rainfall in the watershed, which should be converted to a runoff after satisfying the infiltration losses. However, satellites first detect information about precipitation, which is usually received by sensors and then converted to rainfall data. In some cases, the sensors may detect false precipitation signals from non-raining cold clouds covering large areas over the Earth. The satellite rainfall data may further be calibrated with gauge rainfall data from a basin-wide area. Therefore, this process is not a direct rainfall measurement method and errors may occur during this process that affects the next step of rainfall estimation. The amount of precipitation estimated by the satellite may be biased during the detection, receiving of the information, or calibration of the received data. This is the reason why satellite rainfall-based modeling in the Gilgel Abay watershed was less accurate than runoff modeling using gauge-based rainfall data.

The result showed that there were performance differences among the proposed satellite-based rainfall products (see Table 11). For example, the CMORPH-based rainfall-runoff modeling was more accurate than the 3B42RT and 3B42-based runoff modeling. The possible cause for the deviations in the performances could be the

precision of satellite sensors to retrieve rainfall information and the topographic heterogeneity of the study area. Gebremichael et al., (2014) presented that the CMORPH, 3B42RT, and 3B42 satellite rainfall sources might overrate daily rainfall in lowland and underrate it in plateau areas. The topography of the Gilgel watershed is heterogeneous and diverges between 1866m and 3543m above sea level (see Fig. 14), therefore, the rainfall is more prone to topographic influence. The accuracy of satellite rainfall estimation could also be influenced by algorithms they used to transform the retrieved information into the rainfall. In this regard, the sensors that used microwave-based algorithms indicated superiority over infrared wave-based algorithms (Bitew & Gebremichael, 2010). As indicated in Table 11, the microwave algorithm-based CMORPH reproduced runoff more accurately than the infrared-microwave combination-based 3B42RT and infrared-based 3B42 rainfall products.

The other modeling strategy employed in this study was a fusion of rainfall datasets from all sources. The gauge and the "bias-uncorrected" satellite data (CMORPH, 3B42RT, and 3B42) were combined and forced into the proposed models. It was assumed that the discrepancies and limitations of each rainfall data set would be updated and modified in the course of modeling. It can be seen that the input fusion significantly improved the performance of the rainfall-runoff modeling compared to the first stage modeling. The reason for the improved performance of the models could be that the models capture the best reliable rainfall value from each imposed rainfall product imposed for a given day of observation so that it could be aggregated to the final results of the individual models. This modeling strategy particularly improved the performance of satellite rainfall-based rainfall-runoff modeling, which may be due to the correction of biases due to rainfall fusion mechanisms. In this study, another dimension of the satellite rainfall bias correction technique was introduced, which is the combination of satellite rainfall data with gauge rainfall data. In the fusion, it is believed that the actual gauge rainfall data smoothed the underestimated and overestimated satellite rainfall products at corresponding period of observation. In other words, the gauge rainfall corrected the biases that occurred in the various steps of the satellite rainfall measurement.

To further improve the modeling capacity, linear and non-linear ensemble techniques have been used. In principle, these methods can be used to improve rainfall-runoff modeling by aggregating the advantages of each model into a single entity. The nonlinear ensemble (NNE) method reproduced runoff more accurately than the linear ensemble methods (SAE and WAE) in all scenarios considered in this study.

The linear ensemble techniques could only improve the performance of less performed models and showed no significant change in high performed models. It can be seen that both linear ensemble models perform approximately similarly for the corresponding scenarios. The performance of the linear ensemble techniques was better in scenario 1 than in scenario 2 because the individual models included in scenario 1 showed better performance than the models in scenario 2. Therefore, the merits of the individual models in Scenario 1 were also applied to the ensemble techniques.

The superiority of NNE over SAE and WAE may lie in the ability of the nonlinear models to well understand the nonlinear and complicated physical relationship between rainfall and runoff. The linear models have shown lower performance than NNE for the following reasons. Unlike the NNE methods, the SAE and WAE methods are linear and may only work well when the direct relationship between inputs and outputs of the models is examined. Therefore, the drawbacks of the individual models could propagate and syndicate through linear ensemble models as the models linearly combine the outputs of the individual models.

CHAPTER VI

Conclusion and Recommendations

Conclusions

This study was inspired on rainfall-runoff modeling by SWAT, HEC-HMS, HBV, ANFIS, FFNN, and SVR using 5 gauging stations (Gundel, Wetet Abay, Sekela, Dangila, and Adet) and three satellite-based rainfall datasets (CMORPH, 3B42RT, and 3B42) in the Gilgel Abay catchment in the Upper Blue Nile Basin, Ethiopia. To simulate runoff, discharge time series, land use land cover, soil, and slope data of the catchment were forced into the models in addition to rainfall and temperature data. The most sensitive parameters of rain-runoff modeling for each model were investigated using the SUFI-2 algorithm for SWAT, automatic Monte Carlo for HBV, and one at a time preterbution for HEC-HMS. Accordingly, CN2 and ALPHA_BF for SWAT, the initial abstraction and lag time for HEC-HMS, and FC and K2 for HBV were obtained as the most sensitive parameters which could highly affect the runoff. The relevant input sets for AI-based models were also identified using the non-linear sensitivity analysis method and accordingly, discharge and rainfall were sensitive for rainfall-runoff modeling.

Two-stage rainfall-runoff modeling was deployed by each of the proposed models. First, rainfall-runoff modeling was simulated separately by each model using each satellite, gauge, and fusion of rainfall datasets. Second, the runoff simulated by each model using the fusion of rainfall datasets was applied to the ensemble modeling via SAE, WAE, and NNE techniques to enhance modeling precision by considering three different scenarios. Among the satellite rainfall datasets, CMORPH provided better performance for all models still; it tends to overestimate the low flows. The rainfall-runoff results simulated using 3B42 and 3B42RT underestimates peak flow, and in particular, 3B42 produced random pseudo peaks in the dry season. The accuracy of satellite rainfall products depends on the types of signals they used to collect information about rainfall. Satellites which use microwave-based algorithms are more accurate than those which use infrared rays -based algorithms for rainfall estimation. Accordingly,

CMORPH which uses microwave algorithms indicated superiority over 3B42RT which uses a microwave-infrared combination and 3B42 which uses only infrared rays for rainfall estimation.

From the AI-based models, ANFIS, using both individual rainfalls from each source and their fusion, was found to be superior to the other models. This could be because ANFIS can combine the training capacity of neural networks and fuzzy logic in a given structure. The back-propagation training algorithm of the ANFIS could be able to assign the weights for each input and tuned them, then connected with fuzzy if-then rules thus, provides the output with high accuracy.

Among the semi-distributed models, the rainfall-runoff modeling performance of the SWAT model surpasses that of the HBV and HEC-HMS models, using rainfall data from both gauge and satellite sources. This could be due to the model's ability to well extricate the physical relationship at each HRU since it uses multiple layers of spatial datasets lumped in a single entity.

The fusion of rainfall datasets from diverse sources showed a significant improvement over the rainfall-runoff modeling results using only satellite rainfall datasets, and it also revealed a slight improvement over gauge rainfall-based runoff modeling. This was due to the discrepancies and limitations of each rainfall data set that would be updated and modified in the course of modeling.

To further improve modeling accuracy, two linear (SAE and WAE) and nonlinear (NNE) ensemble techniques were applied in 3 different scenarios. The ensemble scenarios were i) an ensemble of AI-based models, ii) an ensemble of physically-based models, iii) an ensemble of all models using the fusion of rainfall data from gauges and satellite sources. In all ensemble scenarios, NNE improved the performance of modeling in both the calibration and validation phases. The NNE technique in scenario 3 improved the accuracy of the low-performing modeling of HEC-HMS, HBV, SWAT, SVR, FFNN, and ANFIS in the validation phase by up to 21.2%, 19.7%, 19.2%, 18%, 17%, and 14.7%, respectively. It also improved rainfall fusion-based modeling accuracy of HEC-HMS, HBV, SWAT, SVR, FFNN, and ANFIS by 15.7%, 12.6%, 11.8%, 12.1%, 11.2%, and 6%, respectively, in the validation phase. Among the ensemble techniques

used, NNE was a powerful and accurate ensemble method for rainfall-runoff simulation because the model was able to explore the nonlinear relationships of the hydrologic process.

Recommendations

Based on the results obtained from this study, the following points were recommended for future studies as well as implementations.

- ✓ The outcome of the current study would be a groundbreaking step towards utilizing rainfall datasets combined from multiple satellite sources in data-sparse, ungaged, and unevenly gauged catchments.
- ✓ The satellite rainfall products could be a good option to get reliable rainfall datasets for hydrological modeling, water resources management, and planning activities in developing countries.
- ✓ Season-based modeling could provide better result for each rainfall data sets and it can help to identify the performance of each model at different seasons
- ✓ Furthermore, future studies should focus on downscaling and validating satellite rainfall products using the local rain-gauge time series data as the reference data; hence the relevance and credibility of satellite datasets would be better verified.
- ✓ The rating curve used for discharge measurement could be updated regularly and the more ground-based rain gauge and hydro-metric stations should be installed uniformly throughout the watershed
- ✓ In addition, future studies should investigate the effects of regional and global climate change on the rainfall-runoff process using a satellite rainfall dataset.

REFERENCES

- Abba, S. I., Linh, N. T. T., Abdullahi, J., Ali, S. I. A., Pham, Q. B., Abdulkadir, R. A., Costache, R., Nam, V. T., & Anh, D. T. (2020). Hybrid machine learning ensemble techniques for modeling dissolved oxygen concentration. *IEEE Access*, 8, 157218–157237. <https://doi.org/10.1109/ACCESS.2020.3017743>
- Abbaspour, K. C. (2015). *SWAT - CUP SWAT Calibration and Uncertainty Programs*.
- Abbot, J., & Marohasy, J. (2017). Forecasting extreme monthly rainfall events in regions of Queensland, Australia using artificial neural networks. *International Journal of Sustainable Development and Planning*, 12(7), 1117–1131. <https://doi.org/10.2495/SDP-V12-N7-1117-1131>
- Abushandi, E., & Merkel, B. (2013). Modelling Rainfall Runoff Relations Using HEC-HMS and IHACRES for a Single Rain Event in an Arid Region of Jordan. *Water Resources Management*, 27(7), 2391–2409. <https://doi.org/10.1007/s11269-013-0293-4>
- Adamowski, J., Chan, H. F., Prasher, S. O., Ozga-Zielinski, B., & Sliusarieva, A. (2012). Comparison of multiple linear and nonlinear regression, autoregressive integrated moving average, artificial neural network, and wavelet artificial neural network methods for urban water demand forecasting in Montreal, Canada. 48,. *Water Resources Res.*, 48, W01528.
- Al-Safi, H. I. J., & Sarukkalgige, P. R. (2019). The application of conceptual modelling approach to evaluate the impacts of climate change on the future streamflow in three unregulated catchments of the Australian hydrologic reference stations. *International Journal of Hydrology Science and Technology*, 9(5), 494–525. <https://doi.org/10.1504/IJHST.2019.102913>
- Ali, A. F., Xiao, C. de, Zhang, X. peng, Adnan, M., Iqbal, M., & Khan, G. (2018). Projection of future streamflow of the Hunza River Basin, Karakoram Range (Pakistan) using HBV hydrological model. *Journal of Mountain Science*, 15(10), 2218–2235. <https://doi.org/10.1007/s11629-018-4907-4>
- Alizadeh, M. J., Kavianpour, M. R., Kisi, O., & Nourani, V. (2017). A new approach for simulating and forecasting the rainfall-runoff process within the next two months. *Journal of Hydrology*, 548, 588–597. <https://doi.org/10.1016/j.jhydrol.2017.03.032>

- Altunkaynak, A., & Nigussie, T. A. (2015). Prediction of daily rainfall by a hybrid wavelet-season-neuro technique. *Journal of Hydrology*, 529(P1), 287–301. <https://doi.org/10.1016/j.jhydrol.2015.07.046>
- Arnold, J. G., & Allen, P. M. (1996). Estimating Hydrological Budgets for Three Illinois Watersheds. *Journal of Hydrology*, 176, 57–77.
- Arnold, J. G., & Fohrer, N. (2005). Arnold, J.G., Fohrer, N., SWAT2000: Current capabilities and research opportunities in applied watershed modelling. *Hydrol. Process*, 16, 563-572.
- Arnold, J. G., Srinivasan, R., Mutiah, R. S., & Williams, J. R. (1998). Large area hydrologic modeling and assessment part I: model development. *J. Am. Water Resource.*, 34, 73–89.
- Asadi, S., Shahrabi, J., Abbaszadeh, P., & Tabanmehr, S. (2013). A new hybrid artificial neural networks for rainfall-runoff process modeling. *Neurocomputing*, 121, 470–480. <https://doi.org/10.1016/j.neucom.2013.05.023>
- Ateeq-ur-Rauf, Ghumman, A. R., Ahmad, S., & Hashmi, H. N. (2018). Performance assessment of artificial neural networks and support vector regression models for stream flow predictions. *Environmental Monitoring and Assessment*, 190(12). <https://doi.org/10.1007/s10661-018-7012-9>
- Bartoletti, N., Casagli, F., Marsili-Libelli, S., Nardi, A., & Palandri, L. (2018). Data-driven rainfall/runoff modelling based on a neuro-fuzzy inference system. *Environmental Modelling and Software*, 106, 35–47. <https://doi.org/10.1016/j.envsoft.2017.11.026>
- Bates, A. J. M., & Granger, C. W. J. (2016). *The Combination of Forecasts* Stable URL : <http://www.jstor.org/stable/3008764> REFERENCES Linked references are available on JSTOR for this article : *The Combination of Forecasts*. 20(4), 451–468.
- Beven, K. J. (2002). Towards an alternative blueprint for a physically based digitally simulated hydrologic response modelling system. *Hydrological Processes*, 16, 189–206.
- Bitew, G. T., Mulugeta, A. Belete, & Miegel, K. (2019). Application of HEC-HMS Model for Flow Simulation in the Lake Tana Basin: The Case of Gilgel Abay

- Catchment, Upper Blue Nile Basin, Ethiopia. *Hydrology*, 6(21).
<https://doi.org/10.3390/hydrology6010021>
- Bitew, M. M., & Gebremichael, M. (2010). Assessment of high-resolution satellite rainfall for streamflow simulation in medium watersheds of the East African highlands. *Hydrology and Earth System Sciences Discussions*, 7(5), 8213–8232.
<https://doi.org/10.5194/hessd-7-8213-2010>
- Bitew, Menberu M., Gebremichael, M., Ghebremichael, L. T., & Bayissa, Y. A. (2012). Evaluation of high-resolution satellite rainfall products through streamflow simulation in a hydrological modeling of a small mountainous watershed in Ethiopia. *Journal of Hydrometeorology*, 13(1), 338–350.
<https://doi.org/10.1175/2011JHM1292.1>
- Bizuneh, B. B., Moges, M. A., Sinshaw, B. G., & Kerebih, M. S. (2021). SWAT and HBV models' response to streamflow estimation in the upper Blue Nile Basin, Ethiopia. *Water-Energy Nexus*, 4, 41–53. <https://doi.org/10.1016/j.wen.2021.03.001>
- Busico, G., Colombani, N., Fronzi, D., Pellegrini, M., Tazioli, A., & Mastrocicco, M. (2020). Evaluating SWAT model performance, considering different soils data input, to quantify actual and future runoff susceptibility in a highly urbanized basin. *Journal of Environmental Management*, 266(March).
<https://doi.org/10.1016/j.jenvman.2020.110625>
- Chandwani, V., Vyas, S. K., Agrawal, V., & Sharma, G. (2015). Soft Computing Approach for Rainfall-runoff Modelling: A Review. *Aquatic Procedia*, 4(Icwrcoe), 1054–1061. <https://doi.org/10.1016/j.aqpro.2015.02.133>
- Chang, F. J., & Tsai, M. J. (2016). A nonlinear spatio-temporal lumping of radar rainfall for modeling multi-step-ahead inflow forecasts by data-driven techniques. *Journal of Hydrology*, 535, 256–269. <https://doi.org/10.1016/j.jhydrol.2016.01.056>
- Chen, H., Yang, D., Hong, Y., Gourley, J. J., & Zhang, Y. (2013). Hydrological data assimilation with the Ensemble Square-Root-Filter: Use of streamflow observations to update model states for real-time flash flood forecasting. *Advances in Water Resources*, 59, 209–220. <https://doi.org/10.1016/j.advwatres.2013.06.010>
- Chen, Y., Xu, C. Y., Chen, X., Xu, Y., Yin, Y., Gao, L., & Liu, M. (2019). Uncertainty in simulation of land-use change impacts on catchment runoff with multi-

- timescales based on the comparison of the HSPF and SWAT models. *Journal of Hydrology*, 573, 486–500. <https://doi.org/10.1016/j.jhydrol.2019.03.091>
- Chua, L. H. C., & Wong, T. S. W. (2010). Improving event-based rainfall-runoff modeling using a combined artificial neural network-kinematic wave approach. *Journal of Hydrology*, 390(1–2), 92–107. <https://doi.org/10.1016/j.jhydrol.2010.06.037>
- Chua, L. H. C., Wong, T. S. W., & Wang, X. H. (2011). Information recovery from measured data by linear artificial neural networks - An example from rainfall-runoff modeling. *Applied Soft Computing Journal*, 11(1), 373–381. <https://doi.org/10.1016/j.asoc.2009.11.028>
- Ciupak, M., Ozga-Zielinski, B., Adamowski, J., Deo, R. C., & Kochanek, K. (2019). Correcting satellite precipitation data and assimilating satellite-derived soil moisture data to generate ensemble hydrological forecasts within the HBV rainfall-runoff model. *Water (Switzerland)*, 11(10). <https://doi.org/10.3390/w11102138>
- Collins, M., Achuta Rao, K., Ashok, K., Bhandari, S., Mitra, A. K., Prakash, S., Srivastava, R., & Turner, A. (2013). Observational challenges in evaluating climate models. *Nat. Clim. Change*, 3(11), 940–941.
- Deng, P., Zhang, M., Bing, J., Jia, J., & Zhang, D. (2019). Evaluation of the GSMaP_Gauge products using rain gauge observations and SWAT model in the Upper Hanjiang River Basin. *Atmospheric Research*, 219(September 2018), 153–165. <https://doi.org/10.1016/j.atmosres.2018.12.032>
- Devia, G. K., Ganasri, B. P., & Dwarakish, G. S. (2015). A review on hydrological models. *Aquat. Procedia*, 4, 1001–1007.
- Dile, Y. T., Karlberg, L., Daggupati, P., Srinivasan, R., Wiberg, D., & Rockström, J. (2016). Assessing the implications of water harvesting intensification on upstreamecosystem services: a case study in the Lake Tana basin. *Sci. Total Environ.*, 542, 22–35.
- Dinku, T., Ceccato, P., Grover-Kopec, E., Lemma, M., Connor, S. J., & Ropelewski, C. F. (2007). Validation of satellite rainfall products over East Africa's complex topography. *International Journal of Remote Sensing*, 28(7), 1503–1526. <https://doi.org/10.1080/01431160600954688>

- Esmaeili-Gisavandani, H., Lotfirad, M., Sofla, M. S. D., & Ashrafzadeh, A. (2021). Improving the performance of rainfall-runoff models using the gene expression programming approach. *Journal of Water and Climate Change*, *12*(7), 3308–3329. <https://doi.org/10.2166/wcc.2021.064>
- Evsukoff, A. G., Cataldi, M., & De Lima, B. S. L. P. (2012). A multi-model approach for long-term runoff modeling using rainfall forecasts. *Expert Systems with Applications*, *39*(5), 4938–4946. <https://doi.org/10.1016/j.eswa.2011.10.023>
- Fanta, S. S., & Sime, C. H. (2022). Performance assessment of SWAT and HEC-HMS model for runoff simulation of Toba watershed, Ethiopia. *Sustainable Water Resources Management*, *8*(1), 1–17. <https://doi.org/10.1007/s40899-021-00596-8>
- Feldman, A. D. (2000). *Hydrologic Modeling System HEC-HMS. Technical Reference Manual. U.S. Army Corps of Engineers, Hydrologic Engineering Center, HEC.*, Davis.
- Fowler, K. J. A., Peel, M. C., Western, A. W., Zhang, L., & Peterson, T. J. (2016). Simulating runoff under changing climatic conditions: Revisiting an apparent deficiency of conceptual rainfall-runoff models. *Water Resources Research*, *5*(3), 2–2. <https://doi.org/10.1111/j.1752-1688.1969.tb04897.x>
- Gao, F., Zhang, Y., Chen, Q., Wang, P., Yang, H., Yao, Y., & Cai, W. (2018). Comparison of two long-term and high-resolution satellite precipitation datasets in Xinjiang, China. *Atmospheric Research*, *212*(October 2017), 150–157. <https://doi.org/10.1016/j.atmosres.2018.05.016>
- Gao, Z., Long, D., Tang, G., Zeng, C., Huang, J., & Hong, Y. (2017). Assessing the potential of satellite-based precipitation estimates for flood frequency analysis in ungauged or poorly gauged tributaries of China's Yangtze River basin. *Journal of Hydrology*, *550*, 478–496. <https://doi.org/10.1016/j.jhydrol.2017.05.025>
- Garret, C., Boongaling, K., Faustino-eslava, D. V, & Lansigan, F. P. (2018). Modeling land use change impacts on hydrology and the use of landscape metrics as tools for watershed management : The case of an ungauged catchment in the Philippines. *Land Use Policy*, *72*(December 2017), 116–128. <https://doi.org/10.1016/j.landusepol.2017.12.042>
- Gassman, P., Reyes, M., Green, C., & Arnold, J. (2007). (2007). The soil and water

- assessment tool historical development, applications, and future research directions. *Trans. ASABE*, 50, 901–910.
- Gebre, S. L. (2015). Application of the HEC-HMS Model for Runoff Simulation of Upper Blue Nile River Basin. *Journal of Waste Water Treatment & Analysis*, 06(02). <https://doi.org/10.4172/2157-7587.1000199>
- Gebremichael, M., Bitew, M. M., Hirpa, F. A., & Tesfay, G. N. (2014). Accuracy of satellite rainfall estimates in the Blue Nile Basin: Lowland plain versus highland mountain. *Water Resources Research*, 50, 8775–8790. <https://doi.org/10.1002/2013WR014500>.Received
- Glavan, M., & Marina, P. (2012). Strengths, Weaknesses, Opportunities and Threats of Catchment Modelling with Soil and Water Assessment Tool (SWAT) Model. In N. Purna (Ed.), *Water Resources Management and Modeling*. Intech Open. <http://www.intechopen.com/books/trends-in-telecommunications-technologies/gps-total-electron-content-tec-prediction-at-ionosphere-layer-over-the-equatorial-region%0AInTec>
- Graumlich, L. J. (1987). Precipitation variation in the Pacific Northwest (1675–1975) as reconstructed from tree rings. *Ann. Assoc. Am. Geogr.*, 77(1), 19–29.
- Güner, H. A. A., & Yumuk, H. A. (2014). Application of a fuzzy inference system for the prediction of longshore sediment transport. *Physics Procedia*, 48, 162–175. <https://doi.org/10.1016/j.apor.2014.08.008>
- Halwatura, D., & Najim, M. M. M. (2013). Application of the HEC-HMS model for runoff simulation in a tropical catchment. *Environmental Modelling and Software*, 46, 155–162. <https://doi.org/10.1016/j.envsoft.2013.03.006>
- Hamby, D. M. (1994). A review of techniques for parameter sensitivity. *Environmental Monitoring and Assessment*, 32(c), 135–154. https://deepblue.lib.umich.edu/bitstream/handle/2027.42/42691/10661_2004_Article_BF00547132.pdf?sequence=1
- Hosseini, S. M., & Mahjouri, N. (2016). Integrating Support Vector Regression and a geomorphologic Artificial Neural Network for daily rainfall-runoff modeling. *Applied Soft Computing Journal*, 38, 329–345. <https://doi.org/10.1016/j.asoc.2015.09.049>

- Hsu, K., Gupta, H. V., & Sorooshian, S. (1995). Artificial neural network modeling of rainfall runoff process. *Water Resources Res.*, *31*, 2517–2530.
- Hsu, K. L., Gupta, H. V., & Sorooshian, S. (1995). Artificial neural network modeling of the rainfall–runoff process. *Water Resour. Res.*, *31*, 2517–2530.
- Huang, S., Eisner, S., Magnusson, J. O., Lussana, C., Yang, X., & Beldring, S. (2019). Improvements of the spatially distributed hydrological modelling using the HBV model at 1 km resolution for Norway. *Journal of Hydrology*, *577*.
<https://doi.org/10.1016/j.jhydrol.2019.03.051>
- Jain, A., Sudheer, K. P., & Srinivasulu, S. (2004). Identification of physical processes inherent in artificial neural network rainfall–runoff models. *Hydrol. Process.*, *18*, 571–581.
- Jaiswal, R. K., Ali, S., & Bharti, B. (2020). Comparative evaluation of conceptual and physical rainfall–runoff models. *Applied Water Science*, *10*(1), 1–14.
<https://doi.org/10.1007/s13201-019-1122-6>
- Jang, J.S.R., Sun, C. T., & Mizutani, E. (1997). *Neurofuzzy and Soft Computing: A Computational Approach to Learning and Machine Intelligence*. PrenticeHall.
- Jang, Jyh Shing Roger. (1993). ANFIS: Adaptive-Network-Based Fuzzy Inference System. *IEEE Transactions on Systems, Man and Cybernetics*, *23*(3), 665–685.
<https://doi.org/10.1109/21.256541>
- Jia, Q. Y., & Sun, F. H. (2012). Modeling and forecasting process using the HBV model in Liao river delta. *Procedia Environmental Sciences*, *13*, 122–128.
<https://doi.org/10.1016/j.proenv.2012.01.012>
- Joyce, R. J., Janowiak, J. E., Arkin, P. A., & Xie, P. (2004). CMORPH: A method that produces global precipitation estimation from passive microwave and infrared data at high spatial and temporal resolution. *J. Hydrometeorol.*, *5*, 487–503,.
- Joyce, Robert J., Janowiak, J. E., Arkin, P. A., & Xie, P. (2004). CMORPH: A method that produces global precipitation estimates from passive microwave and infrared data at high spatial and temporal resolution. *Journal of Hydrometeorology*, *5*(3), 487–503. [https://doi.org/10.1175/1525-7541\(2004\)005<0487:CAMTPG>2.0.CO;2](https://doi.org/10.1175/1525-7541(2004)005<0487:CAMTPG>2.0.CO;2)
- Kalteh, A. M. (2013). Monthly river flow forecasting using artificial neural network and support vector regression models coupled with wavelet transform. *Computers and*

- Geosciences*, 54, 1–8. <https://doi.org/10.1016/j.cageo.2012.11.015>
- Kasiviswanathan, K. S., Cibin, R., Sudheer, K. P., & Chaubey, I. (2013). Constructing prediction interval for artificial neural network rainfall runoff models based on ensemble simulations. *Journal of Hydrology*, 499, 275–288. <https://doi.org/10.1016/j.jhydrol.2013.06.043>
- Kazemi, H., Sarukkalghe, R., & Badrzadeh, H. (2019). Evaluation of streamflow changes due to climate variation and human activities using the Budyko approach. *Environmental Earth Sciences*, 78(24), 12665. <https://doi.org/10.1007/s12665-019-8735-9>
- Kiran, N. R., & Ravi, V. (2008). Software reliability prediction by soft computing techniques. *Journal of Systems and Software*, 81(4), 576–583.
- Kisi, O., Shiri, J., & Tombul, M. (2013). Modeling rainfall-runoff process using soft computing techniques. *Computers and Geosciences*, 51, 108–117. <https://doi.org/10.1016/j.cageo.2012.07.001>
- Kumar, A., Singh, R., Jena, P. P., Chatterjee, C., & Mishra, A. (2015). Identification of the best multi-model combination for simulating river discharge. *Journal of Hydrology*, 525, 313–325. <https://doi.org/10.1016/j.jhydrol.2015.03.060>
- Kurtulus, B., & Razack, M. (2010). Modeling daily discharge responses of a large karstic aquifer using soft computing methods: Artificial neural network and neuro-fuzzy. *Journal of Hydrology*, 381(1–2), 101–111. <https://doi.org/10.1016/j.jhydrol.2009.11.029>
- Kwin, C. T., Talei, A., Alaghmand, S., & Chua, L. H. C. (2016). Rainfall-runoff Modeling Using Dynamic Evolving Neural Fuzzy Inference System with Online Learning. *Procedia Engineering*, 154, 1103–1109. <https://doi.org/10.1016/j.proeng.2016.07.518>
- Le, M. H., Lakshmi, V., Bolten, J., & Bui, D. Du. (2020). Adequacy of Satellite-derived Precipitation Estimate for Hydrological Modeling in Vietnam Basins. *Journal of Hydrology*, 586(February), 124820. <https://doi.org/10.1016/j.jhydrol.2020.124820>
- Lemma, H., Nyssen, J., Frankl, A., Poesen, J., Adgo, E., & Billi, P. (2019). Bedload transport measurements in the Gilgel Abay River, Lake Tana Basin, Ethiopia. *Journal of Hydrology*, 577(July), 123968.

<https://doi.org/10.1016/j.jhydrol.2019.123968>

- Leong, M., & Yang, X. (2020). Effect of rainfall station density, distribution and missing values on SWAT outputs in tropical region. *Journal of Hydrology*, 584(September 2019), 124660. <https://doi.org/10.1016/j.jhydrol.2020.124660>
- Li, D., Christakos, G., Ding, X., & Wu, J. (2018). Adequacy of TRMM satellite rainfall data in driving the SWAT modeling of Tiaoxi catchment (Taihu lake basin, China). *Journal of Hydrology*, 556, 1139–1152. <https://doi.org/10.1016/j.jhydrol.2017.01.006>
- Lindström, G., Johansson, B., Persson, M., Gardelin, M., & Bergström, S. (1997). Development and test of the distributed HBV-96 hydrological model. *Journal of Hydrology*, 201(1997), 272–288.
- Liu, S., Xu, J., Zhao, J., Xie, X., & Zhang, W. (2014). Efficiency enhancement of a process-based rainfall-runoff model using a new modified AdaBoost.RT technique. *Applied Soft Computing Journal*, 23, 521–529. <https://doi.org/10.1016/j.asoc.2014.05.033>
- Ma, Y., Yang, Y., Han, Z., Tang, G., Maguire, L., Chu, Z., & Hong, Y. (2018). Comprehensive evaluation of Ensemble Multi-Satellite Precipitation Dataset using the Dynamic Bayesian Model Averaging scheme over the Tibetan plateau. *Journal of Hydrology*, 556, 634–644. <https://doi.org/10.1016/j.jhydrol.2017.11.050>
- Makridakis, S., Andersen, A., Carbone, R., Fildes, R., Hibon, M., Lewandowski, R., Newton, J., Parzen, E., & Winkler, R. (1982). The accuracy of extrapolation (time series) methods: results of a forecasting competition. *Journal of Forecasting*, 1(111–153).
- Mamdani, E. H., & Assilian, S. (1975). An experiment in linguistic synthesis with a fuzzy logic controller. *International Journal of Man Machine Studies*, 7(1), 1–13.
- Mandal, A., Stephenson, T. S., Brown, A. A., Campbell, J. D., Taylor, M. A., & Lumsden, T. L. (2016). Rainfall-runoff simulations using the CARIWIG Simple Model for Advection of Storms and Hurricanes and HEC-HMS: Implications of Hurricane Ivan over the Jamaica Hope River watershed. *Natural Hazards*, 83(3), 1635–1659. <https://doi.org/10.1007/s11069-016-2380-3>
- Mathias, S. A., McIntyre, N., & Oughton, R. H. (2016). A study of non-linearity in

- rainfall-runoff response using 120 UK catchments. *Journal of Hydrology*, 540, 423–436. <https://doi.org/10.1016/j.jhydrol.2016.06.039>
- Noori, R., Safavi, S., & Nateghi Shahrokni, S. A. (2013). A reduced-order adaptive neuro-fuzzy inference system model as a software sensor for rapid estimation of five-day biochemical oxygen demand. *Journal of Hydrology*, 495, 175–185. <https://doi.org/10.1016/j.jhydrol.2013.04.052>
- Nourani, V. (2017). An Emotional ANN (EANN) approach to modeling rainfall-runoff process. *Journal of Hydrology*, 544, 267–277. <https://doi.org/10.1016/j.jhydrol.2016.11.033>
- Nourani, V., Alami, M. T., & Aminfar, M. H. (2009). A combined neural-wavelet model for prediction of Ligvanchai watershed precipitation. *Engineering Applications of Artificial Intelligence*, 22(3), 466–472. <https://doi.org/10.1016/j.engappai.2008.09.003>
- Nourani, V., Elkiran, G., & Abdullahi, J. (2019). Multi-station artificial intelligence based ensemble modeling of reference evapotranspiration using pan evaporation measurements. *Journal of Hydrology*, 577(March), 123958. <https://doi.org/10.1016/j.jhydrol.2019.123958>
- Nourani, V., Elkiran, G., Abdullahi, J., & Tahsin, A. (2019). Multi-region Modeling of Daily Global Solar Radiation with Artificial Intelligence Ensemble. *Natural Resources Research*, 28(4), 1217–1238. <https://doi.org/10.1007/s11053-018-09450-9>
- Nourani, V., Gokcekus, H., & Gelete, G. (2021). Estimation of Suspended Sediment Load Using Artificial Intelligence-Based Ensemble Model. *Complexity*, 2021. <https://doi.org/10.1155/2021/6633760>
- Nourani, V., Gökçekuş, H., & Gichamo, T. (2021). Ensemble data-driven rainfall-runoff modeling using multi-source satellite and gauge rainfall data input fusion. *Earth Science Informatics*. <https://doi.org/10.1007/s12145-021-00615-4>
- Nourani, V., Gökçekuş, H., & Umar, I. K. (2020). Artificial intelligence based ensemble model for prediction of vehicular traffic noise. *Environmental Research*, 180(October 2019), 108852. <https://doi.org/10.1016/j.envres.2019.108852>
- Nourani, V., Hosseini, A., Adamowski, J., & Gebremichael, M. (2013). Using self-

- organizing maps and wavelet transforms for space – time pre-processing of satellite precipitation and runoff data in neural network based rainfall – runoff modeling. *Journal of Hydrology*, 476, 228–243. <https://doi.org/10.1016/j.jhydrol.2012.10.054>
- Nourani, V., Kisi, Ö., & Komasi, M. (2011). Two hybrid Artificial Intelligence approaches for modeling rainfall – runoff process. *Journal of Hydrology*, 402(1–2), 41–59. <https://doi.org/10.1016/j.jhydrol.2011.03.002>
- Nourani, V., & Komasi, M. (2013). A geomorphology-based ANFIS model for multi-station modeling of rainfall-runoff process. *Journal of Hydrology*, 490, 41–55. <https://doi.org/10.1016/j.jhydrol.2013.03.024>
- Nourani, V., & Sayyah Fard, M. (2012). Sensitivity analysis of the artificial neural network outputs in simulation of the evaporation process at different climatologic regimes. *Advances in Engineering Software*, 47(1), 127–146. <https://doi.org/10.1016/j.advengsoft.2011.12.014>
- Ochoa, A., Pineda, L., Crespo, P., & Willems, P. (2014). Evaluation of TRMM 3B42 precipitation estimates and WRF retrospective precipitation simulation over the Pacific-Andean region of Ecuador and Peru. *Hydrol. Earth Syst. Sci.*, 18, 3179–3193. <https://doi.org/http://dx.doi.org/10.5194/hess-18-3179-2014>
- Pervin, L., Gan, T. Y., Scheepers, H., & Islam, M. S. (2021). Application of the HBV model for the future projections of water levels using dynamically downscaled global climate model data. *Journal of Water and Climate Change*, 12(6), 2364–2377. <https://doi.org/10.2166/wcc.2021.302>
- Piotrowski, A. P., & Napiorkowski, J. J. (2013). A comparison of methods to avoid overfitting in neural networks training in the case of catchment runoff modelling. *Journal of Hydrology*, 476, 97–111. <https://doi.org/10.1016/j.jhydrol.2012.10.019>
- Prakash, S., Mitra, A. K., Aghakouchak, A., Liu, Z., Norouzi, H., & Pai, D. S. (2018). A preliminary assessment of GPM-based multi-satellite precipitation estimates over a monsoon dominated region. *Journal of Hydrology*, 556(February 2014), 865–876. <https://doi.org/10.1016/j.jhydrol.2016.01.029>
- Rajae, T. (2011). Wavelet and ANN combination model for prediction of daily suspended sediment load in rivers. *Science of the Total Environment*, 409(15), 2917–2928. <https://doi.org/10.1016/j.scitotenv.2010.11.028>

- Rajurkar, M. P., Kothyari, U. C., & Chaube, U. C. (2004). Modeling of the daily rainfall-runoff relationship with artificial neural network. *Journal of Hydrology*, 285(1–4), 96–113. <https://doi.org/10.1016/j.jhydrol.2003.08.011>
- Reza Eini, M., Javadi, S., Delavar, M., Gassman, P. W., & Jarihani, B. (2020). Development of alternative SWAT-based models for simulating water budget components and streamflow for a karstic-influenced watershed. *Catena*, 195(January), 104801. <https://doi.org/10.1016/j.catena.2020.104801>
- Salas, J. D., Delleur, J. W., Yevjevich, V., & Lane, W. L. (1980). *Applied Modeling of Hydrological Time Series*, (first ed.). Water Resources Publications.
- Sardoii, E. R., Rostami, N., Sigaroudi, S. K., & Taheri, S. (2012). Calibration of loss estimation methods in HEC-HMS for simulation of surface runoff (case study: Amirkabir dam watershed, Iran). *Advances in Environmental Biology*, 6(1), 343–348.
- Seong, C.-H., Kim, S.-M., & Park, S.-W. (2008). A Comparative Study of Unit Hydrograph Models for Flood Runoff Simulation at a Small Watershed. In *Journal of The Korean Society of Agricultural Engineers* (Vol. 50, Issue 3, pp. 17–27). <https://doi.org/10.5389/ksae.2008.50.3.017>
- Setegn, S. G., Srinivasan, R., & Dargahi, B. (2008). Hydrological Modelling in the Lake Tana Basin, Ethiopia Using SWAT Model. *The Open Hydrology Journal*, 2(1), 49–62. <https://doi.org/10.2174/1874378100802010049>
- Shamseldin, A. Y., & Connor, K. M. O. (1999). A real-time combination method for the outputs of different rainfall-runoff models. *Hydrological Sciences Journal*, 44(6), 895–912. <https://doi.org/10.1080/02626669909492288>
- Shamseldin, A. Y., Connor, K. M. O., & Liang, G. C. (1997). Methods for combining the outputs of different rainfall – runoff models. *Journal of Hydrology*, 197, 203–229.
- Sharghi, E., Nourani, V., & Behfar, N. (2018a). Earthfill dam seepage analysis using ensemble artificial intelligence based modeling. *Journal of Hydroinformatics*, jh2018151. <https://doi.org/10.2166/hydro.2018.151>
- Sharghi, E., Nourani, V., & Behfar, N. (2018b). Earthfill dam seepage analysis using ensemble artificial intelligence based modeling. *Journal of Hydroinformatics*,

- 20(5), 1071–1084. <https://doi.org/10.2166/hydro.2018.151>
- Shi, B., Wang, P., Jiang, J., & Liu, R. (2018). Applying high-frequency surrogate measurements and a wavelet-ANN model to provide early warnings of rapid surface water quality anomalies. *Science of the Total Environment*, 610–611, 1390–1399. <https://doi.org/10.1016/j.scitotenv.2017.08.232>
- Si, J., Feng, Q., Wen, X., Xi, H., Yu, T., Li, W., & Zhao, C. (2015). Modeling soil water content in extreme arid area using an adaptive neuro-fuzzy inference system. *Journal of Hydrology*, 527, 679–687. <https://doi.org/10.1016/j.jhydrol.2015.05.034>
- Singh, V., Bankar, N., Salunkhe, S. S., Bera, A. K., & Sharma, J. R. (2013). Hydrological stream flow modelling on tungabhadra catchment: Parameterization and uncertainty analysis using SWAT CUP. *Current Science*, 104(9), 1187–1199.
- Srinivasulu, S., & Jain, A. (2006). A comparative analysis of training methods for artificial neural network rainfall-runoff models. *Applied Soft Computing Journal*, 6(3), 295–306. <https://doi.org/10.1016/j.asoc.2005.02.002>
- Stanley Raj, A., Hudson Oliver, D., Srinivas, Y., & Viswanath, J. (2017). Wavelet based analysis on rainfall and water table depth forecasting using Neural Networks in Kanyakumari district, Tamil Nadu, India. *Groundwater for Sustainable Development*, 5(May), 178–186. <https://doi.org/10.1016/j.gsd.2017.06.009>
- Takagi, T., & Sugeno, M. (1985). Fuzzy identification of systems and its application to modeling and control. *IEEE Transactions on System*, 15 (1),. *Man and Cybernetics*, 15(1), 116–132.
- Talei, A., Chua, L. H. C., Quek, C., & P.E. Jansson. (2013). Runoff forecasting using a Takagi-Sugeno neuro-fuzzy model with online learning. *J. Hydrol.*, 488, 17–32.
- Talei, Amin, Chua, L. H. C., & Wong, T. S. W. (2010). Evaluation of rainfall and discharge inputs used by Adaptive Network-based Fuzzy Inference Systems (ANFIS) in rainfall-runoff modeling. *Journal of Hydrology*, 391(3–4), 248–262. <https://doi.org/10.1016/j.jhydrol.2010.07.023>
- Talei, Amin, Hock, L., Chua, C., & Quek, C. (2010). A novel application of a neuro-fuzzy computational technique in event-based rainfall – runoff modeling. *Expert Systems With Applications*, 37(12), 7456–7468. <https://doi.org/10.1016/j.eswa.2010.04.015>

- Tang, L., & Hossain, F. (2012). Investigating the similarity of satellite rainfall error metrics as a function of Koppen climate classification. *Atmospheric Research*, *104*(105), 182–192.
- Tapiador, F. J., Turk, F. J., Petersen, W., Hou, A. Y., Garcia-Ortega, E., Machado, L. A. T., Angelis, C. F., Salio, P., Kidd, C., Huffman, G. J., & de Castro, M. (2012). Global precipitation measurement: methods, datasets and applications. *Atmos. Res.*, *104*(105), 70–97.
- Te Chow, V. (1964). *Handbook of applied hydrology: a compendium of water-resources technology*.
- Thavhana, M. P., Savage, M. J., & Moeletsi, M. E. (2018). SWAT model uncertainty analysis, calibration and validation for runoff simulation in the Luvuvhu River catchment, South Africa. *Physics and Chemistry of the Earth*, *105*(January), 115–124. <https://doi.org/10.1016/j.pce.2018.03.012>
- Thorsten, W., Howard, W., & Hoshin, G. (2003). Rainfall-runoff modeling in gauged and ungauged catchments. In *Imperial Collage Press*. Imperial Collage Press.
- Tongal, H., & Booij, M. J. (2018). Simulation and forecasting of streamflows using machine learning models coupled with base flow separation. *Journal of Hydrology*, *564*(June), 266–282. <https://doi.org/10.1016/j.jhydrol.2018.07.004>
- Uhlenbrook, S., Mohamed, Y., & Gragne, A. S. (2010). Analyzing catchment behavior through catchment modeling in the Gilgel Abay, Upper Blue Nile River Basin, Ethiopia. *Hydrology and Earth System Sciences*, *14*(10), 2153–2165. <https://doi.org/10.5194/hess-14-2153-2010>
- Velázquez, J. A., Anctil, F., Ramos, M. H., & Perrin, C. (2011). Can a multi-model approach improve hydrological ensemble forecasting? A study on 29 French catchments using 16 hydrological model structures. *Advances in Geosciences*, *29*, 33–42. <https://doi.org/10.5194/adgeo-29-33-2011>
- Venkata Ramana, R., Krishna, B., Kumar, S. R., & Pandey, N. G. (2013). Monthly Rainfall Prediction Using Wavelet Neural Network Analysis. *Water Resources Management*, *27*(10), 3697–3711. <https://doi.org/10.1007/s11269-013-0374-4>
- Wale, A., Rientjes, T. H. M., Gieske, A. S. M., & Getachew, H. A. (2009). Ungauged catchment contributions to Lake Tana's water balance. *Hydrol. Process.*, *23*(26),

3682–3693.

- Wang, H., & Hu, D. (2005). Comparison of SVM and LS-SVM for regression. *Neural Netw Brain, 1*, 2079–2283.
- Wang, W. C., Xu, D. M., Chau, K. W., & Chen, S. (2013). Improved annual rainfall-runoff forecasting using PSO–SVM model based on EEMD. *J. Hydroinf., 15*(4), 1377–1390.
- Welde, K., & Gebremariam, B. (2017). International Soil and Water Conservation Research Effect of land use land cover dynamics on hydrological response of watershed : Case study of Tekeze Dam watershed , northern Ethiopia ☆. *International Soil and Water Conservation Research, 5*(1), 1–16.
<https://doi.org/10.1016/j.iswcr.2017.03.002>
- Wen, X., Si, J., He, Z., & Shao, H. (2015). Support-Vector-Machine-Based Models for Modeling Daily Reference Evapotranspiration With Limited Climatic Data in Extreme Arid Regions. *Water Resour Manage, 29*(July), 3195–3209.
<https://doi.org/10.1007/s11269-015-0990-2>
- Winkler, R. . (1983). Combining forecasts: a philosophical basis and some current issues. *Journal of Forecasting, 5*, 605–609.
- Wittwer, C. (2013). *WMO/UNESCO-IHP guideline for flood forecasting, Regional Workshop on hydrological forecasting and impact of climate change on water resources.*
- WMO, & Organization, W. M. (1992). Simulated real-time intercomparison of hydrological models. *Operational Hydrology, 38*.
- Worqlul, A. W., Yen, H., Collick, A. S., Tilahun, S. A., Langan, S., & Steenhuis, T. S. (2017). Catena Evaluation of CFSR , TMPA 3B42 and ground-based rainfall data as input for hydrological models , in data-scarce regions : The upper Blue Nile. *Catena, 152*, 242–251. <https://doi.org/10.1016/j.catena.2017.01.019>
- Yamashkin, S., Radovanovic, M., Yamashkin, A., & Vukovic, D. (2018). Using ensemble systems to study natural processes. *Journal of Hydroinformatics, 24*(4), 753–765.
- Yaseen, Z. M., Jaafar, O., Deo, R. C., Kisi, O., Adamowski, J., Quilty, J., & El-Shafie, A. (2016). Stream-flow forecasting using extreme learning machines: A case study

- in a semi-arid region in Iraq. *Journal of Hydrology*, 542, 603–614.
<https://doi.org/10.1016/j.jhydrol.2016.09.035>
- Yong, B., Liu, D., Gourley, J. J., Tian, Y., Huffman, G. J., Ren, L., & Hong, Y. (2015). Global view of real-time TRMM multisatellite precipitation analysis: implications for its successor global precipitation measurement mission. *Bull. Am. Meteorol. Soc.*, 96(283–296).
- Young, C. C., Liu, W. C., & Wu, M. C. (2017). A physically based and machine learning hybrid approach for accurate rainfall-runoff modeling during extreme typhoon events. *Applied Soft Computing Journal*, 53, 205–216.
<https://doi.org/10.1016/j.asoc.2016.12.052>
- Yu, P. S., Chen, S. T., & Chang, I. F. (2006). Support vector regression for real-time flood stage forecasting. *Journal of Hydrology*, 328(3–4), 704–716.
<https://doi.org/10.1016/j.jhydrol.2006.01.021>
- Zegelew, D. G., & Melesse, A. M. (2018). Applicability of a spatially semi-distributed hydrological model for watershed scale runoff estimation in Northwest Ethiopia. *Water (Switzerland)*, 10(7), 10–12. <https://doi.org/10.3390/w10070923>
- Zeynoddin, M., Bonakdari, H., Azari, A., Ebtehaj, I., Gharabaghi, B., & Riahi Madavar, H. (2018). Novel hybrid linear stochastic with non-linear extreme learning machine methods for forecasting monthly rainfall a tropical climate. *Journal of Environmental Management*, 222(May), 190–206.
<https://doi.org/10.1016/j.jenvman.2018.05.072>
- Zhang, G. P. (2003). Time series forecasting using a hybrid ARIMA and neural network model. *Neurocomputing*, 50, 159–175.
- Zhang, G. P., & Savenije, H. H. G. (2005). Rainfall-runoff modelling in a catchment with a complex groundwater flow system: Application of the Representative Elementary Watershed (REW) approach. *Hydrology and Earth System Sciences*, 9(3), 243–261. <https://doi.org/10.5194/hess-9-243-2005>
- Zhang, H., Wang, B., Liu, D. L., Zhang, M., Leslie, L. M., & Yu, Q. (2020). Using an improved SWAT model to simulate hydrological responses to land use change: A case study of a catchment in tropical Australia. *Journal of Hydrology*, 585(February), 124822. <https://doi.org/10.1016/j.jhydrol.2020.124822>

- Zhang, Q., Wang, B. D., He, B., Peng, Y., & Ren, M. L. (2011). Singular spectrum analysis and ARIMA hybrid model for annual runoff forecasting. *Manage. Water Resources*, 25, 2683–2703.
- Zhou, Y., Guo, S., & Chang, F. J. (2019). Explore an evolutionary recurrent ANFIS for modelling multi-step-ahead flood forecasts. *Journal of Hydrology*, 570(November 2018), 343–355. <https://doi.org/10.1016/j.jhydrol.2018.12.040>

APPENDIX 1

Curriculum Vitae



1. *Personal details*

| | |
|------------------|------------------------------------------------------------------|
| ❖ Name | Tagesse Gichamo Lafamo |
| ❖ Sex | Male |
| ❖ Place Of Birth | Hadiya Zone, Soro woreda, Ethiopia |
| ❖ Date Of Birth | Oct 12,1988 |
| ❖ Marital Status | Married |
| ❖ Nationality | Ethiopian |
| ❖ Address | Tagesse Gichamo Addis Abeba |
| | Telephone (Mobile) +251911285604 |
| | Email tagesseg@gmail.com |

2. *Educational background*

- Received MSc from Hawassa University (Water Resource Engineering and Management) with **CGAP of 3.82 at Nov 214**.
- Graduated BSc. From Wollega University (**Soil Resource and Watershed Management**) With **CGAP 3.81** at June 2011.
- Grade 11-12 Gimbichu Preparatory School at Gimbichu (2007/8)
- Grade 9-10 Gimbichu Preparatory School at Gimbichu (2005/6).
- Grade 1-8 Gimbichu Junior school at Gimbichu (1997/2004).

3. *Award received*

- Certificate from Cech Republic Development Cooperation on Research Proposal Preparation (Jan, 2014).

- Certificate of higher diploma program (HDP)/ Pedagogical skills from Adama science and Technology University (2012).
- Certificate of Research paper presentation from Dilla University, June, 2016
- Certificate of Research paper presentation from Hawassa University, Oct, 2016
- Certificate of Completion SWAT model from Addis Ababa Technology Institute, Jan, 2017
- Certificate of paper presentation on 11th international conference on green environment and sustainability, Dilla University, Ethiopia, May 2016,
- Certificate of paper presentation on 2nd international conference on natural resource management and food security, Hawassa University, Ethiopia, June 2015
- Certificate of paper presentation on 2nd International conference on Water problems in the Mediterranean Countries, Near East University, Cyprus. May, 2019

4. Additional courses

- Basic Computer Skills (Ms Word ,Excel ,Power Point)
- Advanced software's which are very important for water resource management and climate change such as SWAT, HEC-HMS, HBV, CROP WAT, EPANET, ERDAS IMAGINE, MODFLOW, MATLAB, and Arc GIS

5. Work experience

- Part-time Lecturer at Near East University Sep 2018 to Sep 2019
- Research Assistant at Near East University October 2019 to Present
- Lecturer and Researcher at Arsi University November 2014 to present
- Assistant Lecturer at Adama science and Technology University (2011- 2012)

6. Language

- Hadiyegna (Mother tongue)
- English – Proficient
- Amharic (Fluent speaker, Reading, Writing)
- Afan-Oromo (Fluent speaker, Reading, Writing)

7. Publications

1. Ensemble data-driven rainfall-runoff modeling using multi-source satellite and gauge rainfall data input fusion. *Earth Science Informatics* (<https://link.springer.com/article/10.1007/s12145-021-00615-4>)
2. Analysis of Water Balance and Hydrodynamics of Lake Beseka, Ethiopia. *Journal of Water and climate change* (<https://doi.org/10.2166/wcc.2022.323>)
3. Impact of climate change on the hydrology of Blue Nile basin, Ethiopia: a review. *Journal of Water and climate change* (<https://doi.org/10.2166/wcc.2019.014>)
4. Evaluating disinfection techniques of water treatment. *Desalination and Water Treatment* (https://www.deswater.com/DWT_articles/vol_177_papers/177_2020_408.pdf)
5. Interrelation between climate change and solid waste, A review, (<https://translateyar.ir/wp-content/uploads/2020/12/Interrelation-between-Climate-Change-and-Solid-Waste.pdf>)
6. Evaluation of different natural wastewater treatment alternatives by fuzzy PROMETHEE method. *Desalination and Water Treatment* (doi: 10.5004/dwt.2020.25049)
7. Ranking of Natural Wastewater Treatment Techniques by Multi-criteria Decision Making (MCDM) Methods (Book Chapter, Springer) (https://link.springer.com/chapter/10.1007/978-3-030-64765-0_11)
8. Evaluating Disinfection Techniques of Water Treatment Using Multi-criteria Decision-Making Method. (Book Chapter, Springer) (DOI: 10.1007/978-3-030-64765-0_12)
9. Ensemble rainfall-runoff modeling of physically-based semi-distributed models using multi-source rainfall data fusion (*ongoing*)
10. Ensemble rainfall-runoff modeling of Artificial-Intelligence and physically-based semi-distributed models using multi-source rainfall data fusion (*ongoing*)

8. Conferences Organized

- Member, Organization Committee, 2nd International conference on the environment survival and sustainability, 7 – 11 October 2019. Near East University, Nicosia, Cyprus.

- Member, Organization Committee, 2nd International conference on Water problems in the Mediterranean Countries (WPMC 2019), 06 – 10 May, 2019. Near East University, Nicosia, Cyprus.
- Member, Organization Committee, 2nd International conference on the Cyprus Issue: Past, Present and the Vision for the Future, 1 – 3 April, 2019. Near East University, Nicosia, Cyprus

9. Conferences participated

- Impacts of biogas plants on securing rural energy demands, presented on 11th international conference on green environment and sustainability, May 2016, Organized by Dilla University, Ethiopia
- Development of small scale irrigation schemes on food security of pro-poor farmers, presented on 2nd international conference on natural resource management and food security, June 2015, Organized by Hawassa University, Ethiopia
- Evaluation of different natural wastewater treatment alternatives by fuzzy PROMETHEE method presented on 2nd International conference on Water problems in the Mediterranean Countries (WPMC 2019), 06 – 10 May, 2019. Near East University, Nicosia, Cyprus.

10. Courses Thought (2011-2022):

- Irrigation Engineering
- Introduction to Water Resources Management
- Drainage Engineering.
- Soil and Water Conservation Engineering
- Fluid Mechanics
- Water Resource Engineering II
- Engineering Hydrology
- Engineering Geology
- Sanitation Engineering
- Unit operation
- Water Harvesting Technology
- Management of Irrigation water on Saline soils

Sports

Football and Ground tennis

HOBBIES

Reading, Hiking

APPENDIX 2

Graphical Presentation of Each Models Result

Figure 28

The results of SWAT Using Gauge and CMORPH Rainfall Datasets a) at Calibration, b) at Validation Phase

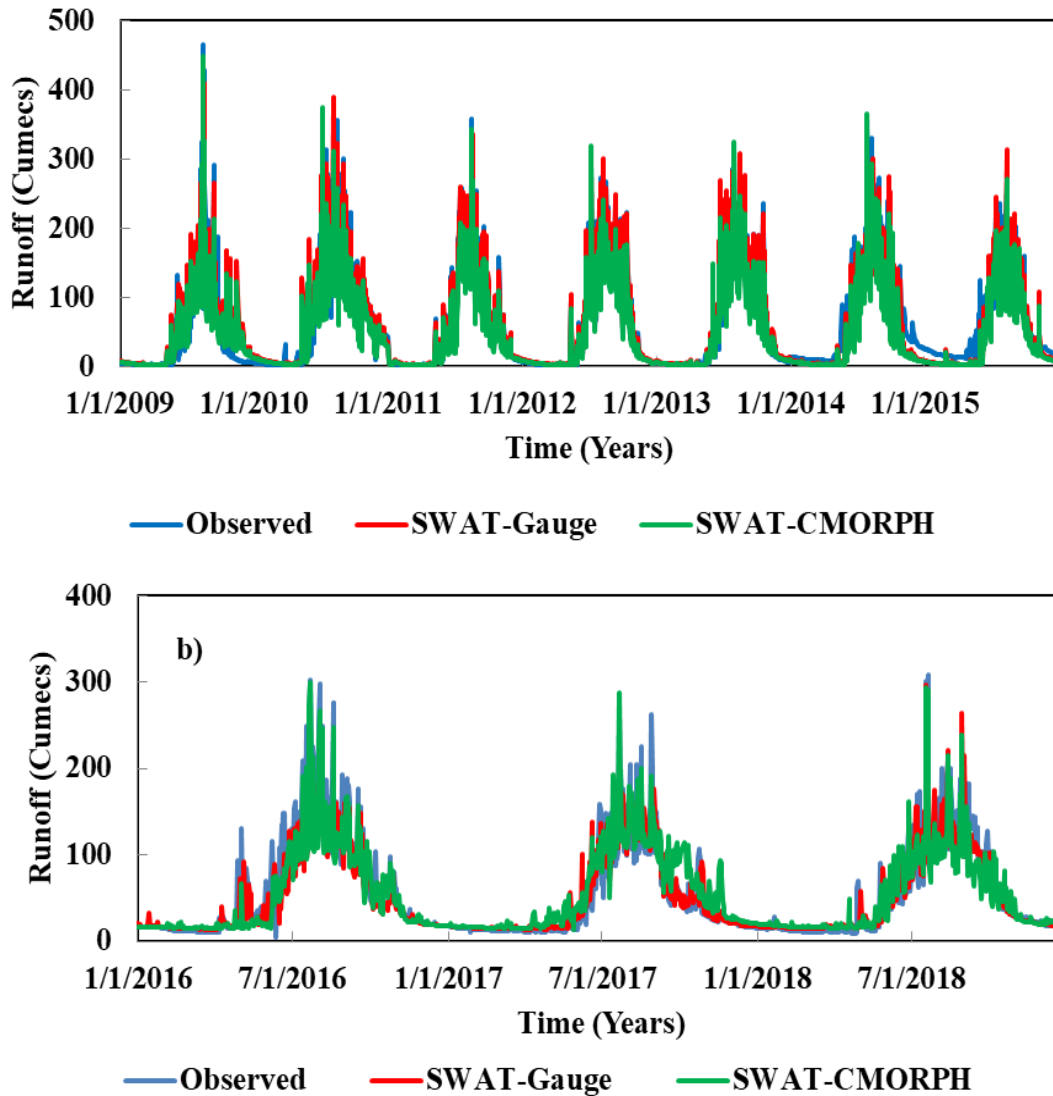


Figure 29

The Results of HEC-HMS Using Gauge and CMORPH Rainfall Datasets a) at Calibration, b) at Validation Phase

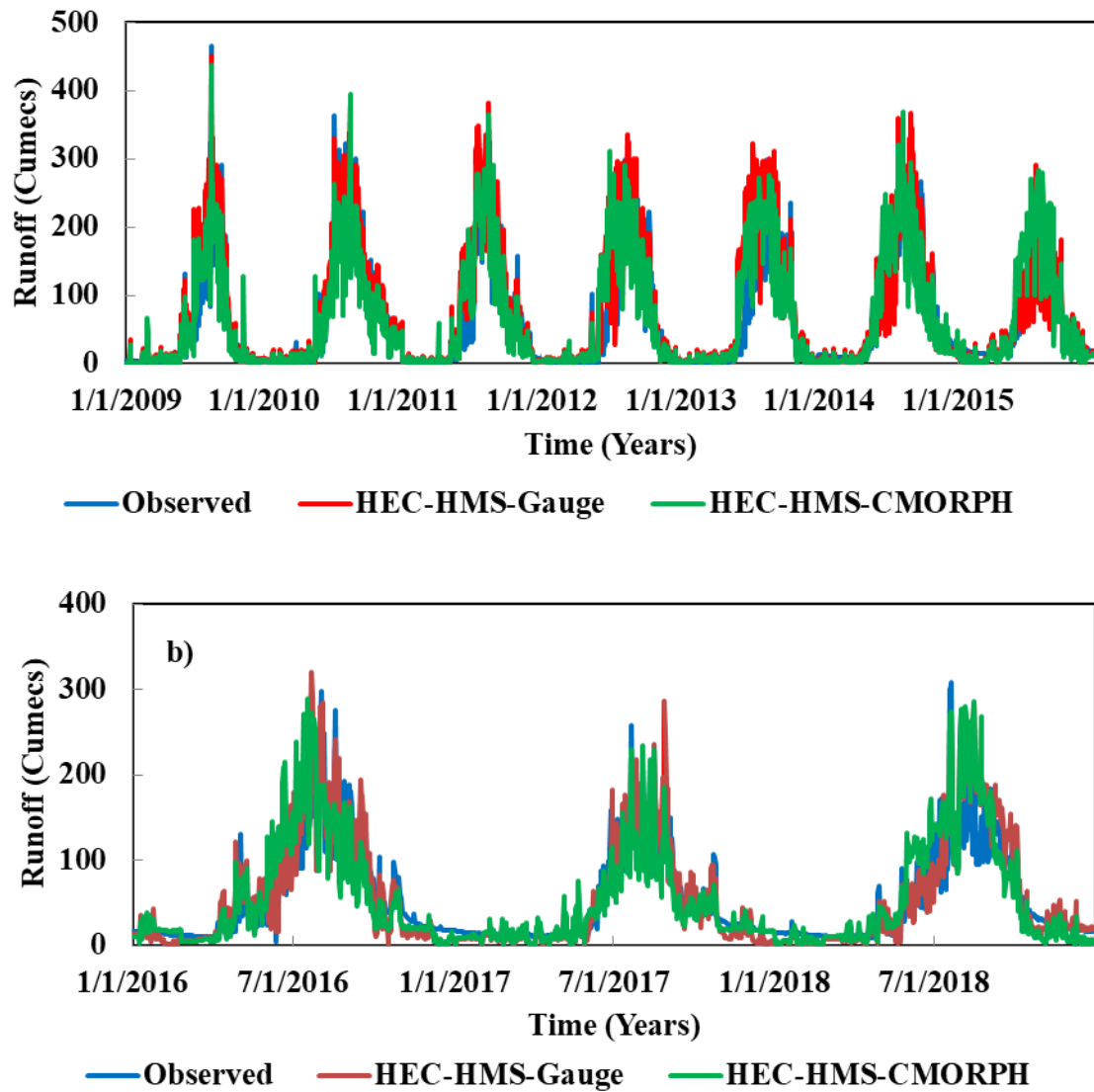


Figure 30

The Results of HBV Using Gauge and CMORPH Rainfall Datasets a) at Calibration, b) at Validation Phase

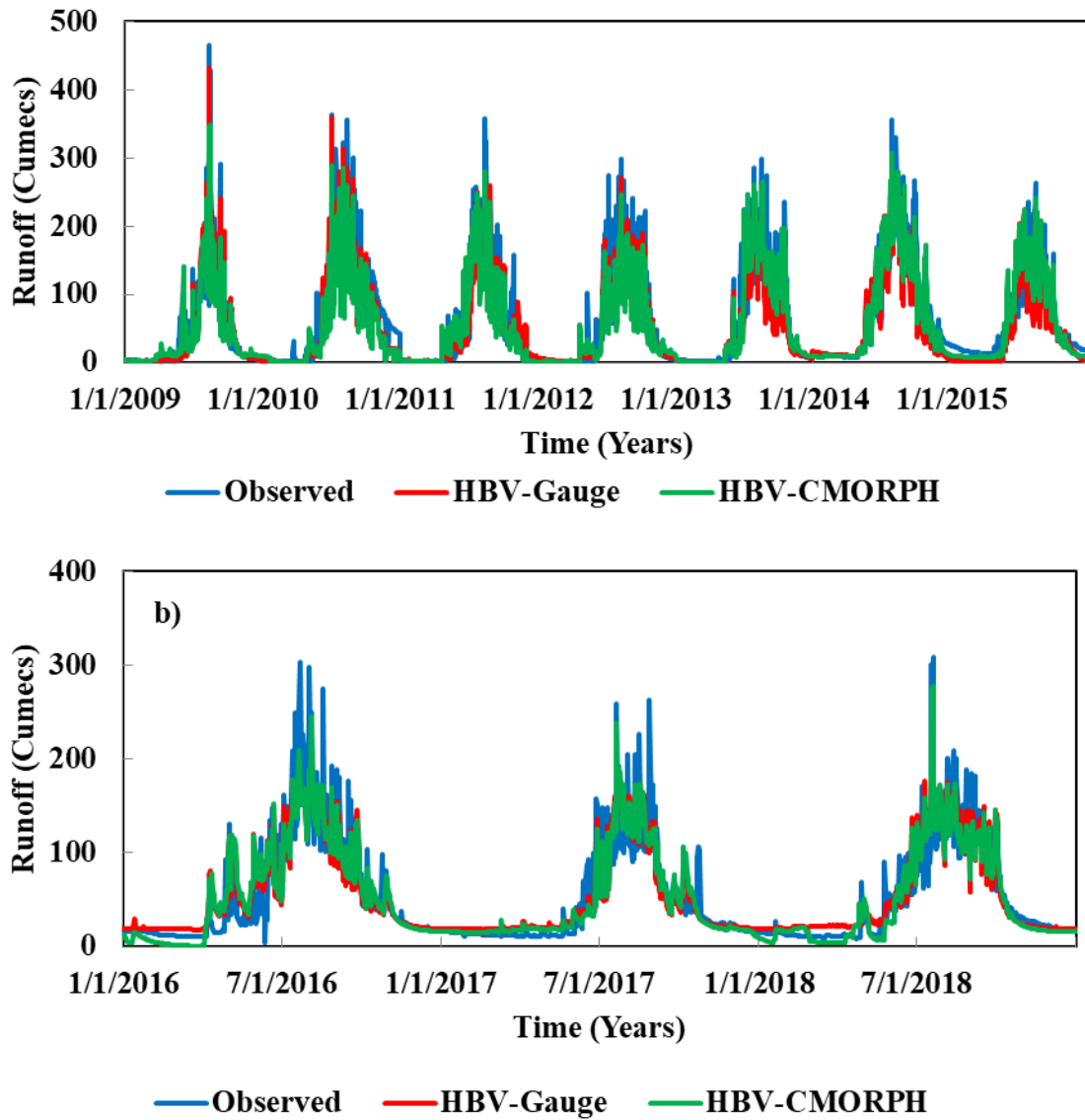


Figure 31

The Results of ANFIS Using Gauge and CMORPH Rainfall Datasets a) at Calibration, b) at Validation Phase

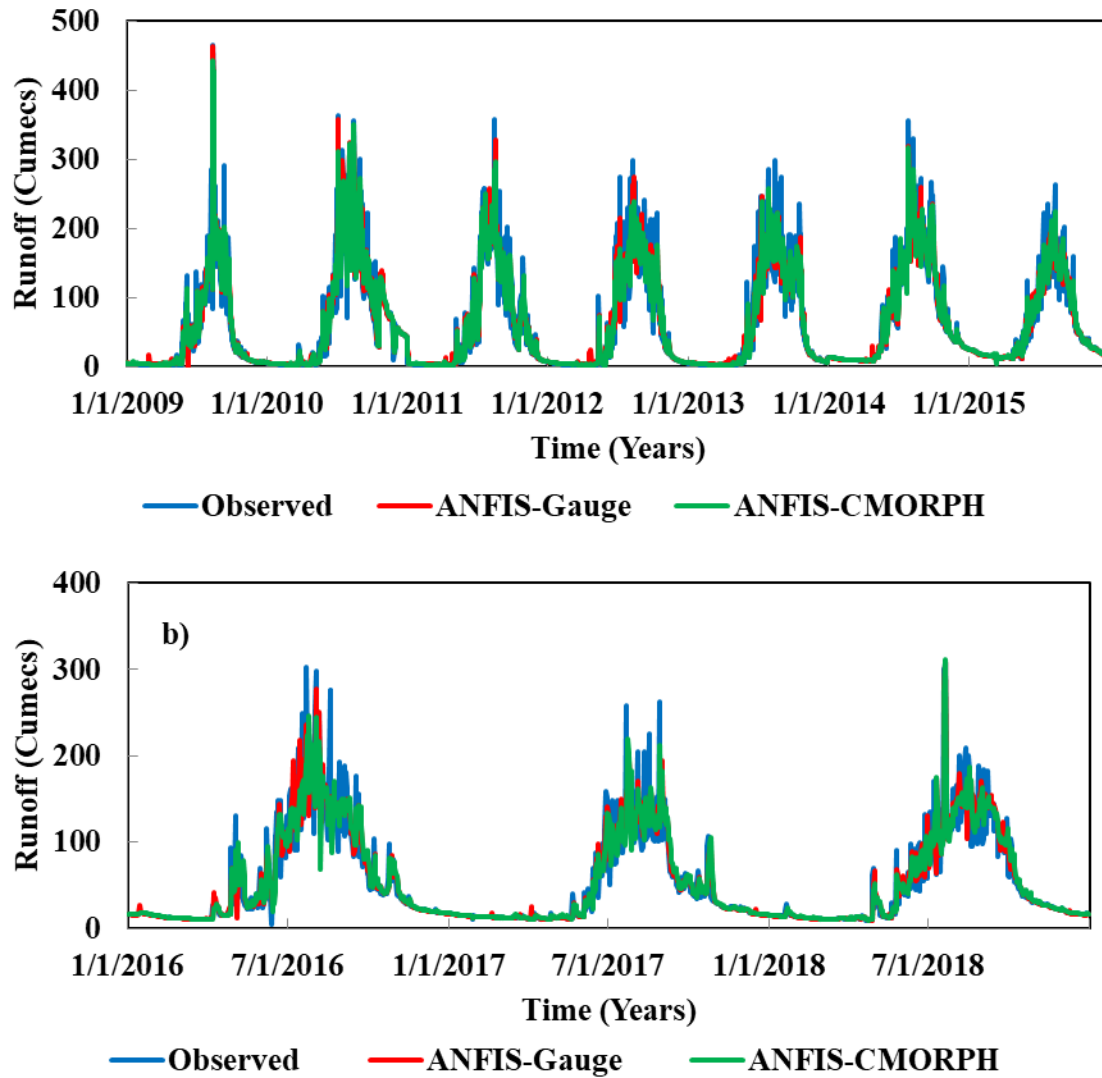


Figure 32

The Results of FFNN Using Gauge and CMORPH Rainfall Datasets a) at Calibration, b) at Validation Phase

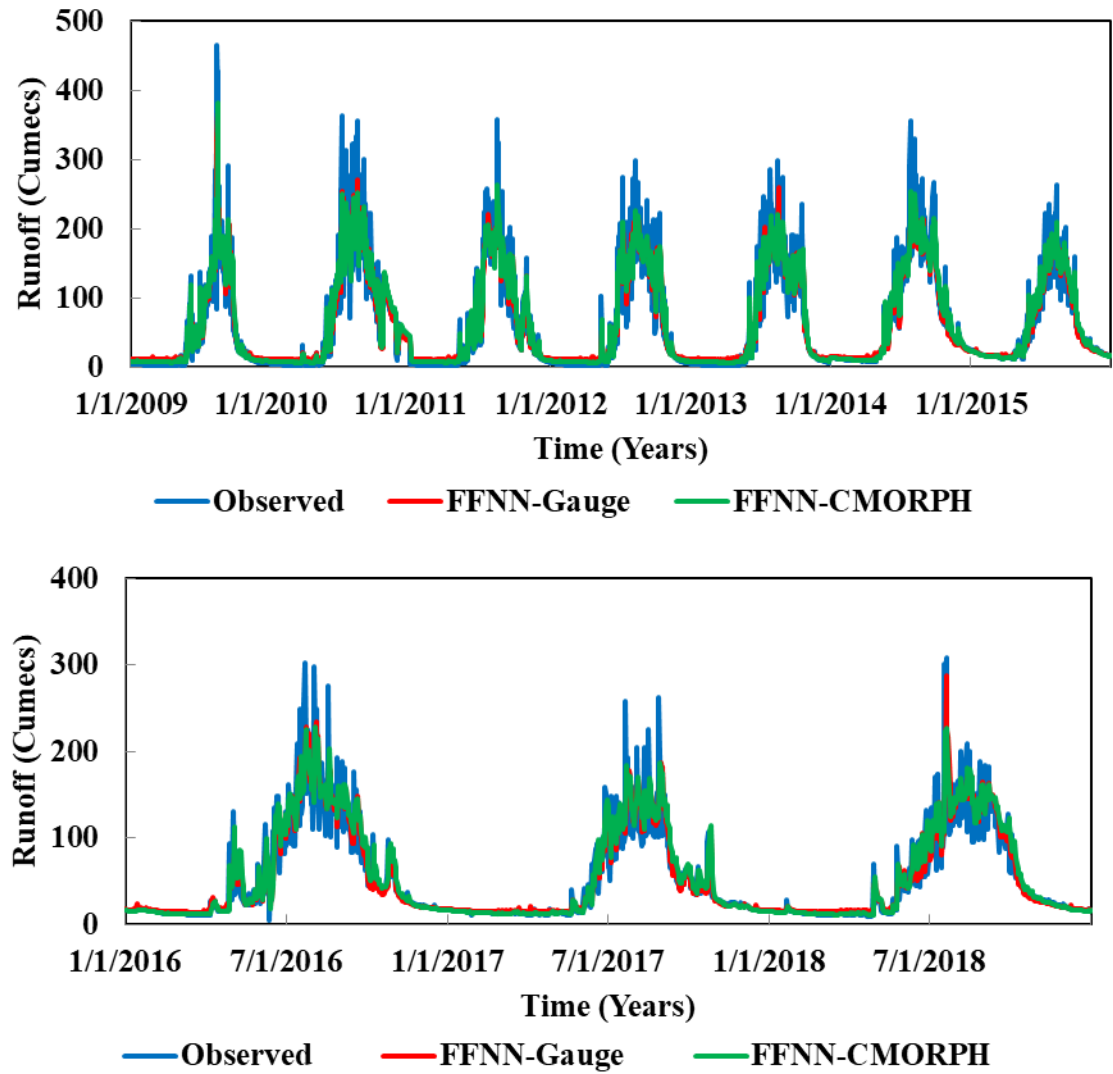
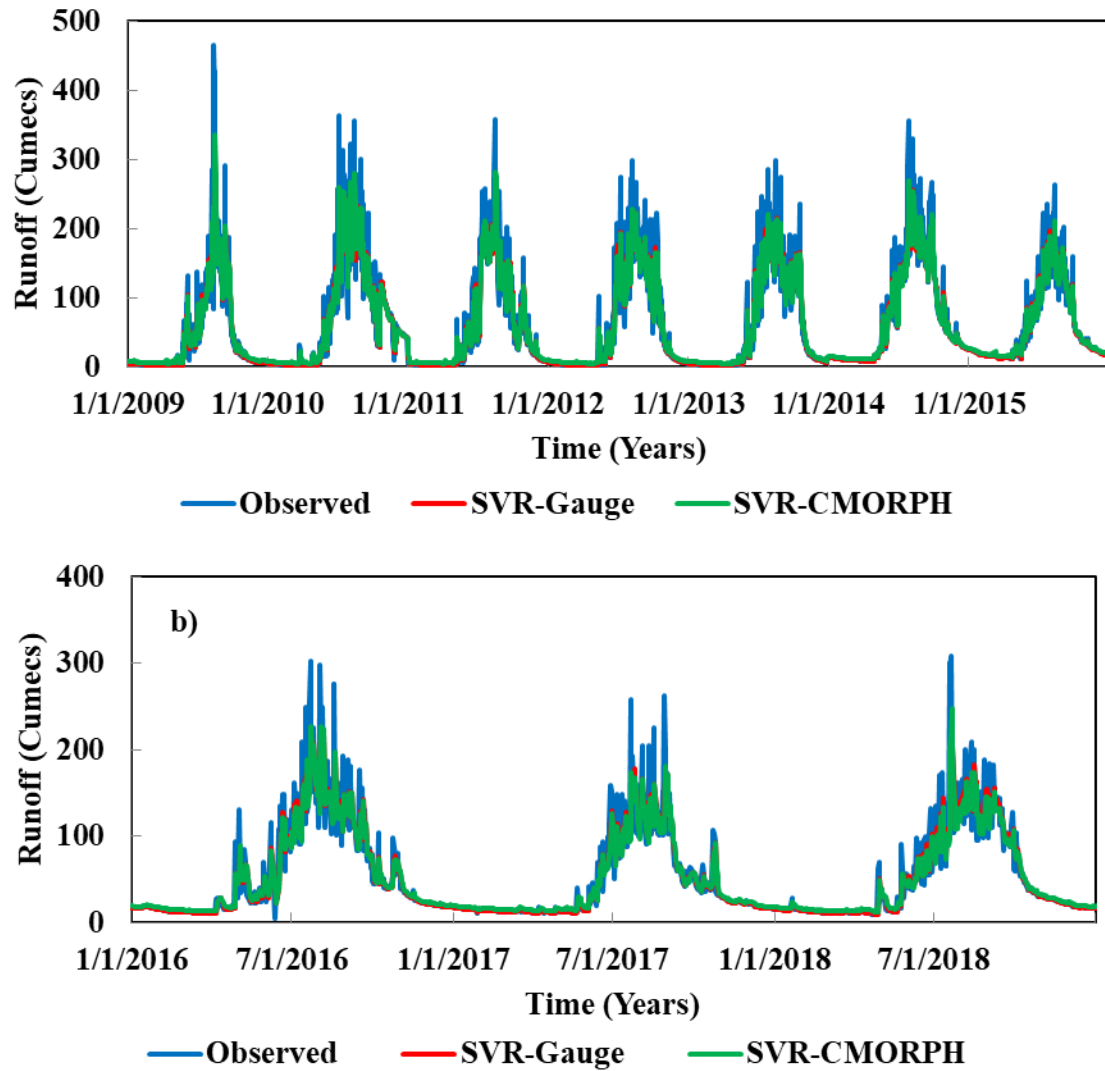


Figure 33

The Results of SVR Using Gauge and CMORPH Rainfall datasets a) at Calibration, b) at Validation Phase



APPENDIX 3

Graphical Summary of Raw Data

Figure 34

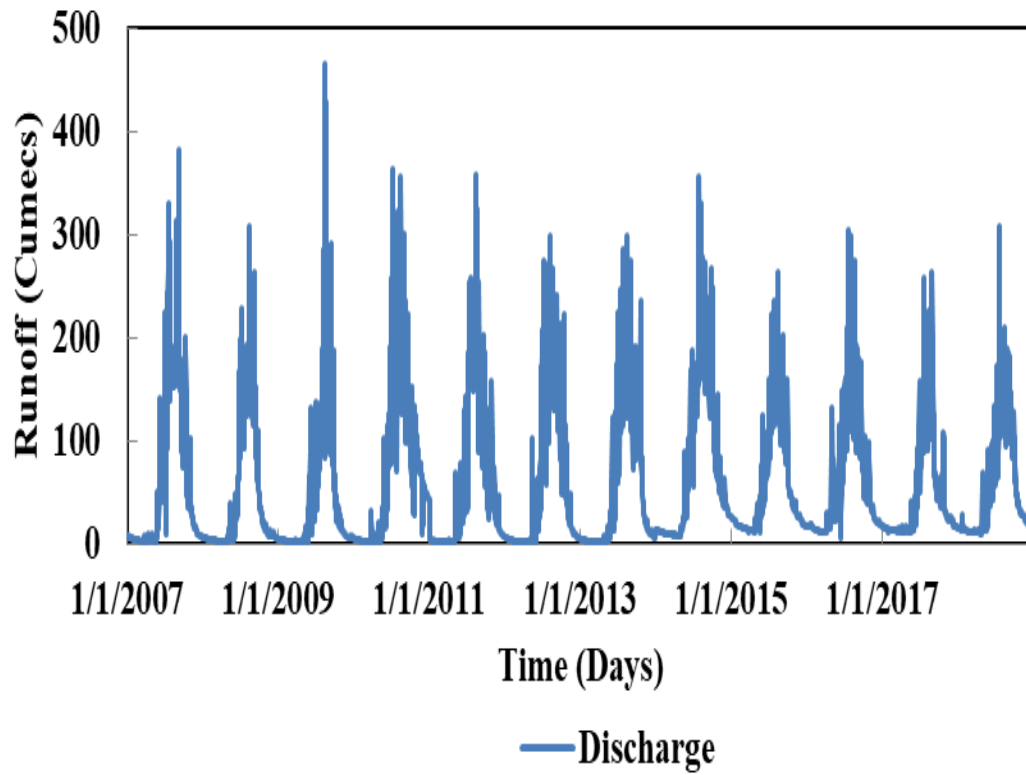
Discharge Time Series

Figure 35

Climatic Time Series of Dangila Station

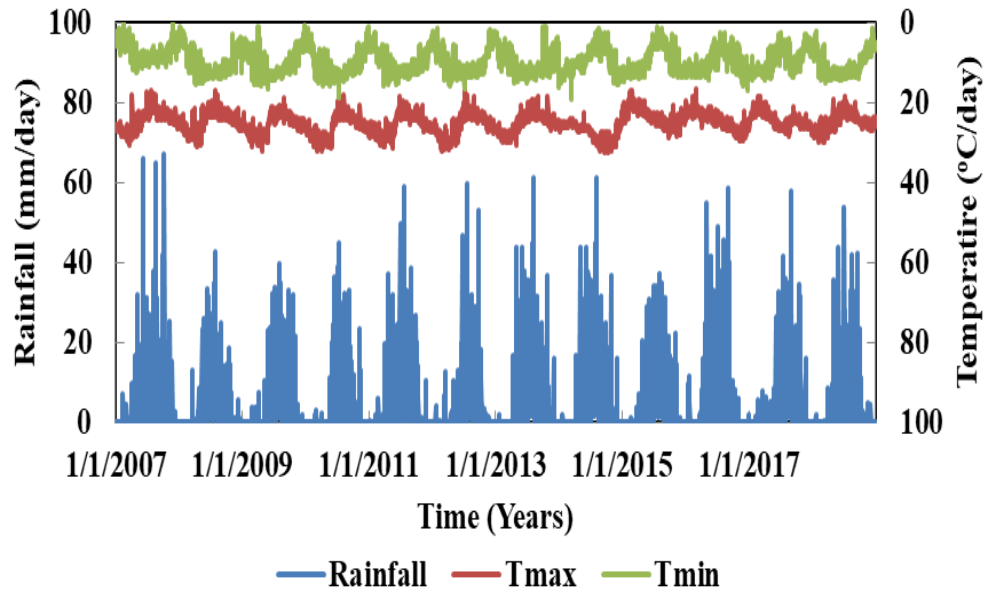


Figure 36

Climatic Time Series of Adet Station

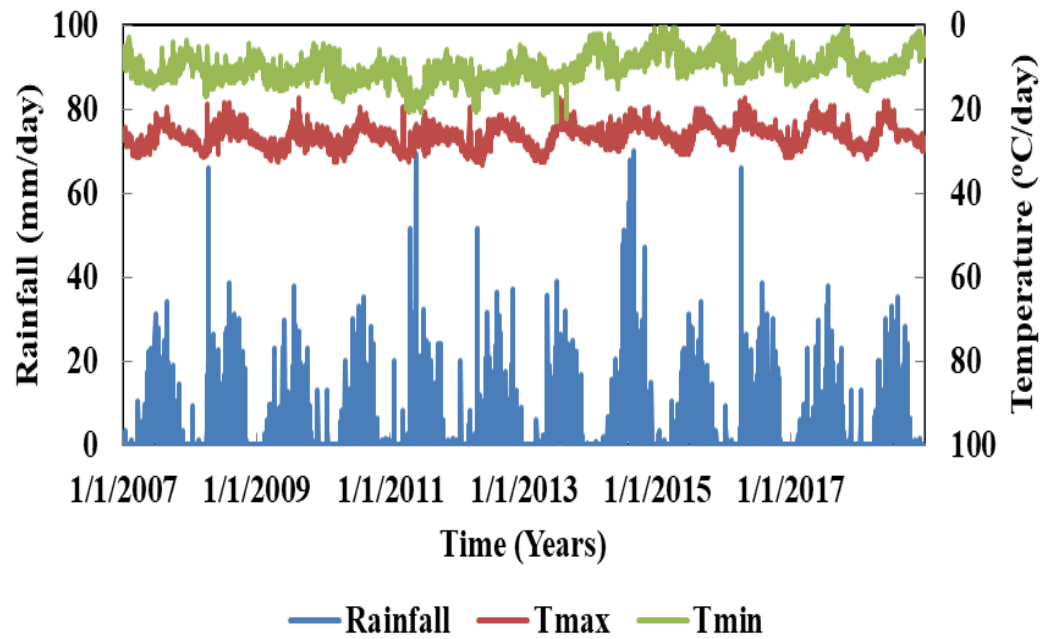


Figure 37

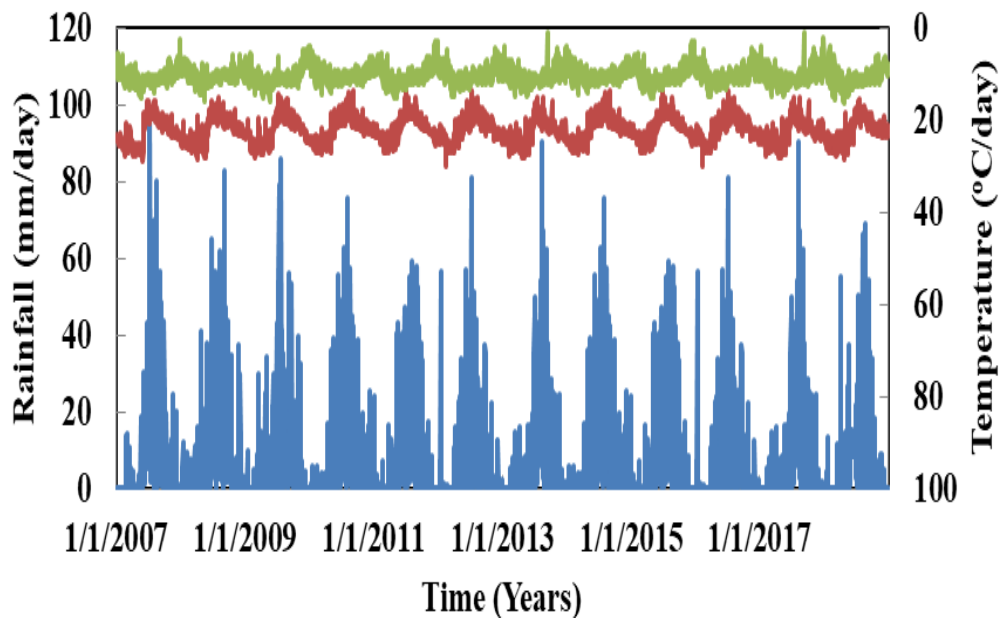
Climatic Time Series of Gundil Station

Figure 38

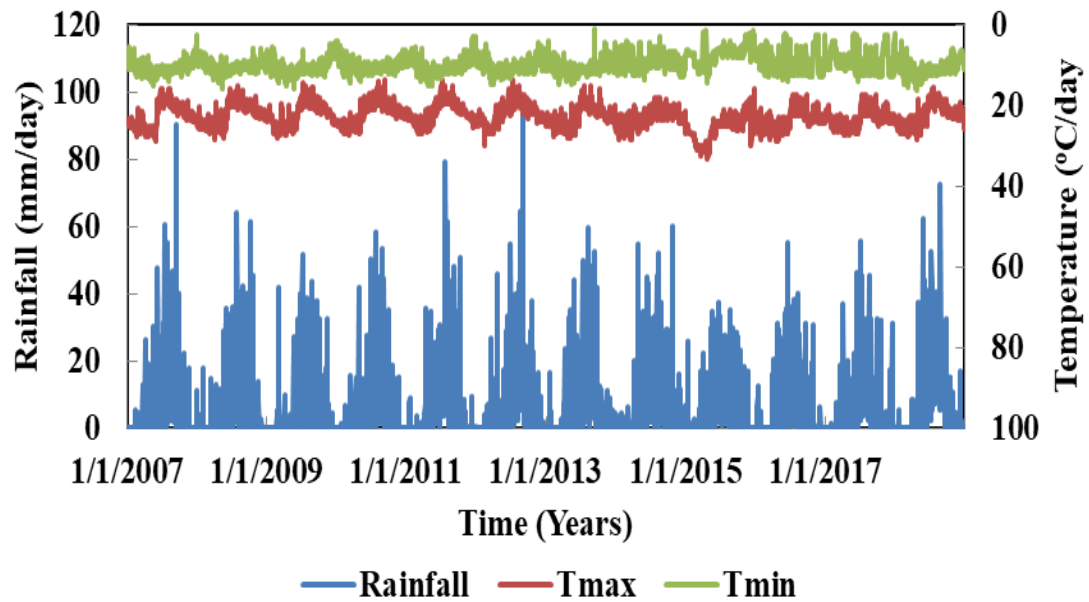
Climatic Time Series of Sekela Station

Figure 39

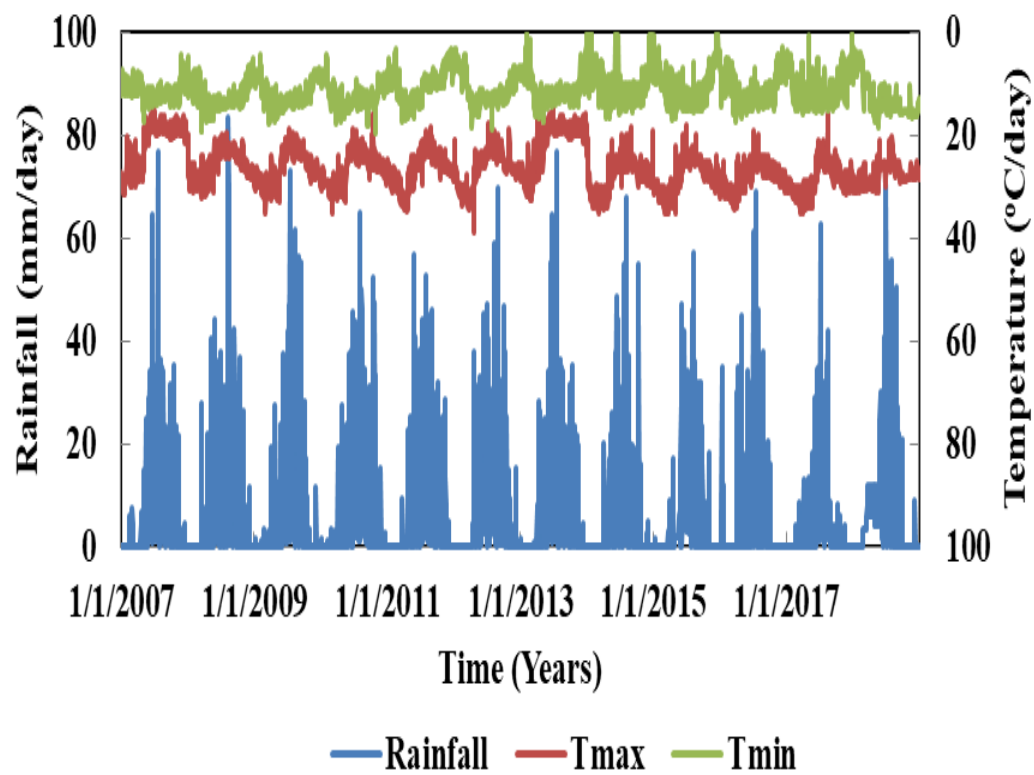
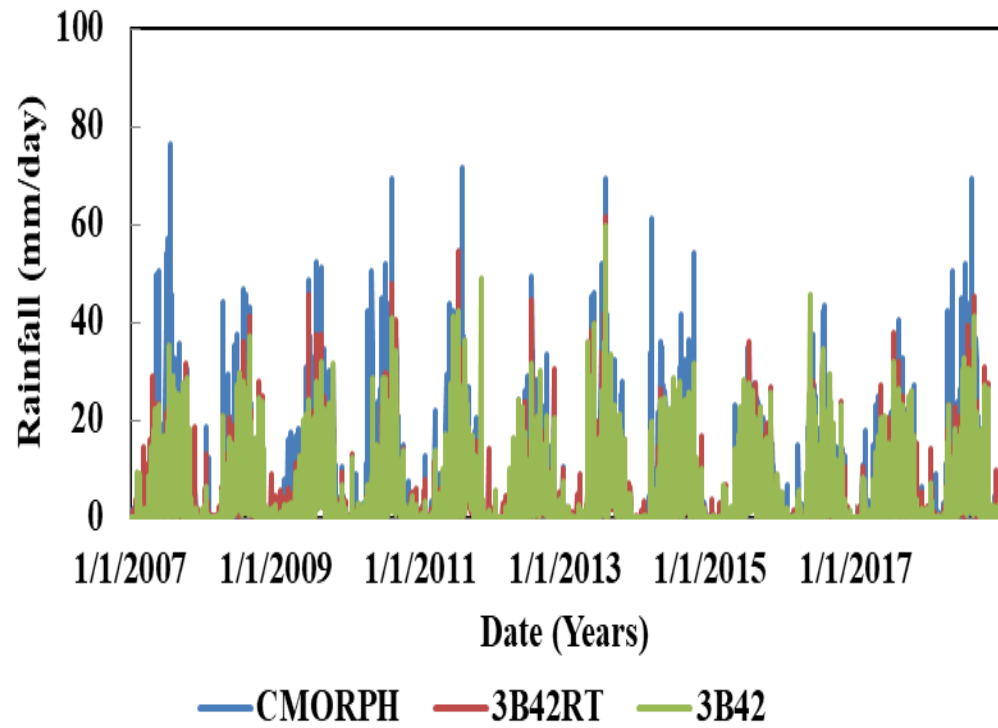
Climatic Time Series of Wetat Abay Station

Figure 40

Satellite Rainfall Time Series

APPENDIX 4

Ethical Approval Letter

Date: 6th June, 2022

To the Institute of Graduate Study

REFERENCE: TAGESSE GICHAMO LAFAMO (20176900)

I would like to inform you that the above candidate is one of our postgraduate students in Civil Engineering Department. He is taking thesis under my supervision and the thesis title is **“Ensemble Rainfall Ensemble Runoff Modeling Using Rain Gauge And Satellite Based Data, case of Gilgel Abay, Ethiopia.”** has been evaluated. Since the researcher(s) will not collect primary data from humans, animals, plants or earth, this project does not need to go through the ethics committee.

Please do not hesitate to contact me if you have any further queries or questions.

Thank you very much indeed.



Prof. Dr. Huseyin Gokcekus

Dean, Faculty of Civil and Environmental Engineering

Near East Boulevard, ZIP: 99138

Nicosia/TRNC, North Cyprus,

Mersin 10 – Turkey.

Email: huseyin.gokcekus@neu.edu.tr

APPENDIX 5

Similarity Report



Assignments Students Grade Book Libraries Calendar Discussion Preferences

NOW VIEWING: HOME > SIMILARITY CHECK > TAGESSE GICHAMO LAFAMO THESIS

About this page

This is your assignment inbox. To view a paper, select the paper's title. To view a Similarity Report, select the paper's Similarity Report icon in the similarity column. A ghosted icon indicates that the Similarity Report has not yet been generated.

Tagesse Gichamo Lafamo Thesis

INBOX | NOW VIEWING: NEW PAPERS ▾

| Submit File | | Online Grading Report Edit assignment settings Email non-submitters | | | | | | | |
|--------------------------|-------------------------|-------------------------------------------------------------------------|------------|-------|----------|------|------------|-------------|--|
| <input type="checkbox"/> | AUTHOR | TITLE | SIMILARITY | GRADE | RESPONSE | FILE | PAPER ID | DATE | |
| <input type="checkbox"/> | Tagesse Gichamo Lafa... | Abstract | 0% | -- | -- | | 1886311213 | 24-Aug-2022 | |
| <input type="checkbox"/> | Tagesse Gichamo Lafa... | Chapter VI Conclusion and Recommendation... | 0% | -- | -- | | 1885928062 | 23-Aug-2022 | |
| <input type="checkbox"/> | Tagesse Gichamo Lafa... | Chapter V Discussion | 3% | -- | -- | | 1885926958 | 23-Aug-2022 | |
| <input type="checkbox"/> | Tagesse Gichamo Lafa... | Chapter IV Findings and Discussion | 5% | -- | -- | | 1885925541 | 23-Aug-2022 | |
| <input type="checkbox"/> | Tagesse Gichamo Lafa... | Chapter I Introduction | 6% | -- | -- | | 1885920992 | 23-Aug-2022 | |
| <input type="checkbox"/> | Tagesse Gichamo Lafa... | Chapter II Literature review | 7% | -- | -- | | 1885921839 | 23-Aug-2022 | |
| <input type="checkbox"/> | Tagesse Gichamo Lafa... | Full thesis | 15% | -- | -- | | 1885914762 | 23-Aug-2022 | |
| <input type="checkbox"/> | Tagesse Gichamo Lafa... | Chapter III Methodology | 19% | -- | -- | | 1886004583 | 23-Aug-2022 | |

Prof. Dr. Hüseyin Gökçekuş